2004

Electrical, optical and structural properties of e-beam deposited manganese dioxide (MnO2) thin films for selective surface application

Khatun, Mst. Shefaly

University of Rajshahi

ELECTRICAL, OPTICAL AND STRUCTURAL PROPERTIES OF E-BEAM DEPOSITED MANGANESE DIOXIDE (MnO_2) THIN FILMS FOR SELECTIVE SURFACE APPLICATION

A Thesis
Submitted to the University of Rajshahi in Fulfillment
of the Requirements for the Degree of
Master of Philosophy

BY
MST. SHEFALY KHATUN

DEPARTMENT OF APPLIED PHYSICS AND ELECTRONICS
UNIVERSITY OF RAJSHAHI, RAJSHAHI-6205, BANGLADESH

APRIL, 2004

DEDICATED TO
MY
PARENTS

ফলিত পদার্থ বিজ্ঞান ও ইলেকট্রনিক্স
বিভাগ, রাজশাহী বিশ্ববিদ্যালয়,
রাজশাহী-৬২০৫,
বাংলাদেশ

Department of Applied physics
and Electronics. University of
Rajshahi, Rajshahi-6205,
Bangladesh

CERTIFICATE

The thesis entitled " **Electrical, optical and structural properties of e-beam deposited manganese dioxide (MnO_2) thin films for selective surface application** "submitted by Mst. shefaly khatun , embodies the results of research carried out by her under our direct supervision and guidance. We certify that this work has not been presented for any degree or prize elsewhere.

(Dr. Khairul Alam Khan)
Professor
Department of Applied Physics & Electronics
University of Rajshahi, Rajshahi
Bangladesh

(Dr. Osman Gani Talukdar)
Professor
Department of Applied Physics & Electronics
University of Rajshahi, Rajshahi
Bangladesh

ACKNOWLEDGEMENT

I wish to express my deepest sense of gratitude to my reverent teacher **Dr. M. Khairul Alam Khan** and **Dr. Osman Gani Talukdar,** Professor, Department of Applied Physics and Electronics, Rajshahi University, Rajshahi, for their kind and constant guidance, active help, cooperation, untold patience, valuable suggestion and encouragement during the research work.

I wish to express my gratefulness to professor M.A. Sobhan, Chairman and Professor M.. A. Aziz miah, former Chairman of this department for providing necessary facilities to carry out this work.

Thanks are also due to all my respectable teachers of this department for their valuable suggestions and inspirations throughout the course of the research work. I am particularly grateful to Professor Mr. Rejwan Ali, who always became glad whenever I approached him for my problem regarding this study.

I am indebted to Mr. A.L. Talukder, principle Instrument Engineer, Mr. M.S. Islam, Instrument Engineer, for their help regarding instrumental troubles. I express my thanks also to Mr. Ayub Ali, caretaker of our laboratory.

I have deep sense of gratitude to the staff of Department of physics, BUET, Dhaka, for their kind help to using the X-ray Diffractometer for XRD measurement.

Finally, I would like to express my heartfelt gratitude to my parents and other family members for their constant support and encouragement during my study.

The Author.

ABSTRACT

MnO_2 thin films of thickness ranging from 55 to 250 nm have been prepared by e-beam deposition technique onto glass substrate at two pressures, namely at about $2x10^{-5}$ torr and at about $6x10^{-6}$ torr, respectively and the deposition rate was about 3 nm/sec.

MnO_2 thin films were characterized through X-ray diffraction technique. These studies hint that the films are amorphous in nature.

Electrical conductivity was measured as a function of temperature ranging from 303 to 403K and exhibits an anomaly in conductivity at a temperature 323 K. The films deposited at about $2x10^{-5}$ torr show the electrical conductivity metallic in character by indicating positive Temperature Coefficient of Resistance (TCR), whereas a negative Temperature Coefficient of Resistance (TCR) indicating semiconducting behaviour exhibits on the films deposited at a pressure of about $6x10^{-6}$ torr. This result, therefore, suggests that preparation and properties of MnO_2 films are very much dependent on ambient pressure.

It is seen that the activation energy for the samples are fairly low. It is also observed that the activation energy was inversely proportional with the film thickness above the anomaly and was directly proportional below the anomaly temperature.

Thickness-dependent electrical conductivity study was done in semiconducting MnO_2 films and it was seen that below 200nm thickness, the film shows thickness-dependent property and above this range the film has thickness-independent behaviour which is in good agreement with **Fuchs-Sondheimer** theory.

The conductivity of the as-deposited films was increased whenever it was annealed to a certain temperature, however, its order of conductivity does not change appreciably.

Aging effect were studied for the semiconducting films and it was found that thicker films slowly degrade than the thinner ones which may be caused due to oxidation or contamination of the films.

The measurements of Hall coefficient are found to increase with decreasing magnetic field. The Hall mobility varies with increasing thickness while the carrier concentration increases with increasing thickness. The value and sign of the Hall voltage of the measured samples signify that the samples are n-type in character. The band gap was found at approximately 0.27 eV.

The thermal e.m.f. was directly proportional with temperature and the thermoelectric power was negative in all cases. The negative value of thermoelectric power indicates that the electrons are the majority carriers. Similar observation was also obtained from Hall effect measurement. The transport properties in these samples are controlled mainly by the ionized impurity scattering process corresponding to a scattering index of -1.5 obtained from thermoelectric power data. In the room temperature region coefficient of activation energy has strong thickness dependency while in the high-temperature region it is almost thickness independent.

Optical measurement were done for the semiconducting films in the wavelength range $0.3<\lambda<2.5$ μm and the films show highly transparent both in the visible and infrared regions. From the optical measurements, the band gap was calculated and it was found to be $\approx$ 0.25 eV. The value of optical band gap is very close to the value obtained from electrically measured band gap 0.27 eV, which is well agreed with reports of previous workers. The integrated values of luminous transmittance (T_{lum}) and solar transmittance (T_{sol}) are of high order indicating that the material is a potential candidate for the applications in selective surface devices.

CONTENTS

CHAPTER ONE

INTRODUCTION

INTRODUCTION

1.1 OVERVIEW

The tremendous development of the microelectronics device technology in the past several decades is possible mainly due to the advancement of the "Physics of Thin Films". Thin films have been extensively studied for over a century because of their potential applications.

The investigation of the physical properties of matter has progressed so much during the last century that today physics is divided into a large group of special branches. Thin film is such an important branch of physics. The systems which are investigated in this branch have a common characteristic that one of their dimensions is very small i.e. negligible in comparison to the other.

Film means a layer of coating of a material onto another material (called substrate), which is non-reactive except for sufficient adhesion. A solid material is said to be **"Thin Film"** when it is built up as a thin layer on a solid support, called substrate, by controlled condensation of the individual atomic, molecular, or ionic species either directly by a physical process or via a chemical and/or electrochemical reaction. The word **"Thin"** gives a relative measurement of any dimension but not to any absolute value and **"Film"** means a coating of layer. The term thin as it applies to thin films is quite ambiguous. It is used to define a layer of thickness, which is comparable with the mean free path (mfp) of the

conduction electrons. Its value differs from material to material. In practice, this branch deals with films having thickness between the tenths of a nanometer and a few micrometers.

Thin films are most commonly deposited by thermal evaporation techniques where the atoms are condensed from the vapor phase onto a substrate. Deposition of thin films in such a process is achieved by one or more phase transformation and the study of the thermodynamics and kinetics of these phase transformations reveal the formation of thin films. Thin films exhibit different electrical, optical, mechanical, structural and magnetic properties than their corresponding bulk bodies. These are the consequences of their planner geometry, size and unique structure.

The reduction of one dimension of material to an order of only several atomic layers creates an intermediate system between micro-system and molecular system, thus providing us with a method of investigation of the microphysical nature of various processes. Probably these are the important reasons why thin films have attracted the attention of a large number of physicists and researches all over the world.

1.2 HISTORICAL BACKGROUND OF THIN FILM

For the last three centuries non-solid films have been studied and were familiar to the scientist. Thin solid films were probably first obtained by electrolysis in 1838 and were studied for their technological value and fantastic applications in the field of research. However according the recoded literature, metal films obtained by means of a chemical reaction

and glow-discharge sputtering, **(Bunsen, 1852).** First metal films obtain by thermal evaporation on explosion of a current carrying metal wire **(Faraday, 1857).** Edison and others in 1883 while experiencing with carbon filament lamp probably first discovered free evaporation and condensation of thin films in vacuum. The possibility of depositing thin metal films in a vacuum by Joule heating of platinum wires was tested **(Nahrwold, 1887)** and a year later adapted **(Kundt, 1888)** for the purpose of measuring refractive indices of metal films.

In the following decades, evaporated thin films remained in the domain of academic interest until the development of vacuum equipment had progressed enough to permit large-scale applications and control of films properties. During the last 40 years, evaporated films have found industrial usage in the manufacture of cathode ray tubes, in electronic circuit and lastly selective surface coating for energy efficient devices.

In most cases, a film below a few micrometers in thickness can be regarded as thin film technology. The technology and understanding of films less than 1 micron thick have made tremendous advances in the last decades, primarily because of industrial demand for reliable thin film microelectronic devices to fulfill the urgent needs of electronic era. The most recent thin film technology in the microelectronic industry based on two features, namely, its compactness and integration. Compactness results from very thin. Integration is accomplished by fabricating interconnected components on each other to form very thin film integrated circuits. Very large-scale integrated circuits like

microprocessor and other memory devices are the greatest contribution of thin film technology on computer era.

The properties of thin films are rather different from the balk material. Theoretical explanations regarding the properties of thin films were done. The **"size-effect"** theory explain the high electrical resistivity of thin film specimen as compared with that of balk material (**Thomson , 1901).** The "size-effect" theory was also explained for a spherical Fermi-surface and a free electron model **(Fuchs, 1938)** and later explained the galvanometric effect**(Sondheimer, 1950).**

Thin film technology had a rapid growth between the beginning and the middle of twentieth century when the vacuum evaporated metal and dielectric films were used in optics (for mirrors and antireflection coating respectively). The development of high vacuum diffusion pump made possible the construction of high vacuum systems. This progress made possible to fabricated high quality thin films and a new branch of optical technology has emerged which is based on optical film interference system. The most modern development in the field of thin film physics is that of the electronics devices. Now-a-days extensive studies on different properties of thin films proceeded along different lines throughout the world. Recently an even greater application known as thin film microelectronics has emerged in the field of electronics and consequently a rapid development occurred in microelectronics industry.

1.3 CHARACTERISTICS OF THIN FILM

Thin films are commonly prepared by the condensation of atoms from vapor phase of atom by atom onto a cooler substrate. The properties of thin film changes appreciably when it is cooled to a very low temperature or heated to a higher temperature (above room temperature). A study of the changes in the properties of a thin film, when the films are heated to higher temperature provides a great deal of information about the properties of films.

In general the physical properties of thin films are determinated by a number of factor, such as:

(i) **The nature of substrate:** It may be non-crystalline, crystalline or glass and films characteristics may be different for each substrate.

(ii) **The temperature of the substrate during deposition of films:** At low temperature polycrystalline films with high densities of structural imperfections are formed on both vitreous and crystalline substrate, but a high temperature oriented single-crystal films are formed on crystalline substrates.

(iii) **Deposition conditions:** The properties of thin films depend on the deposition conditions, such as source temperature, pressure, current, deposition angle, distance between source to substrate etc.

(iv) **The annealing temperature:** The relative values of the minimum annealing temperature, i.e., heating the films to a higher temperature after deposition and cooling it back to room temperature.

(v) **Annealing cycle:** Annealing cycle, however, also plays an important role for the surface mobility of the atoms at the temperature of the substrate during deposition.

1.4 APPLICATION AREAS OF THIN FILM

Thin films are widely used in today's technology and their applications are expected to be even more widespread in the future. It is not possible to give an exhaustive survey over thin film applications, but a list of them is given below.

(a) **Mechanically functional**

- Hard coating for cutting tools
- Lubrication coatings
- Wear and erosion resistant coatings

(b) **Electrically functional**

- Super-conductors
- Conductors
- Insulators (resistors, capacitors)
- Solar cells
- Microelectronic devices

(c) **Optically functional**

- Spacecraft temperature control
- Architectural glazing

- Antireflection coatings
- Solar absorbing coatings
- Automotive windows
- Mirrors

(d) **Chemically functional**

- Diffusion batteries
- Catalytic coatings
- Corrosion resistant layer

(e) **Decorative**

- Costume jewelry
- Watch bezels and bands
- Eyeglass frames

FRONTIER AREAS OF TEIN FILM TECHNOLOGY

- Coatings for energy efficiency and solar applications
- Superconductors with high critical temperature
- Laser mirrors
- Sub-micron microelectronics
- Thin film photovoltaic
- Coatings for advanced cutting tools
- Corrosion/erosion resistant coatings for high temperature applications
- Wear-resistant coatings, particularly for high temperatures
- Catalytic materials
- Ultra-high strength ceramic layers

- Biomedical devices
- Thermonuclear reactor vessels
- Materials conservation

1.5 INFORMATION ABOUT MnO_2

Research and development on surface coatings for energy efficient devices has led to the conclusion that different classes of materials are of particular interest for different applications. The key concepts of the coating in the spectral selectivity, i.e. the films should have qualitatively different optical properties in different wavelength range.

Manganese dioxide, a gray to black in color, occurs in ores such as pyrolusite, where it is usually nonstoichiometric. It is an element of group IV in the periodic table. Manganese dioxide is a low band gap, high optical constant semiconductor. It has also ferroelectric properties **(Bhide and Damle, 1960).**

Manganese dioxide has a rutile structure and belongs to the tetragonal. The Mn^{4+} ions lie on a body-centered tetragonal lattice with a= 0.4865 nm and c=0.3824 nm. Each Mn ion is connected to two oxygen ions situated at a distance of about 0.17 nm from it. Thus O-Mn-O forms a basis of the body-centered tetragonal structure of MnO_2. The corner Mn^{4+} ions have the oxygen linkage along one of the diagonals of the square face, whereas the central Mn^{4+} ions has a linkage with two oxygen ions along the other diagonal. Previous report **(Bhide , 1960)** in electrical conductivity measurements of this material sometimes show an anomaly

at a temperature of about 50 ^{0}C and no anomaly in conductivity at the curie temperature **(Megraw, 1957).** The conductivity in MnO_2 essentially arises from the controlled valance mechanism. It appears that at the Curie temperature, where the dielectric constant is a maximum, the electrical conductivity is also maximum.

1.6 OBJECTIVE OF THE PRESENT WORK

The purpose of the present work is to prepare MnO_2 thin films by e-beam deposited technique onto glass substrates. It includes the study of electrical, optical and structural properties of the deposited films. To make a study, the following steps are adopted:

- Production of MnO_2 thin films by e-beam deposited technique at Various pressures.
- Characterization of MnO_2 samples by X-ray diffraction pattern.
- Effect of deposition parameters (such as deposition time, ambient pressure, source to substrate distance) on film thickness
- Effect of films thickness on resistivity (ρ), Temperature Coefficient of Resistance (T.C.R.), activation energy.
- Annealing effect.
- Aging effect.
- Hall effect studies.
- Studies on the Thermo electrical power.
- Optical property studies.

CHAPTER TWO

METHOD OF THIN FILM PREPARATION

METHODS OF THIN FILM PREPARATION

2.1 INTRODUCTION

It is well known that the properties of thin film may be quite different from those of bulk material, particularly if the film thickness is very small. These anomalous properties are due to the peculiar structure of the film, and the process, in turn, dictates this structure, which occur during the film formation. Generally thin films are prepared by depositing the film material, atom by atom onto a substrate. One of the examples is the condensation of vapor to give a solid or liquid film. Such process of deposition involves a phase transformation. The best understood process of film formation is that by condensation from the vapor source.

2.2 SURVEYS OVER DEPOSITION TECHNOLOGIES

There is large number of technologies for making surface coatings of different types. Table 2.1 gives a survey, where the technologies are grouped under the following headings:

i) Atomistic deposition
ii) Particulate deposition
iii) Bulk coating
iv) Surface modification

The technologies listed under atomistic deposition and surface modifications are most widely applicable to thin film production whereas the other technologies usually lead to thick film production.

TABLE-2.1 Survey over film fabrication technologies:

Atomistic deposition	**Particulate deposition**	**Bulk coating**	**Surface modification**
1.a) vacuum environment • Evaporation • Molecular beam • Epitaxy • Ion beam deposition 1.b) plasma environment • Sputter deposition • Ion plating • Plasma polymerization • Glow discharge deposition 1.c) Electrolytic environment • Electroplating • Electrolysis deposition 1.d) Chemical vapour environment • Chemical vapour deposition • Spray pyrolysis 1.e) Liquid phase epitaxy	2.a) Thermal spraying • Plasma spraying • Flame spraying • Detonation gun 2.b) Fusion coatings • Enameling • Electrophoresis	3.a) Wetting processes • Painting • Dip coating • Spin coating 3.b) Printing 3.c) Cladding • Explosive • Rollbinding 3.d) Weld coating	4.a)Chemical conversion • Anodic oxidation • Nitridation 4.b) Leaching 4.c) Thermal surface treatment 4.d) Ion implantation 4.e) Laser glazing

An alternative classification of some common technologies for making thin films by deposition is found in Table-2.2. Here the technologies are grouped under the headings:

i) Physical

ii) Chemical

iii) Physico-chemical

TABLE: 2.2 Alternative classifications of major thin film deposition technologies:

Physical	**Chemical**	**Physico-chemical**
• Evaporation • Sputtering • Ion-assisted techniques	• Deposition from solution • Chemical vapor deposition	• Plasma- polymerization • Glow discharge deposition

2.2a VACUUM EVAPORATION

Vacuum evaporation is the most widely used technique for the preparation of thin films. This method is very simple and it has many advantages over the other methods. The most important characteristic feature of this technique is that the transport of vapor from the source of the substrate takes place by physical means. Films of high quality are readily produced with a minimum of interfering conditions. In practice they are applicable to all substances and to a great range of thickness.

The film fabrication by vacuum evaporation is most conveniently introduced looking at a prototype evaporation system as shown in figure 2.1. A vacuum chamber, evacuated to ~10^{-5} torr or below, contains a vapor source, for example a resistive foil source and a substrate. The material to be evaporated is in thermal contact with foil

source. When the vapor source is heated by passing an electric current, the vapor pressure of the evaporate becomes substantial and liberated atoms are sent out into the vacuum chamber and stick to the substrate where a thin film consequently formed

2.2.b STEPS OF EVAPORETION

The following physical stage are found in the process of film formation by evaporation:

i) Transition of a condensed phase, which may be solid or liquid, into the gaseous state.

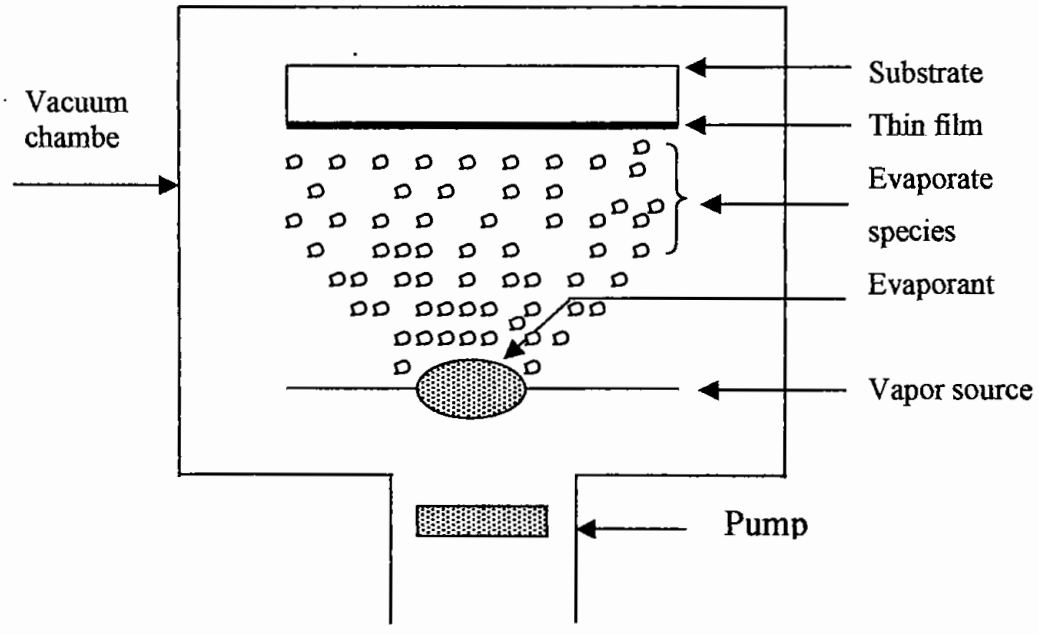

Fig: 2.1 Vacuum evaporation system for thin film preparation.

ii) Vapor traversing the space between the evaporation source and the substrate at reduced gas pressure.

iii) Condensation of the vapor upon arrival on the substrates.

The liquid vapor transformation is called evaporation and solid to vapor transformation is called sublimation.

2.2.c THERMAL EVAPORATION METHODS

Solid materials vaporize when it is heated to sufficiently high temperatures. The condensation of the vapor onto a cooler substrate yields thin films. This method of film formation is known as thermal evaporation method. Thermal evaporation may be achieved directly or indirectly (via a support) by a variety of physical methods. Some of them are briefly described below:

i) Resistive heating: This method consists of heating the material with a resistively heated filament or boat generally made of refractory metals such as W, Mo, Ta, and Nb with or without ceramic coatings. The choose of the support material is primarily determined by the evaporation temperature and resistance to alloying and /or chemical reaction with the evaporate. The material to be evaporated is being placed on a strip or boat. Then electric current is passed through the foil boat, this current produces heat and material is began evaporated.

ii) Flash evaporation: A rapid evaporation of a multicomponent alloy or compound, which tends to distill fractionally, may be obtained by continuously dropping fine particles of the material onto a hot surface, so

that numerous discrete evaporation occur **(Harries, 1948)**. There is evidence **(Ellis, 1967)** that flash evaporated films in some cases can show considerable deviation from the original composition. Further, since the large amount of rapidly released gas produces spattering of particles from the evaporant, this method is not easily controllable **(Beam, 1948)**.

iii) Arc evaporation: By striking an arc between two electrodes of a conducting material, sufficiently high temperatures can be generated to evaporate refractory materials such as Nb and Ta. This method is widely used for the evaporation of carbon for electron-microscope specimens, employs a standard dc arc-welding generator connected to the electrodes with a capacitor across the electrodes. In this method, deposition rate of about 50 A^{o}/sec or higher can be obtained **(Lucas, 1965)** for refractory metals, but this process is not easily reproducible.

iv) Exploding-wire technique: This method consists of exploding a wire by a sudden resistive heating of the wire with a transient high current density approaching 10^{6} A^{0}/cm^{2} **(Conn, 1950)**. This is achieved by discharging a bank of condensers (~10 to 100μF), charged to a voltage ~1 to 10 kV, through a metallic wire. Thus, a catastrophic destruction and vaporization of the wire at some region take place.

v) Laser evaporation: The enormous intensity of a laser may be used to heat and vaporize materials by keeping the laser source outside the vacuum system and focusing the beam on the surface of the material to be evaporated. This promising method **(Smith, 1965)** has not yet been fully exploited. Since the laser penetration depth is small (~ $100A^{o}$), evaporation takes place at the surface only.

vi) RF heating: The induction heating may be supplied to the evaporant directly or indirectly from the crucible material **(Turner, et. al. ,1963)**. It used a crucible thin enough near the surface to offer no shielding of the field and thus allow heating of the Al melt by the 200 kc/sec field **(Ames, 1966)**. However, the crucible was thick enough elsewhere to screen the melt from excessive coupling with the field, thus minimizing turbulence **(Van, 1965)**.

vii) Electron bombardment heating: The simple resistive heating of an evaporation source suffers from the disadvantages of possible contamination from the support material and the limitations of the input power, which make it difficult to evaporate high melting point materials. These drawbacks may be overcome by an efficient source of heating by electron bombardment of the material. In principle, this type of source is capable of evaporating any material at rates ranging from fractions of an angstrom to microns per second. In the present work this method is used for the evaporation of MnO_2.

2.3 DIFFERENT STAGE OF THIN FILM PREPARATION

There are three mechanisms of thin film condensation can be distinguished, depending on the strength of interaction between the atoms of the growing film and between the atoms of the film and substrate. These are:

a) The layer-by-layer growth **(Vander Merwe mechanism)**

b) A three-dimensional nucleation forming, growth and coalescence of islands **(Volmer Weber mechanism)**.

c) Absorption of a monolayer and subsequent nucleation on the top of this layer **(Stranski-Krastanov mechanism)**.

2.3.a CONDENSATION

Condensation simply means the transformation of a gas into a liquid or solid. The condensation of vapor atom is determined by its interaction with the impinged surface in the following manner. The impinging atom is attracted to the surface by the instantaneous dipole and quadruple moments of the surface atoms. As a result, the atom loses its velocity component normal to the surface in a short time, provided the incident kinetic energy is not too high **(Chopra, 1969)**. The vapor atom is then physically absorbed (called "adatom"), but it may or may not be completely thermally equilibrated. It may move over the surface by jumping from one potential well to the others because of thermal activation from the surface of its own kinetic energy parallel to the surface. The adatom has a finite stay or residence time on the surface during which it may interact with other adatoms to form a stable cluster and may chemically absorbed with the release of the heat of condensation. If not absorbed, the adatom re-evaporates into the vapor phase. Therefore, the condensation is the net result of equilibrium between the absorption and desorption processes.

The probability that an impinging atom will be incorporated into the substrate is called the "*condensation*" or "*sticking*" coefficient. It is measured by the ratio of the amount of material condensed on a surface to the total amount impinged. The sticking coefficient is expected to

decrease with increasing substrate temperature .It should be increased with increasing deposit and approach unity for the case of self deposition.

2.3.b NUCLEATION

Nucleation is the birth stage of film. There are two types of nucleation occur during the formation of film; homogeneous and heterogeneous nucleation. A homogeneous nucleation theory which takes into account the total free energy of formation of a cluster of adatom was postulated by Volmer, and Weber **(Volmer and Weber, 1925).** It was later extended to heterogeneous nucleation by Volmer and to the particular shapes of clusters in a thin film case by Pound et al. **(Pound et al., 1954)**. In this theory, clusters are formed by collisions of adatoms on the substrate surface, and in the vapor phase if super saturation is sufficiently high. They develop that with increase in free energy until a critical size is reached, above with growth continues with decrease in free energy.

2.3.c GROWTH

Growth is the final and completion stage of thin film formation. The process of enlargement of the nuclei to finally form a coherent is termed as *growth.* The growth sequence of a film was originally deduced by Andrade from the observed optical transmission behavior of Ag films **(Andrade, 1935)**. This deduction is in remarkable agreement with the electron-microscope observations **(Uyeda, 1942)**. The clusters become larger and ultimately continuous film is produced. Pashley et al.

distinguished four stages of the growth process based on the electron microscope observation **(Pashley et al., 1964)**. They are the following:

i) The island stage

ii) The coalescence stage

iii) The channel stage

iv) The continuous film stage.

The stages of film formation are shown in figure 2.2

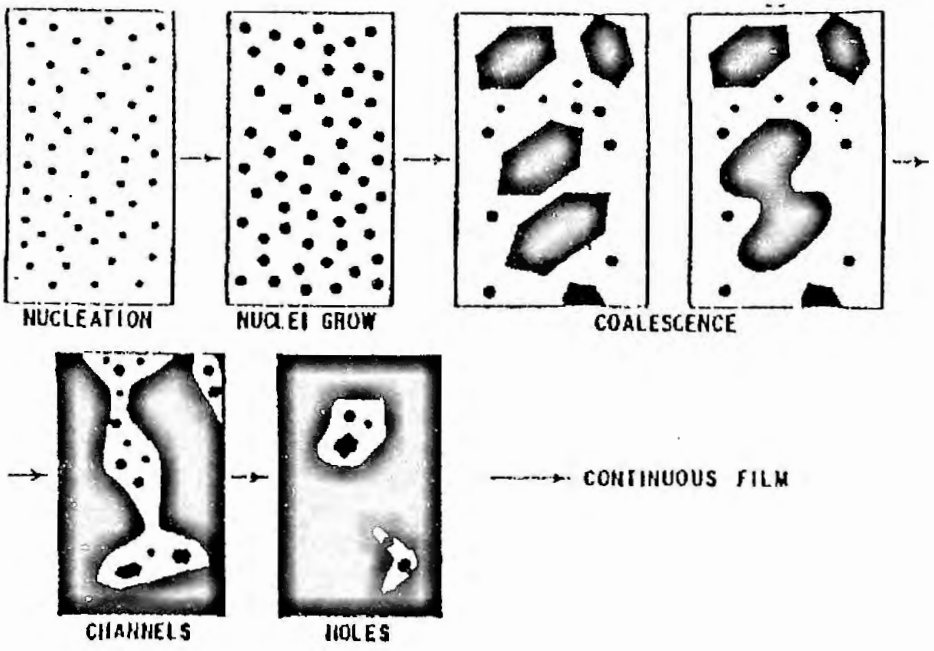

Fig: 2.2 Different stages of film growth

i) The island stage: When a substrate under impingement of condensate monomers is observed in the electron microscope, the first evidence of condensation is a sudden burst of nuclei of fairly uniform size.

(ii) The coalescence stage: As islands increase their size by further deposition and come closer to each-other, the larger one appear to grow by coalescence of the smaller ones. Figure 2.3 illustrates the manner of coalescence of two rounded nuclei. The coalescence occurs in less than 0.1s for the small nuclei and is characterized by a decrease in total projected area of the nuclei on the substrate (and an increase in their height). In addition, nuclei having well-defined crystallographic shapes before coalescence become rounded during the event **(Pashley and Stowell, 1962)**. The composite island takes on a crystallographic shape again if left for a sufficiently long time before interacting with its neighbors. The triangular profile of the crystallites is characteristic of the nucleation stage; after coalescence has taken place, the islands assume a more hexagonal profile and are often faulted. A sequence of micrographs illustrating the effects as shown in figure 2.4, where islands A and B have formed a compound island which eventually becomes crystallographically shaped.

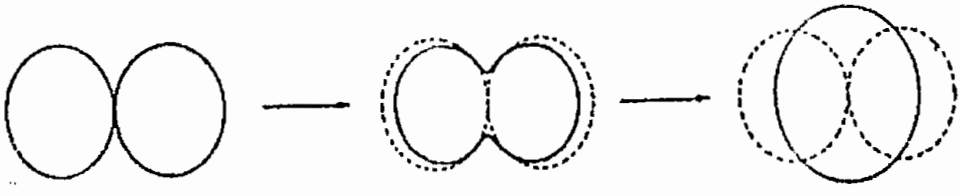

Fig: 2.3 Schematic of shape changes during coalescence of two rounded nuclei (Pashley et al., 1964).

The liquid like character of the coalescence leads to enlargements of the uncovered areas of the substrate, with the result that secondary nuclei form between the islands. This effect becomes noticeable when the primary islands have grown to about 1000 A°, and continues until the final hole-free film is formed. The small nuclei surrounding island B (figure.2.4a) are examples of those secondary nuclei. A secondary nucleus grows until it touches a neighbor, and if this happens to be a much larger island, the secondary nucleus coalesces very rapidly and becomes completely incorporated in the large island.

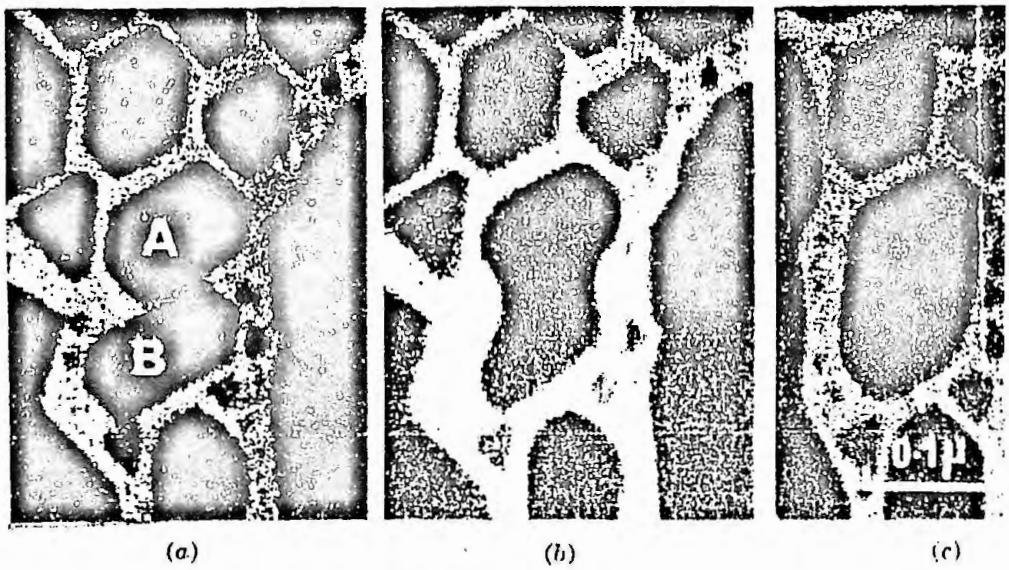

Fig: 2.4 Electron micrograph shows the change in shape of islands during and after coalescence (a) at zero (b) after 1 to 2 sec. (c) after 60 sec. (Pashley 1954).

iii) The channel stage:

As the islands grow, there is a decreasing tendency for them to become completely rounded after coalescence. Large shape changes still occur, but these confined mainly to the regions in the immediate vicinity of the junction of the islands. Consequently, the islands become elongated and join to form a continuous network structure in which the deposit material is separated by long, irregular, and narrow channels of width 50 to 200 A° as shown in figure 2.5(a). As deposition continues, secondary nucleation occurs in these channels, and the nuclei are incorporated into the bulk of the film as they grow and touch the sides of the channel. At the same time, channels are bridged at some points and fill in rapidly in a liquid like manner. A sequence of these events is shown in figure 2.5.

Eventually, most of the channels are eliminated and the film is continuous but contains many small irregular holes. Secondary nucleation takes place on the substrate within these holes, and the growing nuclei are incorporated (in a liquid like manner) into the continuous regions of the deposit. The hole contains many secondary nuclei which coalescence with each other to form secondary islands, which then touch the edge of the hole and coalesce with the main film to leave a clean hole. Further, secondary nuclei then form, and the process is repeated until the hole finally fills in.

iv) The continuous film stage: The final stage of film growth is a slow process of filling the empty channels, which requires a considerable amount of deposits. In channel stage large areas are vacated by coalescence. These empty channels are filled by secondary nucleation, growth and coalescence and in this way a continuous film is formed.

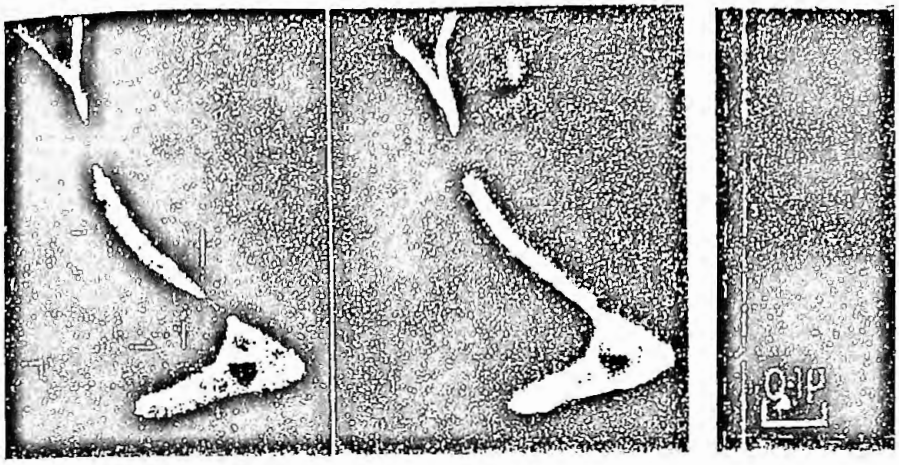

Fig: 2.5 Electron micrographs of Au on MoS_2 at 400°C. Showing channel filling: (a) at zero (b) 0.06s (c) 4s (Pashley et al. 1964).

2.4 THICKNESS DISTRIBUTION

The thickness of thermally evaporated film depends on the shape and size of the source and orientation of the source relative to the substrate. Holland **(Holland, 1956)** has discussed thoroughly the theoretical distribution of vapor from a point, a wire, a small surface, an extended strip and cylindrical ring types of source. For the ideal case of deposition from a clean uniformly emitting point source onto a plane receiver as shown in figure2.6, the rate of deposition varies as $Cos\theta/r^2$ (*Knudsen cosine law*), where r is the radical distance of the receiver from the source and θ is the angle between the radial vector and the normal to the receiver direction.

If t_o and t are the thickness of deposits at the receiver vertically

below the source at a distance h, and at a horizontal distance x from the vertical line, respectively, then the deposit distribution (assuming the same condensation coefficient) is given by

$$\frac{t}{t_o} = \frac{1}{\left[1+\left(\frac{x}{h}\right)^2\right]^{\frac{3}{2}}} \qquad \text{----------(2.1)}$$

For evaporation from a small area onto a parallel plane receiver, the deposition rate is proportional to $\cos^2\theta/r^2$, and the thickness distribution is given by

$$\frac{t}{t_o} = \frac{1}{\left[1+\left(\frac{x}{h}\right)^2\right]^{2}} \qquad \text{----------(2.2)}$$

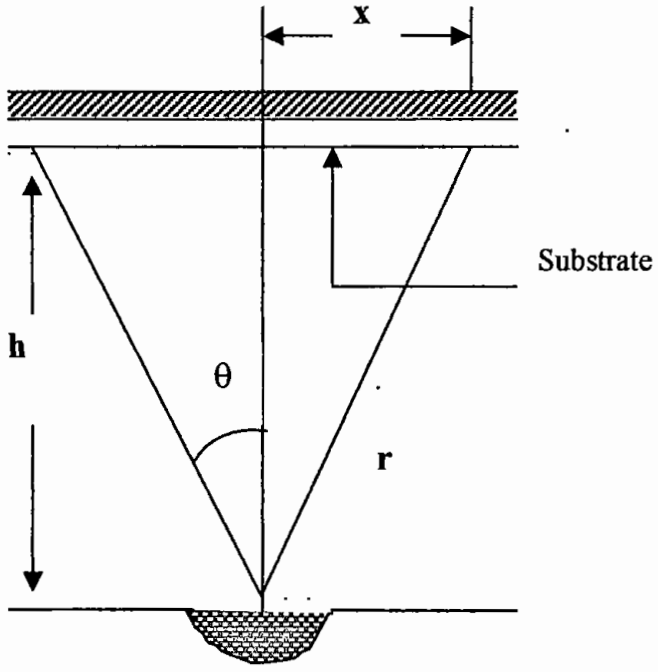

Fig: 2.6 Schematic Illustration of thickness distribution.

2.5 INFLUENCE OF SUBSTRATE AND DEPOSITION CONDITIONS ON FILM GROWTH AND PROPERTIES

(a) Substrate: The single-crystal substrate has a dominant influence on the oriented growth of the deposit. Epitaxy can occur between two substances of completely different crystal structures and of different types of chemical bonds.

(b) Substrate temperature: The most important effect of heating the substrate in vacuum is the additional cleaning of the surface that results from the desorption of contaminants.

An increasing substrate temperature may improve epitaxy by (1) adding the adsorptions of absorbed surface contaminants, (2) lowering super-saturation, thus allowing the dilute gas of atoms sufficient time to reach the equilibrium positions, (3) providing activation energy for atoms to occupy the positions of potential minima, (4) enhancing re crystallization due to the coalescence of islands by increasing surface and volume diffusion and (5) assisting a possible ionization of surface atoms. **(Bruck, 1936).**

(c) Deposition rate: According to Sloope and Tiller **((Sloope and Tiller, 1965)** on evaporated Ge films on CaF_2, NaCl, NaF and Ag on cleaved NaCl, established that, for a given deposition rate R, a minimum epitaxial temperature T_e exists related to R by

$$R \leq A \exp\left(-\frac{Q_d}{KT_e}\right)$$

Here A is constant and Q_d is the energy of surface diffusion. This relation follows from the elementary considerations that an atom should have sufficient time to jump to an equilibrium position of an ordered state by surface diffusion before it interacts with another adatom. For a given system with fixed atomic mobility, this is satisfied if the deposition rate of a monolayer should be less than the jump frequency of adatoms.

(d) Contamination: The main source of contamination in evaporated films are contaminants brought into the vacuum system on the substrate, residual contaminant gases or vapors in the vacuum system, gases released from the evaporant and the heater material itself.

(e) Film thickness: Since the rate of bombardment by residual gas is constant (for constant residual pressure),higher deposition rates produce films containing smaller amounts of residual gas when an active metal is being deposited. The residual gas content of the film may be thickness dependent, the last layers contain less residual gas than the first layers. Residual gas content can be minimized by depositing on a shutter for a relatively long time before starting to collect the deposit.

(f) Annealing effect: Since the material internal stress depends much on the structural order of a film, it is usual to observe its irreversible

changes due to an extent annealing and relate it to the elementary lattice defects and crystallization process.

(g) Source temperature: Most materials to be evaporated require source temperatures in the range of 1000 to 2000 °C, and some means of heating the materials to these temperatures must be provided, where a simple strip or boat of molybdenum, tungsten or tantalum are often used. Many types and shapes of resistance heaters are available. The choose of heater becomes more difficult as the evaporation temperature increases, since the heater must neither soften nor react appreciably with the molten source material.

(h) Electrostatic effect: An applied electric field can enhance coalescence, improve epitaxial growth, and stabilize crystallographic structure other than the normal. A d.c. electronic field in the plane of the substrate surface can induce coalescence at an early stage of film growth and thus the film becomes electrically conductive at a small average thickness **(Chopra, 1969)**.

(i) Deposition methods: Deposition methods are very important for film deposition, because different deposition methods can produce films with different characteristics i.e. the resistivity or mobility can be affected by deposition methods.

(j) Angle of incidence of the evaporant: The angle of incidence, which is the angle between the normal to the surface and trajectory of the arriving atom, can affect the structure of the evaporated film.

A coarse texture develops more rapidly as the angle of incidence increases. As illustrated in figure 2.7, the incident vapor atoms are shielded from depositing on the far side of peaks, which grow in the direction of the source. For some material, this change in texture affects the stress in the film.

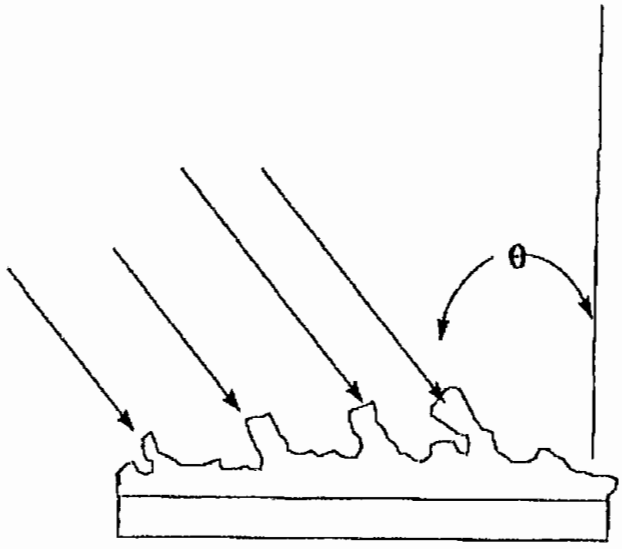

Fig: 2.7 Schematic diagram of an electron photomicrograph showing how the more elevated grains, which grow at the expense of their neighbors, tend to tilt towards the vapor beam.

CHAPTER THREE

THEORICAL CONSIDERATION ON MEASUREMENT

THEORETICAL CONSIDERATIONS ON MEASUREMENT

3.1 RESISTIVITY AND CONDUCTIVITY MEASUREMRNT

Generally the property of a material to resist of electrical current is called the resistance and the resistance per unit length of cross-section is called resistivity. It is denoted by ρ and mathematically defined as

$$\rho = \frac{RA}{L} \text{----------(3.1)}$$

Where A is the cross-sectional area, R is the resistance and L is the length of the material along the direction of current flow. Resistivity is an intrinsic property of a material and depends only on the crystal structure of the material.

Electrical conductivity of a material is reciprocal of resistivity of the material. Conductivity is denoted by σ and defined as

$$\sigma = \frac{1}{\rho} \text{----------(3.2)}$$

Conductivity depends only on the structural and physical property of the material.

A number of methods used to measure the resistivity of a material. Only two of them are discussed below:

3.2 RESISTIVITY MEASUREMENT TECHNIQUES

3.2.a DIRECT METHOD

The resistivity of a thin film can be measured easily by using direct method. The experimental arrangement is shown in figure 3.1. If the current I is flowing along of length L and voltage drop across L is V, then R=V/I and then by using the following equation, one can easily determine the resistivity if the film of thickness t is known

$$\rho = \frac{RWt}{L} \text{ ----------(3.3)}$$

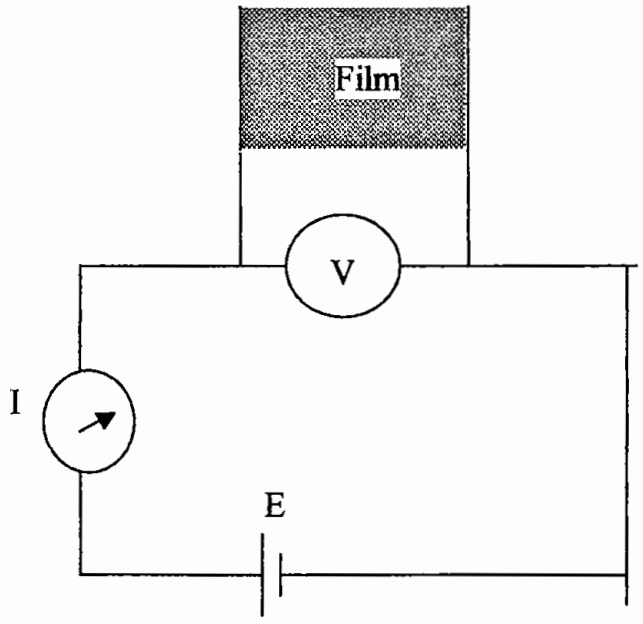

Fig:3.1 Circuit arrangement for resistivity measurement by using direct method.

If W = L i.e. film having square shape, then resistivity equation becomes

$$\rho = Rt \text{ ----------(3.4)}$$

and corresponding conductivity is defined as

$$\sigma = 1/\rho \text{ ----------(3.5)}$$

Thus one can easily determine the resistivity as well conductivity by measuring the sheet resistance R and film thickness t.

3.2.b VAN DER PAUW'S METHOD

Electrical resistivity of metal and semiconductor film of any shape may be measured by using Van der pauw's method. The resistivity or conductivity of a thin film having any arbitrary shape can be uniquely determined by using this method **(Van der pauw's, 1958)**.

Let us consider a film of an arbitrary shape having four contacts A,B,C and D in order as shown in figure 3.2.

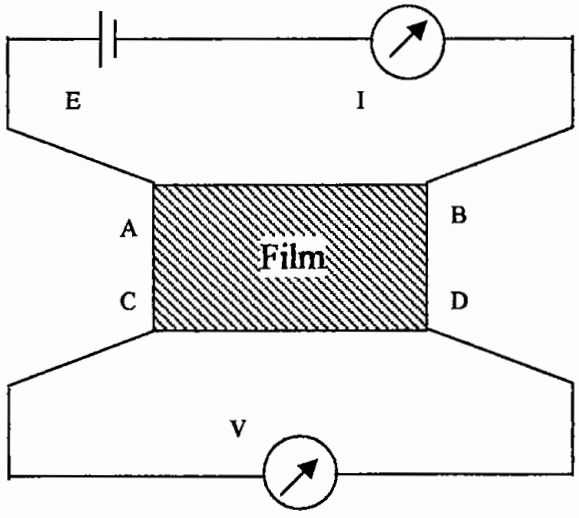

Fig: 3.2 Experimental arrangement for measuring resistivity by using Van der Pauw's method.

If a current I_{AB} entering the film through the contact A and leaving it from the contact B and produces a potential difference V_{DC} between points D and C then

$$R_{AB,CD} = \frac{V_{DC}}{I_{AB}} \text{ ---------- (3.6)}$$

Similarly, we can write

$$R_{CD,AB} = \frac{V_{BA}}{I_{CD}} \text{ ----------(3.7)}$$

$$R_{BC,DA} = \frac{V_{AD}}{I_{BC}} \text{ ----------(3.8)}$$

$$R_{DA,BC} = \frac{V_{CB}}{I_{DA}} \text{ ----------(3.9)}$$

Using reciprocal theorem Van der pauw showed that

$$\rho = 4.543t\left(\frac{R_{AB,CD} + R_{BC,DA}}{2}\right)\int\left(\frac{R_{AB,CD}}{R_{BC,AD}}\right)\Omega - cm \text{ - - - - - - - - - - - -} \quad (3.10)$$

The correction factor $\int$ has been calculated by van der pauw and is equal to unity when $R_{AB,CD} \cong R_{BC,AD}$ and then equation (3.10) becomes

$$\rho = 2.266t(R_{AB,CD} + R_{BC,DA}) \ \Omega\text{-cm} \text{ ----------(3.11)}$$

Where t is the film thickness in cm. and corresponding conductivity is defined as

$$\sigma = \frac{1}{\rho}(\Omega - cm)^{-1} \text{ ----------(3.12)}$$

3.3 SHEET RESISTANCE

The resistance of a thin film directly proportional to the resistivity ρ and inversely proportional to the thickness t and we can write for a rectangular film of length L and width W.

$$R = \left(\frac{\rho}{t}\right) \times \left(\frac{L}{W}\right) = Rs\left(\frac{L}{W}\right) \text{ ----------(3.13)}$$

Where R_S is known as the sheet resistance and expressed in ohms per square.

$$\therefore Rs = \frac{\rho}{t} \text{ ohm per square ----------(3.14)}$$

The ratio (L/W) is called the number of squares. The number of "squares" is a pure number have no dimensions. It is very useful quantity that is widely used for comparing films, particularly those of the same material deposited under similar conditions.

3.4 TEMPERATURE COEFFICIENTS OF RESISTANCE

The Temperature Coefficients of Resistance (T.C.R) plays an important role for film characterization. The resistivity of any metal and semiconductor are temperature dependent **(Ghosh and Deb, 1937).** The relation between resistivity and temperature is given by

$$\rho_T = \rho_o(1+\alpha T+\beta T^2 + \cdots\cdots\cdots\cdots) \text{ ----------(3.15)}$$

Where ρ_o is the resistivity at 0^0C and ρ_T is the resistivity at T^0C and α is the temperature coefficient of resistance and β is a constant. Generally $\alpha >> \beta$ at low temperature, and we can write from first approximation

$$\rho_T = \rho_o (1+\alpha T) \text{ ----------(3.16)}$$

At temperatures T_2 and T_1, the equation (3.16) can be written as

$$\rho_{T2} = \rho_o (1+\alpha T_2) \text{ ----------(3.17)}$$

$$\rho_{T1} = \rho_o (1+\alpha T_1) \text{ ----------(3.18)}$$

From above two equations after some mathematical manipulation we can write

$$\alpha = \frac{(\rho_{T2} - \rho_{T1})}{\rho_{T1}(T_2 - T_1)} \text{ ---------- (3.19)}$$

Generally ρ_{T1} is the resistivity at room temperature and ρ_{T2} is the resistivity at temperature T_2.

3.5 ACTIVATION ENERGY

The energy required to transfer charge from one initially neutral island to another is known as activation energy and denoted by ΔE.This is equivalent to the electrostatic binding energy of the charge to the island. When these charge carriers are excited to at least this energy from the Fermi-level, there will be tunneling from one island to another. These island or small particles are called crystallites. The activation energy is related with film conductivity and given by the relation

$$\sigma = \sigma_o \exp\left(-\frac{\Delta E}{2KT}\right) \text{----------(3.20)}$$

Where σ_o is the conductivity at 0°C and K is the boltzman constant and T is the absolute temperature. Equation (3.20) can be written as

$$\ln \sigma = -\frac{\Delta E}{2KT} + \ln \sigma_o \text{----------(3.21)}$$

Equation (3.21) is equivalent to straight-line equation y = mx+c. So that ΔE can be determined from the slope of the straight line $\ln\sigma = -\frac{\Delta E}{2KT} + \ln\sigma_o$. From the graph of lnσ VS 1/T, ΔE can be calculated by using the following relation

$$\Delta E = -\left\{\frac{\ln\sigma}{\frac{1}{T}}\right\} x2K \text{----------(3.22)}$$

3.6 GRAIN SIZE

A thin film consists of planer array of many small, discrete particles or islands of linear dimension r having dielectric constant ε. The activation energy **(Neugebaur and Webb, 1962)**

$$\Delta E = \frac{e^2}{\varepsilon . r}$$

Or, $$r = \frac{e^2}{\Delta E . e}$$

∴ Grain-size,

$$r = \frac{14.4}{\varepsilon . \Delta E} \overset{o}{A} \text{----------(3.23)}$$

Here r is expressed in angstroms when ΔE is in eV, ε is the dielectric constant and its value is taken as 3, halfway between those of vacuum and glass and e is the electronic charge. The grain size is also thickness dependent. The grain size increases with the increasing film thickness.

3.7 HALL EFFECT MESUREMENT

If a specimen (metal or semiconductor) carrying a current I is placed in a transverse magnetic field of flux density H, an electric field is developed along a direction perpendicular to both H and I. This phenomenon is known as Hall effect and the voltage developed is called Hall voltage **(E. H. Hall, 1879).**

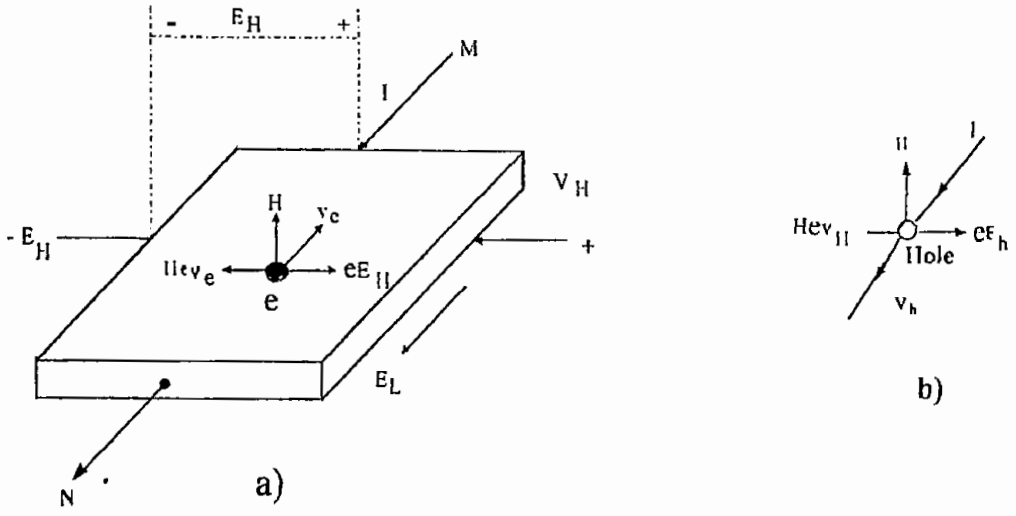

Fig: 3.3 Hall effect measurement a) for n-type material b) for p-type material.

In figure 3.3 (a), a current I is flowing through the semiconductor or metal in the direction MN under the influence of an external applied field E_L. Obviously, electrons comprising this current move along NM with a velocity V_e. Consider one such electron as shown in figure 3.3. The direction of the force exerted on it by the magnetic field H can be found

by using Fleming's left-hand rule and is shown in figure 3.3. The magnitude of this force is equal to Hev_e. Under the influence of this force, electrons will tends to crowd towards the left side of semiconductor or metal. This collection of electrons to one side gives rise to electric potential difference V_H , which is Hall voltage and hence to an electric field E_H . This field beings to prevent additional electrons from arriving there, force exerted this field on the electrons is eE_H. Equilibrium is established when the two oppositely directed magnetic and electric forces acting on the electron become equal in magnitude.

It may be noted that the above treatment is equally applicable to p-type semiconductors where current flow is made up of hole movement. If holes were to move in the same direction (MN) as the electrons in figure 3.3(a), then polarity of Hall voltage V_H would be reverse as shown in figure 3.3(b). So that the polarity of Hall voltage gives the concept of charge carriers. i.e. p-type or n-type ,we can write

$$Hev_e = eE_H \text{ or } Hv_e = E_H$$

Also

$$v_e = eE_L \qquad \text{-----(3.24)}$$

$$\therefore \mu_e = \frac{EH}{HEL} \qquad \text{-----(3.25)}$$

Also current density,

$$J = \frac{I}{A} \qquad \text{-----(3.26)}$$

$$\therefore n = \frac{JH}{eEH} \qquad \text{------- (3.27)}$$

Again Hall coefficient is given by Vander Pauw is

$$R_h = 10^8 R_{AC,BD} \frac{t}{H} \text{ cm}^3/\text{coulb.} \qquad \text{-----(3.28)}$$

Where t is the film thickness in cm . The notation $R_{AC,BD}$ denotes the resistance between A&C when current is passed between B&D . This resistance changes due to an applied magnetic field H in gauss.

Again we know,

$$R_H = \frac{1}{ne}$$

$$\therefore \text{Carrier concentration, } n = \frac{1}{RHe} \text{ --- --- -----(3.29)}$$

$$\therefore \text{Hall mobality, } \mu_H = R_H\sigma \text{ cm}^2\text{/v-sec. ---- ----- (3.30)}$$

$$\therefore \text{Band gap, } E_g = \frac{\ln RH}{1/T} \text{x2k --- ---- ---(3.31)}$$

3.8 SIZE EFFECT THEORY

The size effect is caused by restriction on the mean-free- path of the conduction electrons imposed by the geometry of very thin film. When the thickness of metal or semiconductor film becomes comparable in magnitude with the mean-free- path, the film boundaries impose a geometrical limitation on the movement of the effective value of the mean-free- path. Physical effect arising because of this geometrical limitation of the mean-free- path are termed "mean-free- path" or "size effect".

Thomson was the first who propose a size effect theory to explain the observed high electrical resistivity of thin specimens as compared with that of the same metal in bulk **(Thomson, 1901)**. The size effect theory for a free electron model was worked out by Fuchs **(Fuchs, 1938)** for a special fermi-surface and extended by Sondheimer **(Sondheimer, 1950)** to include galvanomagnetic effects. Lucas **(Lucas, 1965)** generalized the

Fuchs calculations to the case of scattering from the two film surfaces with different parameters.

Among these theories, the Fuchs treatment for free electron model is simple and instructive. In the boundary conditions it was assumed that every free path is determined by collision at the surface so that distribution function of electrons leaving the surface must then be independent of direction and further the relaxation process for surface scattering is the same as for the bulk.

During the growth of film, discrete islands are formed on the substrate result in discontinuous film. In this case the scattering of conduction electrons become large for this growth **(Sondheimer, 1950)**. In fact, the film will be highly resistive and mobility will be very small in value **(Thomson, 1901)**. But due to increase of film thickness, it becomes continuous, as a result the resistivity of the film decreases and conductivity is increased. Therefore the mobility of the film is increased.

3.9 AGING EFFECT

The physical properties of thin films are naturally changed if it is exposed to open air for a considerable period of time, due to partial oxidation or contamination with moisture and dust particles present in the atmosphere. This phenomenon is known as aging effect and can be measured by measuring resistivity, electrical conductivity, sheet resistance, Hall coefficient and concentration etc. after regular interval of

time. In this present work the conductivity was measured with an interval of 48 hours for 10 days.

3.10 THERMAL E.M.F. AND THERMOELECTRIC POWER

If two contacts to a semiconductor are maintained at different temperatures, a potential difference is set up when no electric current flows. This is known as See back effect. The e.m.f produced in this way is known as thermal emf and the current flowing through these junctions is known as thermoelectric current, and the pair of metals is known as thermo-couple. This arises from the rapid diffusion of carriers heated at the hot junction. These carriers diffuse to the cold junction, so that such a contact acquires a potential having the same sign as the diffusing majority carriers.

If the temperature of the hot junction is increased further, the e.m.f increases with temperature up to certain maximum value and then decreases to zero as shown in figure-3.4.

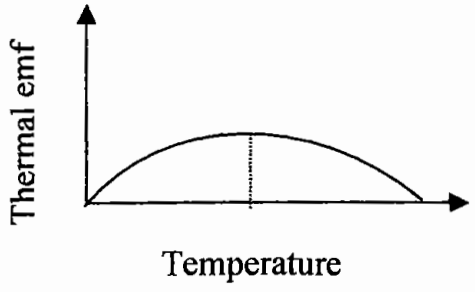

Fig : 3.4 Variation of thermoelectric e.m.f with temperature difference.

To explain the seeback effect, let us consider the figure 3.5.

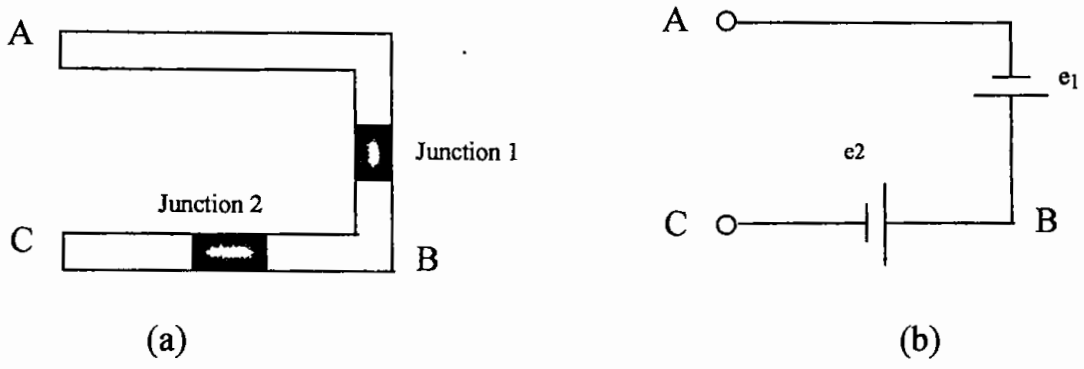

(a) (b)

Fig: 3.5 (a) Two junctions of metal A and B.
(b) Equivalent circuit.

When the temperatures of two junctions are equal then $e_1=e_2$ and net emf across AC is zero. If junction-1 is at higher temperature than that of the junction-2, then $e_1>e_2$ and (e_1-e_2) is positive and if junction-2 is at higher temperature than that of the junction-1 then (e_1-e_2) is negative.

Seeback arranged different metals in a particular order, which gives the thermoelectric power series as given below **(Vasudeva, 1984)**:

Sb	Fe	Cd	Zn	Ag	Au	Rb	Mo	Cr
Sn	Pb	Hg	Mn	Cu	Pt	Co	Ni	Bi

When any two metals of the above series are used with junctions at different temperatures a conventional current flows from the one earlier to the one latter in the series through the cold junction. Thermoelectric power may be defined as the e.m.f produced per unit temperature difference between junctions of two dissimilar metals. Mathematically,

Thermoelectric power,

$$Q = \frac{E}{(T_2 - T_1)} = \frac{E}{\Delta T} \text{ Volt/°K} \text{----------} (3.32)$$

3.11 OPTICAL PROPERTIES OF THIN FILMS

3.11.a ABSORPTION COEFFICENT

The optical behavior of a material is generally utilized to determine its optical constants, n and k. The absorption of radiation by any medium occurs through the excitation of electrons and phonons and the phonon-electron interactions. Then intensity of radiation is generally attenuated in an exponential form of the type exp (-kt), where k is the absorption coefficient and related to the imaginary part of k_o of the refractive index by $k = 4\pi k_0/\lambda$

The absorption coefficient of thin film can be measured by passing monochromatic light through the film under study and measuring the incident and transmitted beam intensity by a photosensitive detector. When a ray of monochromatic light incident perpendicularly to a flat section of the film, a portion of the incident light will be reflected and the remainder part will be transmitted into the film. The transmitted light can be absorbed by the film material.

In the fundamental absorption region the transmission T is given by

$$T = A\exp\left(\frac{-4\pi k_o t}{\lambda}\right) \text{----------} (3.33)$$

Where k_o is the extinction coefficient, t is the film thickness and λ is the wavelength of incident light. If $k_o << n$ then the principal variation of T

occurs in the exponential term and the pre-exponential term A which accounts for reflecting effect is close to unity. Therefore, from equation (3.33) we can write for absorption coefficient

Absorption coefficient,

$$K = \frac{\ln\left(\frac{1}{T}\right)}{t} \text{----------} \quad (3.34)$$

3.11.b OPTICAL BAND GAP DETERMINATION

The separation between conduction band and valence band on the energy level diagram is known as energy gap. The greater the energy gap, more tightly the valence electrons are bound to the nucleus . In order to push an electron from valence band to conduction band, (i.e. to make the valence electron free), external energy equal or greater to the forbidden energy gap must be supplied. In figure 3.6 show the band gap of semiconductor at 0°K. Generally, band gap is important in semiconductor crystal.

Mainly there are two types of band gap found in crystal are

a) Direct band gap

b) Indirect band gap

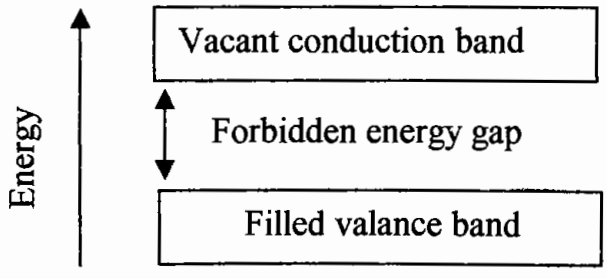

Fig: 3.6 Energy band gap of semiconductor at 0K

a) Direct band gap

If the maximum of valence band and the minimum of conduction band energy exist for the same value of wave vector p in a semiconductor, then the semiconductor is called the direct band gap semiconductor.

The form of the absorption process for a direct band gap semiconductor is shown in the energy momentum sketch of figure 3.7a.Because of the photon momentum is small compared to the crystal momentum, the latter essentially is conserved in the transition. The energy difference between the initial and final state is equal to the energy of the original photon:

$$E_\upsilon - E_i = h\nu \text{----------} (3.35)$$

As the photon energy hυ increases, so does the value of crystal momentum at which the transition occurs (figure 3.7a). A simple theoretical treatment gives the result

$$k(h\nu) = A^* (h\nu - E_g)^{1/2} \text{----------} (3.36)$$

where A* is a constant having the numerical value of $2x10^4$ when k is expressed in cm^{-1} and hυ and E_g are in electron volts (eV).

b) **Indirect band gap**

In the case of an indirect band gap semiconductor, the minimum energy in the conduction band gap and the maximum energy in the valence band occur at different values of crystal momentum (figure 3.7b). Photon energies much larger than the forbidden gap are required to give direct transitions of electrons from the valence to the conduction band.

As indicated in the energy momentum sketch of figure 3.7b, an electron can make a transition from the maximum energy in the valence band to the minimum energy in the conduction band in the presence of photons of suitable energy by the emission or absorption of a photon of the required momentum. Hence, the minimum photon energy required exciting an electron from the valence to conduction band is

$$h\nu=E_g-E_p \text{ ----------} (3.37)$$

Where E_p is the energy of an absorbed photon with the required momentum.

Since the indirect band gap absorption process required that an extra "particle" be involved, the probability of light being absorbed by this process is much less than in the direct band gap case. Hence, the absorption co-efficient is low and light can pass a reasonable distance into the semiconductor prior to absorption.

Since both phonon emission and absorption are possible for $h\nu>E_g+E_p$, the absorption co-efficient is then,

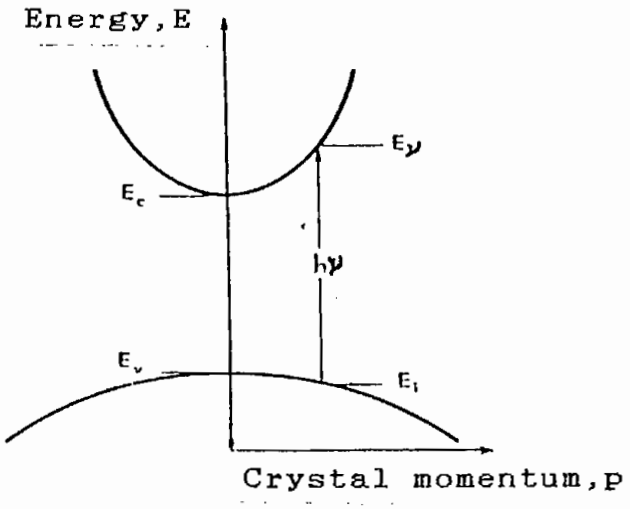

Fig: 3.7a Energy-crystal momentum diagram of a direct-band gap semiconductor, showing the absorption of a photon by the excitation of an electron from the valence to the conduction band.

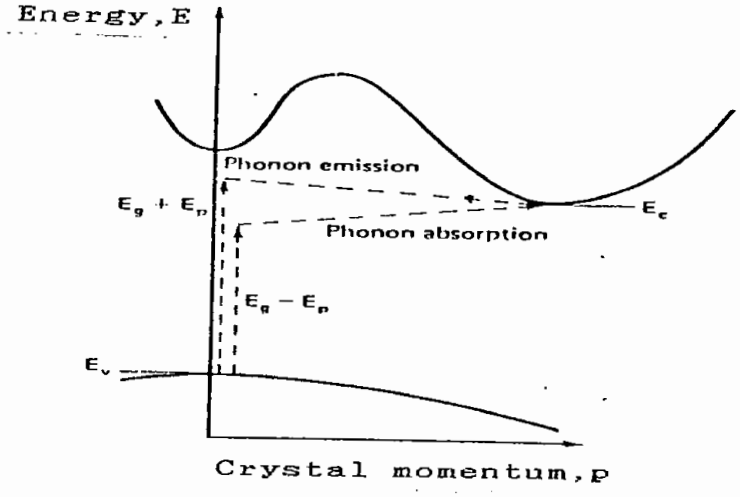

Fig:3.7b Energy-crystal momentum diagram of an indirect-band gap Semiconductor, showing the absorption of a photons by the two step processes involving phonon emission or absorption

$k(h\nu) = k_a(h\nu) + k_e(h\nu)$----------(3.38)

According to Bardeen et. al. the relationships that exit for possible transitions across the energy gap of a semiconductor show that the absorption co-efficient k is proportional to the following expressions for conditions given **(Barden et al., 1965)**

Direct transition:

$$\frac{(h\upsilon - Eg)^r}{h\upsilon}$$

where $r=\frac{1}{2}$ for allowed transitions and $r=\frac{3}{2}$ for forbidden transitions.

Indirect transition:

$$\frac{(h\nu - E_g \pm E_p)^r}{h\nu}$$

where r=2 for allowed transition and r=3 for forbidden transitions.

From all of the above expressions, it is clear that a plot of $(khv)^{1/r}$ versus hv for the various values of r would give the value of band gap E_g when carefully drawn for a particular transition process.

3.12 Selective surface

A selective surface is a surface whose radioactive characteristics vary with wavelength. Generally, optically selective surfaces can be classified into two categories:

1) The reflection absorption type (solar selective absorber) is applied directly to the absorber surface.
2) The reflection transmission type (transparent heat mirror) is applied to the cover plates of the converter system.

Figure 3.8(a) shows the solar radiation that falls on the earth surface, being passed through the atmosphere at the normal incidence, air mass 1 (AM1) **(Sayigh and Thekaera, 1977).** The spectrum of solar radiation AM2, AM3 etc., which falls on the earth surface at different angles, is qualitatively similar to AM1 but they are more attenuated because of their longer travel through the atmosphere. The solar radiation is very intense and is mainly located in the $0.3 < \lambda < 2.5$ μm wavelength range.

Figure 3.8(b) shows spectra for blackbody radiation at three different temperatures **(Touloukian and Dewitt, 1972).** The vertical scale shows the radiated power per area unit and wavelength interval and the horizontal scale shows the wavelength. The spectra indicate that at rising temperature the total amount of radiation increases and the peak wavelength moves towards shorter wavelength.

It is seen from figure 3.8(b) that for the shown temperatures the radiation is confined almost totally to the wavelength range $3 < \lambda < 100$ μm. Comparing figure 3.8(a) and 3.8(b), it is seen that for ambient

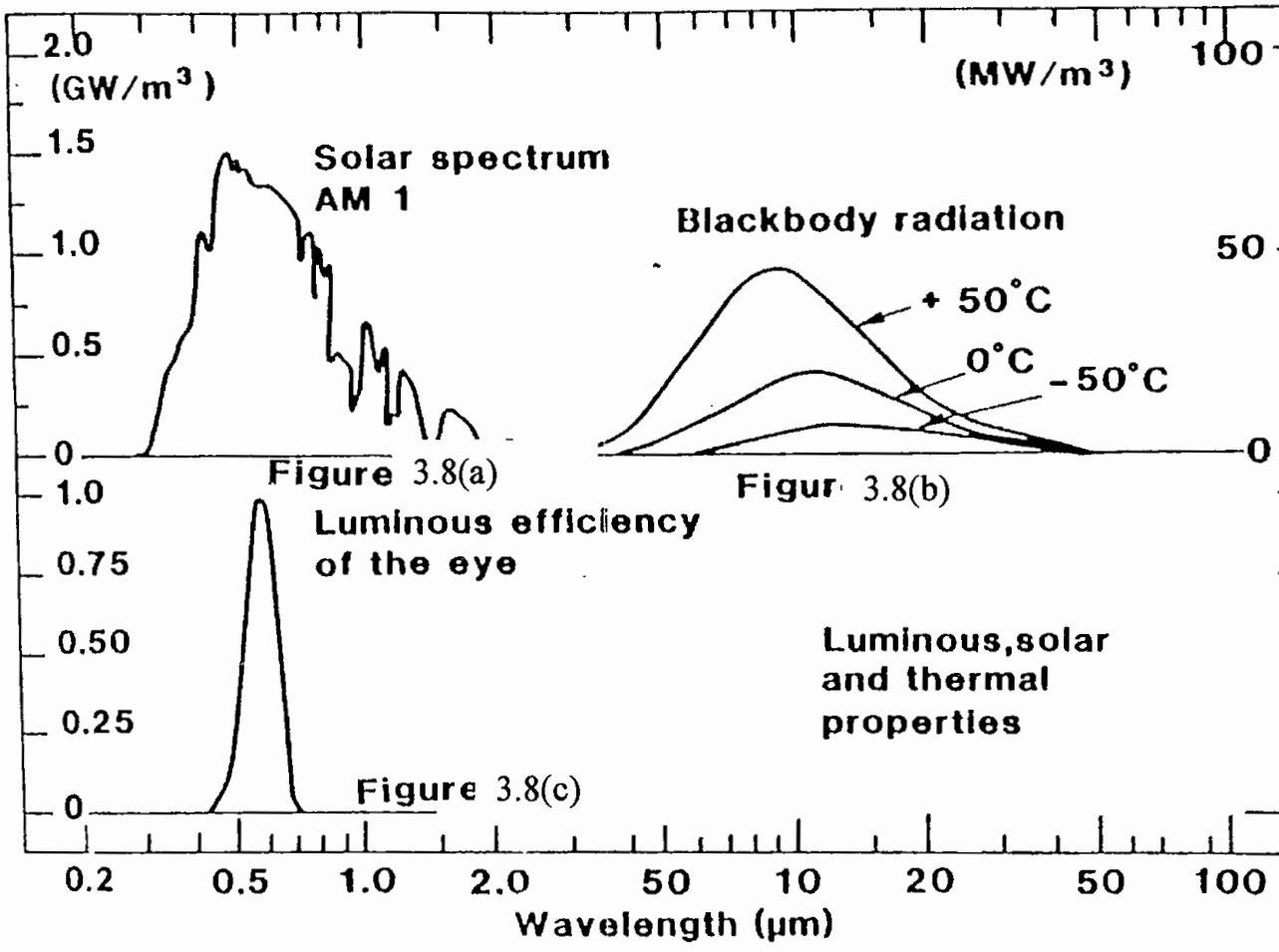

Fig: 3.8(a) ***Solar spectrum for radiation that passed through the atmosphere at normal incidence***

Fig: 3.8(b) ***Blackbody radiation from surfaces at three different temperatures***

Fig: 3.8(c) ***Luminous efficiency of the eye when adapted for day light.***

temperature there is practically no overlap between solar and blackbody spectra.

Figure 3.8(c) shows the spectral sensitivity of the human eye **(Driscoll et. al., 1978)**. The human eye is sensitive only in the $0.4 < \lambda < 0.7$ μm range. Hence only the shorter part of the solar spectra is observed as a visible light. **(Fan and Bachner,1976).**

CHAPTER FOUR

EXPERIMENTAL TECHNIQUES

EXPERIMENTAL TECHNIQUES

4.1 INTRODUCTION

For the preparation of vacuum evaporated MnO_2 thin films, the fundamental requirements are:

(i) Choose of proper substrate and its cleaning

(ii) Choose of support material which do not react with source material

(iii) Vacuum production and well-defined mask for particular measurement.

4.2 THE COATING PLANT

Thin film specimens for all the experimental investigations (e.g. electrical, optical and structural) were prepared by thermal evaporation of E-beam technique in the vacuum coating plant (Edwards, Model: E 306), as shown in figure 4.1. Basically the coating plant consists of three principle parts:

(1) The deposition chamber

(2) The pumping system and

(3) The electrical sources.

The deposition chamber is cylindrical and has a mechanically polished interior. The complete vacuum coating plant and the deposition chamber is shown in figure 4.2. A substrate holder was designed to hold a substrate and another circular stainless steel disc, positioned just under substrate holder had four metal mask fitted to it. The three masks used for the fabrication of sandwich devices. The substrate holder is approximately at a height 10 cm above the source. A mechanical shutter operated from outside, isolated the substances from the evaporate at desired times. A tungsten filament (W) is fitted concentrically with the hearth. The accessory is comprised of a six-hearth turret with rotary drive. The rotary drive hand wheel was turned to check for freedom of movement, such that turret rotated and when the hand wheel was rotated backwards the hearth raised concentrically. The source turret is rotated, raised and lowered by an externally controlled mechanism. The inner side of the chamber is shown in figure 4.3.

The deposition chamber is evacuated with oil diffusion pump, which is controlled by an automatic evacuation system.

The coating plant is provided with Edwards, EBS power supply unit (0-6KV) by using the high tension (3.5 kv) and low tension (100 mA). It is complete with HT voltage and emission current meters and variable transformers for control

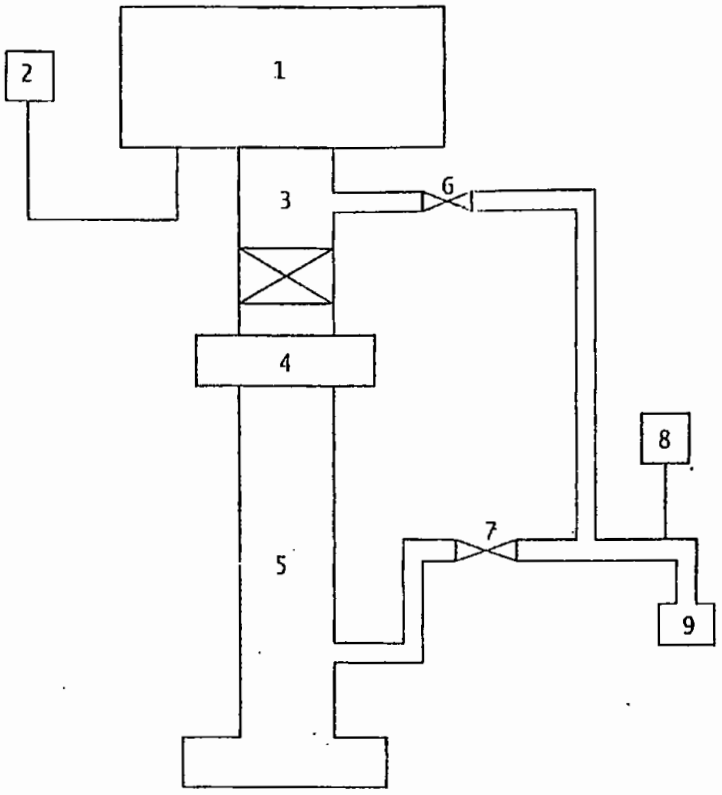

1. Vacuum Chamber 2.Ionization gauge 3. High Vacuum Isolation Valve
4. Liquid Nitrogen Trap 5. Diffusion Pump 6. Roughing Valve
7.Backing valve 8. Pirani Gauge 9. Rotary Pump

Fig: 4.1 Schematic diagram of vacuum chamber

Fig: 4.2 The Photograph of vacuum coating plant (Edward E-306) and the deposition chamber.

Fig: 4.3 The Photograph of the inner side of the chamber.

4.3 EVAPORATION SOURCES

The electron bombardment heating of an evaporation source was used in this investigation. The electron beam sources are used when evaporate reacts adversely with normal resistance heated source materials and also to evaporate materials which have a high melting point. The accessory companies a six-hearth turret with rotary drive and an electron beam gun mounted on battle plate. The assembly is normally mounted on the tripod accessory. Also supplied with the source are cerment hearths tungsten emitters and a 6D electrode.

The simple resistive heating of an evaporation source suffers from the disadvantages of possible contamination from the support material and the limitations of the input power, which make it difficult to evaporate high melting point materials. These draw backs may be over come by an efficient sources of heating by electron bombardment of the material (**Chopra, 1969**). The simplest electron bombardment arrangement consists of tungsten filament (W) to supply electrons with the help of Edwards EBS power supply unit as shown in figure 4.4, which are accelerated by applying a positive potential to the material for evaporation is shown in figure 4.5. The electrons loss their energy in the material very rapidly their range being determined by their energy and the atomic number of the material. Thus the surface of the material becomes a molten drop and evaporates.

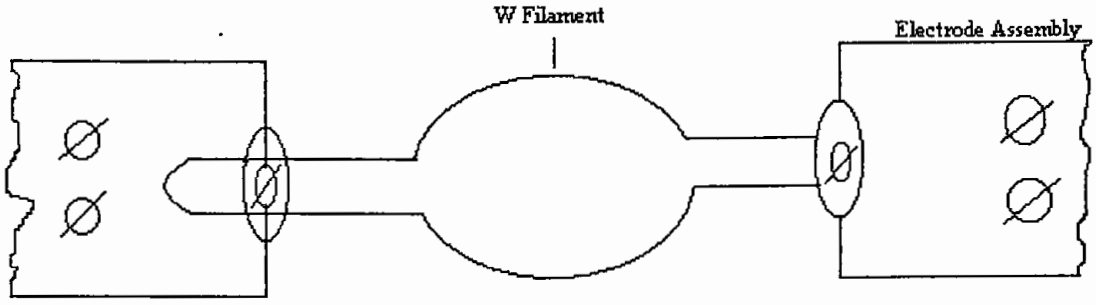

Fig: 4.4 A Filament with electron assembly

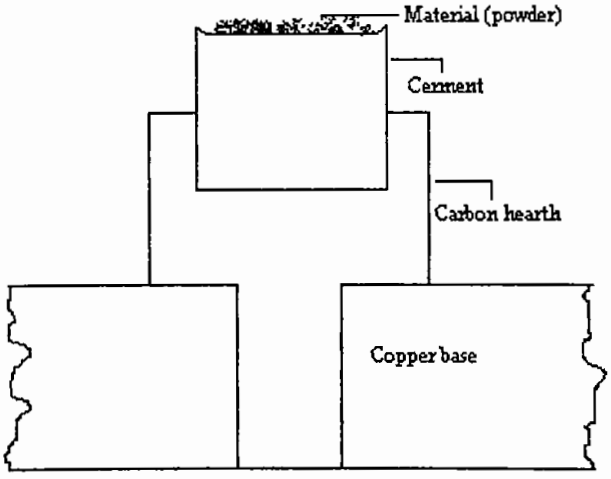

Fig 4.5 A cermet and a base plate(turret) position

4.4 CHOICE OF SUBTRATE AND ITS CLEANING

The choice of substrate is an important factor for thin film deposition. The demands made on the substrates of thin follow from their purpose the substrate serves as a mechanical support for the film and in electronic application, it usually serves as an insulator .The need for long term stability in thin film substrates makes it imperative that no chemical reactions occur which could change the chemical properties of the thin film. The substrate must therefore fulfill certain requirements as to mechanical strength and there must be adequate adhesion of the film to the substrate during large temperature changes. A high dielectric strength and the appropriate heat conductivity are necessary. The substrate surface should also be flat and smooth. In some applications even its weight may be an important factor.

It is general, possible to say that there is no material that would satisfy all requirements. The most widely used substrates for polycrystalline substrates for polycrystalline are glass, quartz and ceramics. Alkali halides, mica, Mgo, Si, Ge etc, are used as single crystal substrate for epitaxial growth. Organic material (e.g. Mylar or Teflon) is used for special cases. In the present work, glass substrates were used.

The properties of evaporated films generally depend on the cleaning of the substrate and hence they must be cleaned adequately deposition of films. There are various techniques of cleaning substrate and hence the choice of a particular technique on the nature of substrates, the nature of contaminants

and the degree of cleanliness required. In the present work substrate were cleaned as follows:

Initially the gross contaminations were removed by dipping the substrate in a solution of $k_2Cr_2O_2$ and H_2SO_4 for a few days.

Then the substrates were cleaned by distilled water and were dried by blowing hot air from hair drier.

The substrates were then rubbed with acetone to minimize surface contamination and dried in hot air.

Finally, the contamination problem was avoided by keeping substrates in dust free dissector, until these were used for deposition purpose.

4.5 PREPARATION OF MASKS

The direct deposition of thin film pattern requires a suitable shaped aperture, commonly referred to as a mask. This may be a metal, graphite or glass plate with the desired pattern cut or etched into it. The mask was placed in proximity to the substrate, thereby allowing condensation of the evaporate only in the exposed substrates areas. The masks were prepared in such a way that the edge of the mask was smooth so that it was helpful for determining the film thickness accurately. In order to study the various properties of the thin film, it is necessary that must be properly patterned. The methods commonly employed are (i) physical masking, (ii) photo resists and (iii) metal asking. Accurate replication of the mask pattern by the as-deposited film depends upon two conditions; first the mean free path of the evaporated

particles must be long compared with the mask to the substrate spacing to avoid random condensation caused by intermolecular collision. Secondly, the sticking coefficient of impinging vapour must be close to unity to prevent re-evaporation and lateral spreading under the masks. In the present work, thin aluminum sheet was used for the preparation of masks. First the sheet was cut in a required shape and size, and then the aperture was cur with the help of precision files. Different shapes were prepared for thickness measurement; resistivity, Hall effect measurement, thermoelectric power measurement and optical measurement and they were cut as shown in figure 4.6. Regardless of mask material and fabrication process all mask should be thoroughly cleaned and inspected before use.

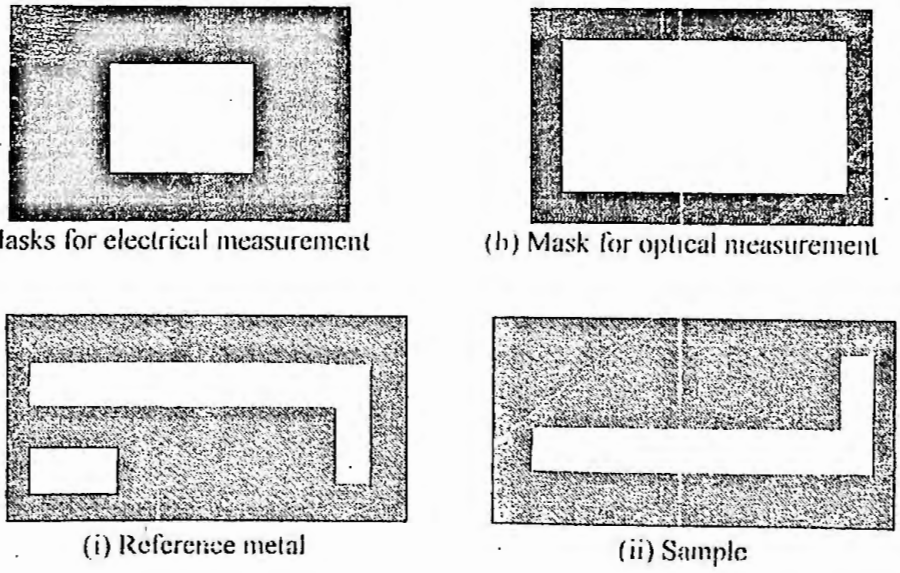

Fig: 4.6 Different types of masks.

4.6 FILM THICKNESS MEASUREMENT

Many of the electrical and optical properties of thin film depend on its thickness. Thus film thickness is one of the most significant film parameter hence care should be taken measure it. Thickness may be directly known by in-site monitoring the rate of deposition or it may be measurement technique may be broadly classified according to physical principles:

(a) Electrical method

(b) Mechanical method

(c) Gravimetric method

(d) Optical method

(e) Radiation-absorption and radiation-emission method.

Weiner was the first who use interference fringes to measure film thickness **(Weiner, 1887)**.Tolansky improved the interference fringes method to a degree of precision and are now accepted as the absolute standard method for film thickness measurement **(Tolansky, 1948)**.In the present work, a low power microscope, a monochromatic source, half silvered glass plates and an interferometer were required for the experimental set up. The Fizeau fringes of equal thickness were obtained in an optical apparatus of the type shown in fig: 4.7.The interferometer consists of two slightly inclined optical flats, one of them supporting the film, which forms a step on the substrate. When the second optical flat (a half silvered plate) was brought in contact with the film surface and the interferometer is illuminated with a parallel monochromatic sodium beam at normal incidence. A fringe system was produced which was viewed with

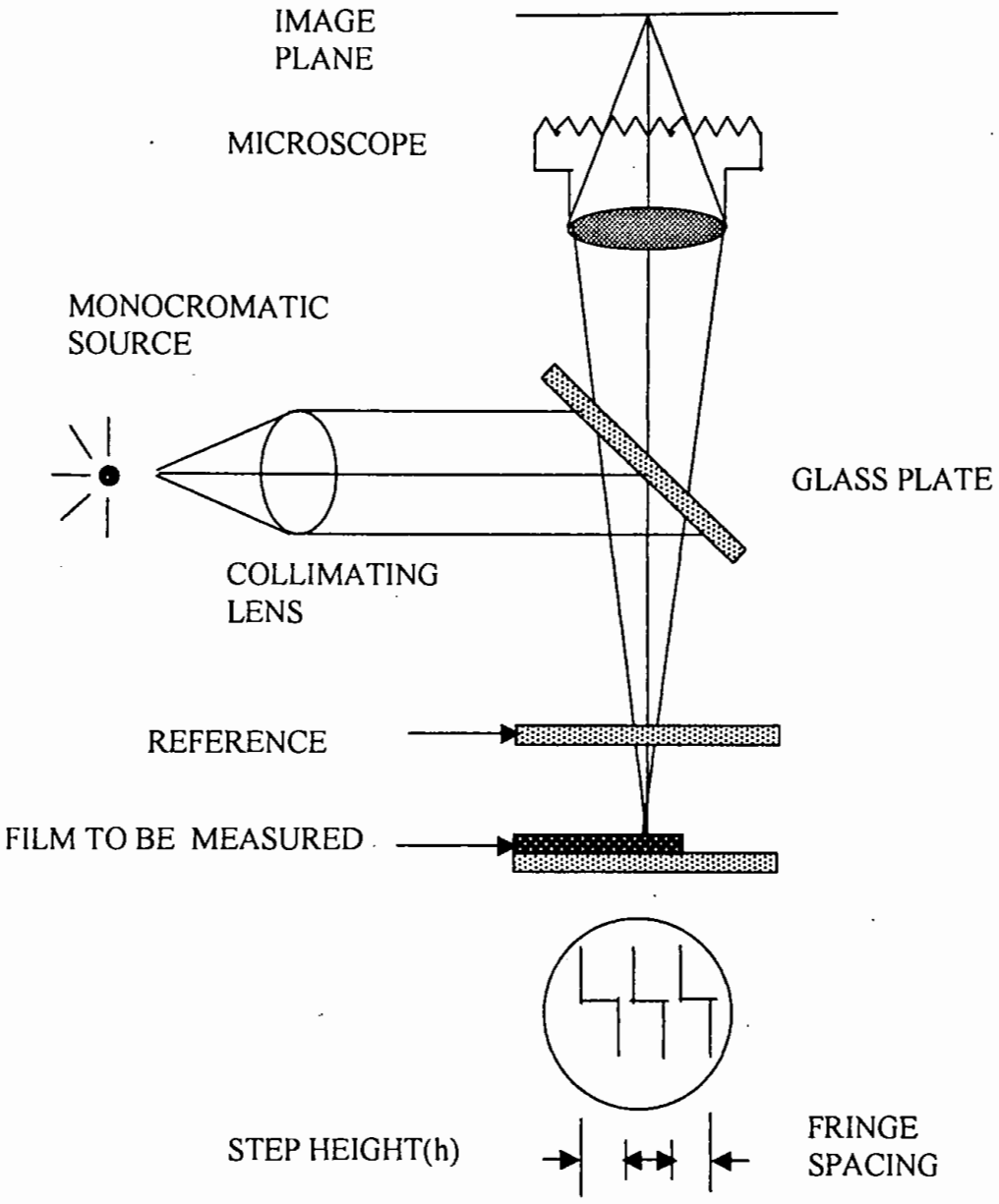

Fig 4.7 Interferometer arrangement for producing reflecting Fizeau fringes of equal thickness

a low power microscope on white background. The wedge shaped air gap was formed by adjusting the relative positions of the flat and it was possible to make fringes in straight lines perpendicular to the steps on the opaque film thickness can be spacing and step height.

Suppose two adjacent fringes are separated by λ/2, where λ is the wavelength of the monochromatic light source. The fringe system is abruptly displaced "h" as they pass over the film step edge and corresponding spacing is 'd'. Since for d spacing the step height is h and for λ /2 spacing, the corresponding step height is given the film thickness, so the thickness

$$t = \frac{h}{d} x \frac{l}{2} \quad \text{---} \quad \text{----} \quad \text{----(4.1)}$$

4.7 DETERMINATION OF STRUCTURE

Attempts were made to study the structure of the films by using x-ray diffraction. The XRD were done using a diffractometer, modelJDX-8P, made in JEOL, JAPAN. In this investigation MoKα radiation (λ-0.710688Å), voltage 30 kv, current 20 mA, scanning speed 2° was used within Bragg angle of 3° to 53° on as deposited samples.

4.8 LEAD ATTACHMENT WITH THE THIN FILMS

For studying electrical properties of thin film, lead attachment with the film is a very important factor.

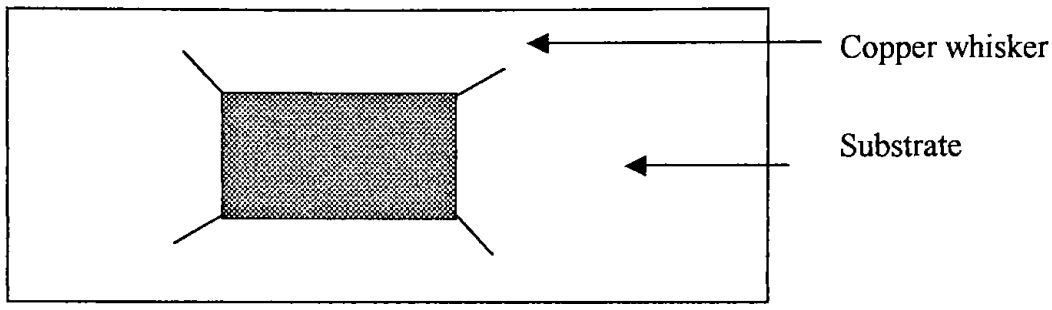

Fig-4.8 ***Diagram of film with lead attachment***

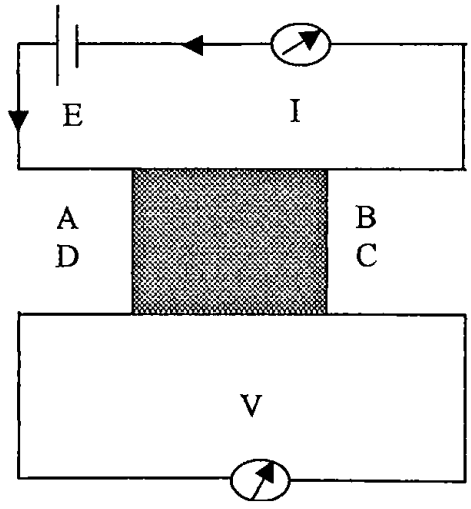

Fig: 4.9 ***Circuit arrangement to measure resistivity by using van-der pauw's method.***

In the present work silver paint (leading silver D 200) is used. One end of a fine copper wire is attached to the film by using a little amount of silver paint on it. By this way ohmic contact is made for this experiment.

4.9 RESISTIVITY AND CONDUCTIVITY MEASUREMENT

Electrical resistivity of thin film may be measured by different methods. In the present work, the resistivity of the films were measured by using Vander Pauw's method. The resistivity was calculated using equation (3.11) and conductivity was calculated using equation (3.12).

4.10 TEMPERATURE COEFFICIENT OF RESISTANCE, SHEET RESISTANCE, ACTIVATION ENERGY AND GRAIN SIZE MEASUREMENT

The measurement of T.C.R. in the present work accomplished by measuring the resistivity of individual film of different temperatures, from room temperature 373^0K.The specimen was heated by a mica insulating heating coil surrounded by an aluminum sheet .The specimen was attached to the aluminum sheet. The temperature on the surface of the aluminium sheet can be kept constant for a considerable period of time. Temperature of the film was varied by varying temperature of the heater, which was measured by the digital thermometer connected to a copper–constant thermocouple. The temperature coefficient of resistivity (T.C.R.) was calculated using equation (3.19). The sheet resistance was measured during resistivity measurement

using equation (3.14). The temperature dependence of sheet resistance was measured during T.C.R. measurement by varying temperature. The activation energy of the film was calculated from the slop of Lnσ versus 1/T curve based on the equation (3.22). The grain size of the corresponding film was calculated using equation (3.23).

4.11 HALL EFFECT MEASURENT

The van-der pauw's in 1958 specimen provided with four electrical contacts used for the measurement of Hall effect (1887). The electrical contacts were made by fine copper wire with silver paint. The specimen was then fixed with sample holder and connected to the electrical circuit as shown in figure 4.10. The total experimental setup is shown in figure 4.11.

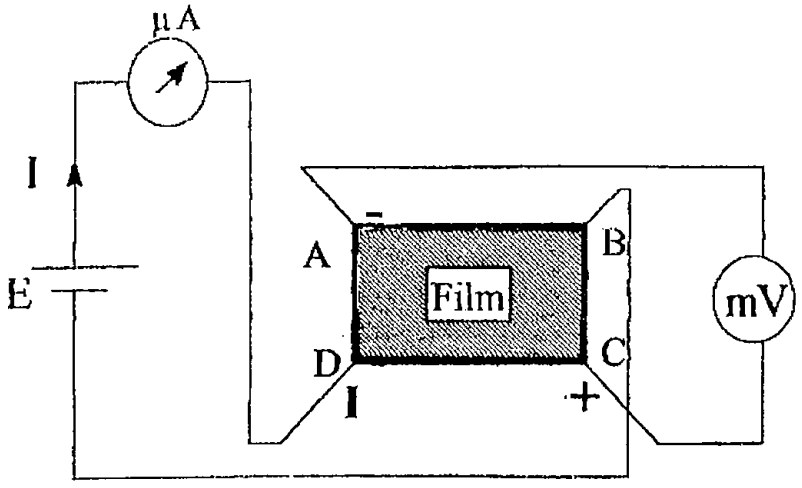

Fig: 4.10 Circuit diagram for Hall effect measurement.

The magnetic field used for the study of Hall effect was provided by an electromagnet designed and produced by Newport Instruments Ltd. England.

Hall effect was measured using conventional D.C. method as a power supply unit dry cell battery was used. With this power supply unit a potentiometer was connected in series to vary the sample current. Current and voltage were measured by a digital multi meter (model, DL-711) and digital electrometer (Keithley, 614) respectively.

A dc voltage from the power supply unit was applied between terminals D and B and the voltage developed between terminals A and C was measured with zero magnetic fields. The magnetic field was then applied perpendicularly to the surface of the film and again the potential difference between A and C was measured. The change in resistance $\Delta R_{BD,AC}$ was calculated by using the relation,

$$\Delta R_{BD,AC} = \frac{V_2 - V_1}{I_{BD}} \quad \text{---} \quad \text{---} \quad \text{---(4.2)}$$

Where V_1 is the voltage with zero magnetic fields, V_2 is the voltage with changing magnetic field and I is the sample current.

In the present work the magnetic field was varied between 4.75 to 7.22 KGS.

Hall coefficient, carrier concentration, Hall mobility were calculated from equations (3.28), (3.29), (3.30) respectively. The effective mass of the electron was assumed equal to rest i.e. $m^*=m$. The band gap measured from the slop of the graph (LnR_H vs. 1/T) and using the relation (3.31).

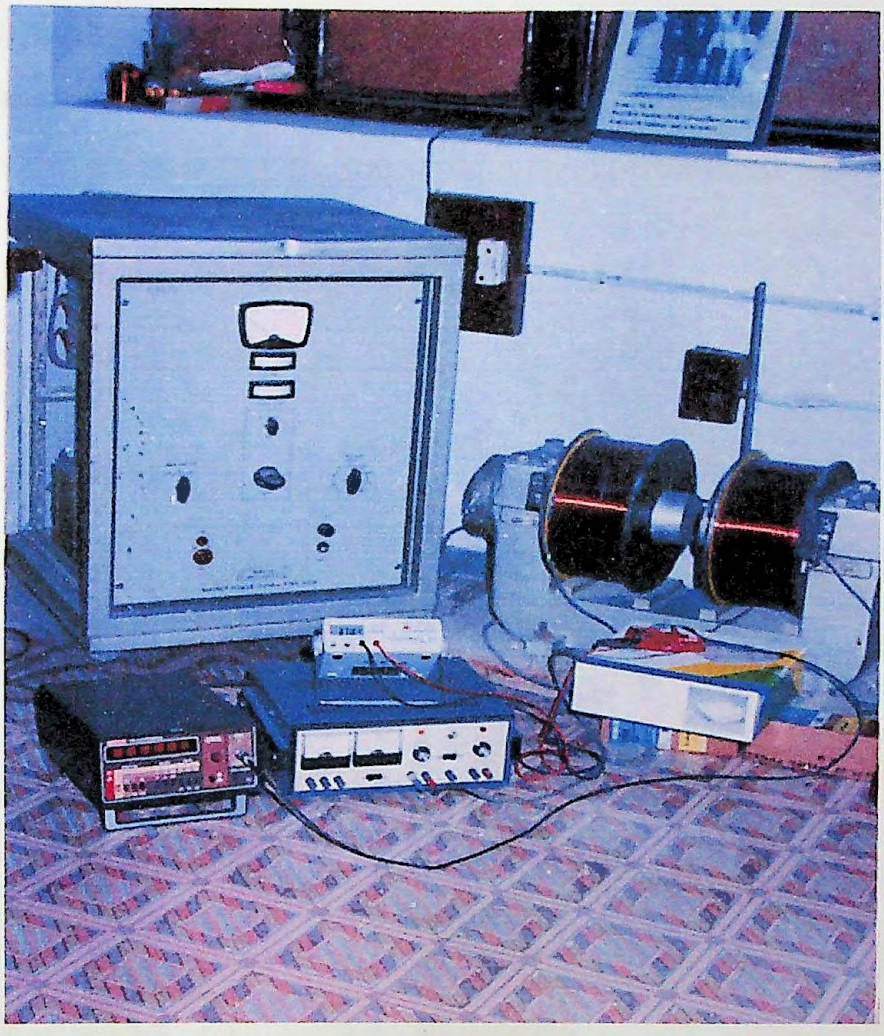

Fig: 4.11 Experimental set-up for Hall effect measurement

4.12 THERMOELECTRIC POWER MEASUREMENT

Figure 4.12 illustrate the experimental arrangement for the measurement of thermoelectric power of MnO_2 thin films. The figure also shows the mask and substrate geometry for the film and junction preparation

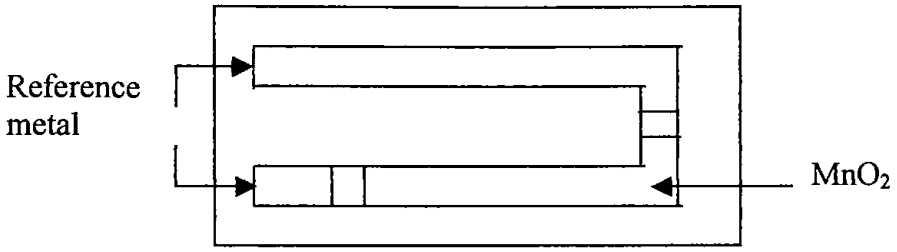

Fig: 4.12(a) The mask and substrate geometry for film

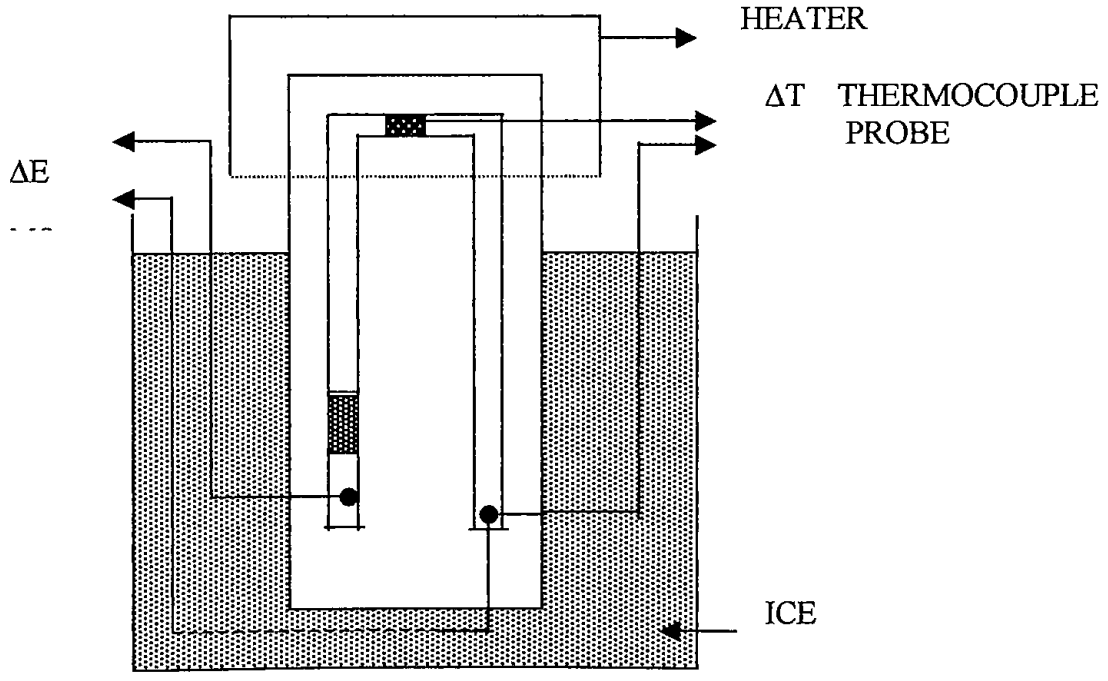

Fig: 4.12(b) Experimental arrangements for the thermoeletric power measurement

Cu. Ag and Pb were chosen as reference metal. The thermoelectric e.m.f. were measured forming junction of two different pair of different metals. But MnO_2 was common for all pair. The technique used for the specimen was held at a fixed temperature 273 ^{0}K (in ice) and other junction was heated to a temperature T was made to vary the range 303^{0}K to about 473^{0}K .The temperature of the sample was varied by special designed heater and was measured by a copper –constant thermocouple connected to a digital thermometer. The thermal e.m.f generated by the specimen was measured by digital electrometer (keithley, 614). Hot junction potential was always measured by connecting the negative probe to the electrometer the temperature dependence of the Seeback coefficient in thermoelectric power Q was calculated by using equation (3.32)

4.13 OPTICAL TRANSMITTANCE, REFLECTANCE AND ABSORPTION COEFFICIENT MEASUREMENTS

For optical measurement of MnO_2 thin films, a PERKIN ELMER LAMBDA-19 spectrometer was used as shown in figure 4.13. The Lambda 19 Spectrophotometer features an all-reflecting, double-monochromatic optical system. The optical components are coated with silica for durability. Halogenographic gratings are used in each monochromatic for the ultraviolet/visible/near infrared (UV/VIS/NIR) range.

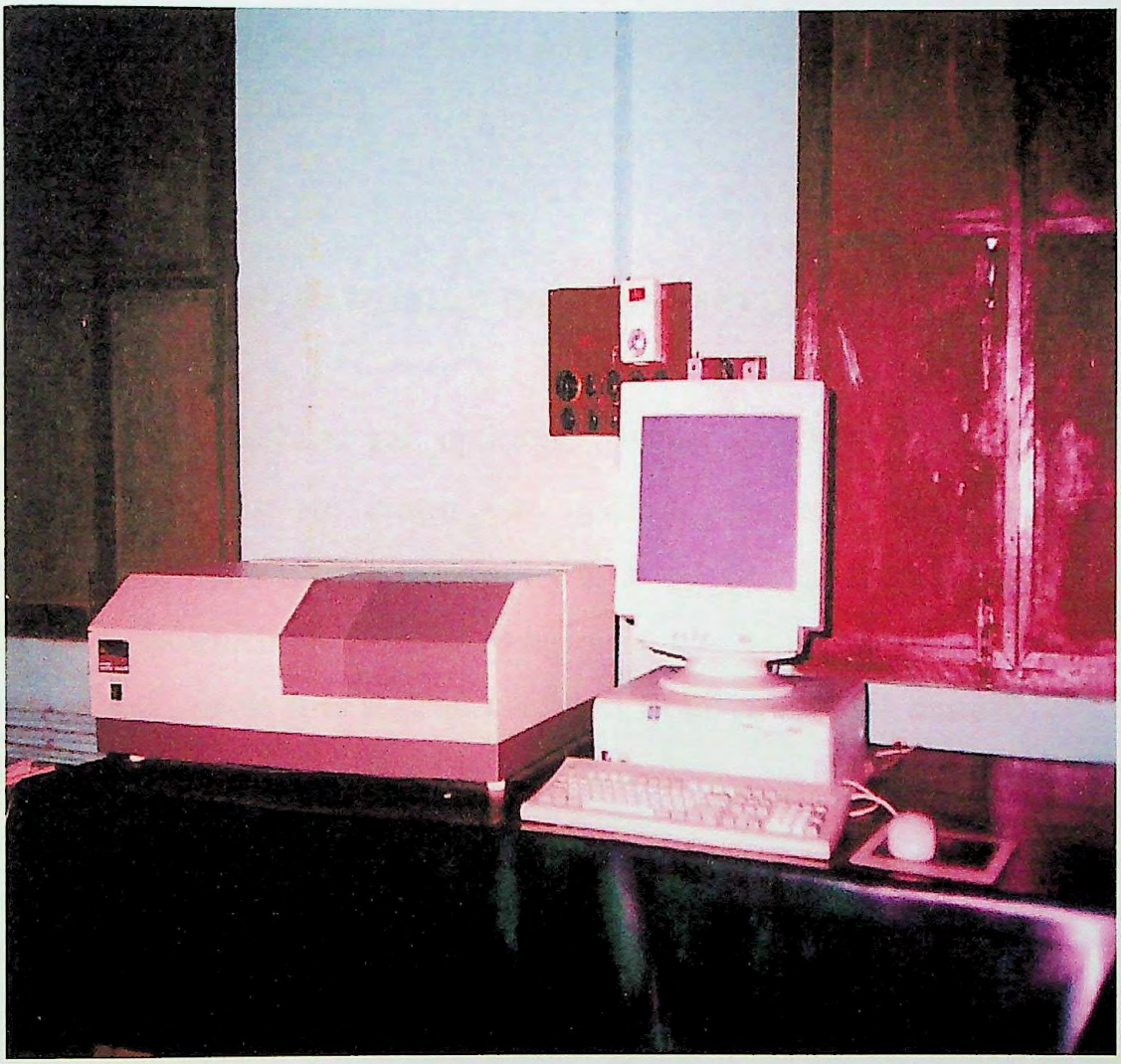

Fig: 4.13 A photograph of PERKIN ELMER LAMBDA-19 Spectrophotometer

The transmittance and reflectance were measured at normal incidence for the $300< \lambda<2500$ nm range with reflectance to glass using an integrating sphere detecting system. Knowing the film thickness and transmittance at the corresponding wavelength, one can determine absorption coefficient by using the equation (3.35).

4.14 OPTICAL BAND GAP DETERMINATION

To determine the band gap optically, the plot of $(kh\nu)^{1/2}$ versus $h\nu$ and $(kh\nu)^2$ versus $h\nu$ are drawn for indirect allowed and direct allowed transitions. The value of the band gap is determined from the tangent of these curves which intersect the energy axis.

From these curves it is seen that indirect fit gives the best linearity and the band gap is determined from this intercepts.

CHAPTER FIVE

EXPERIMENTAL RESULTS

EXPERIMENTAL RESULTS

5.1 EFFECT OF DEPOSITION PARAMETERS ON FILM THICKNESS

The variation of film thickness with deposition time is shown in figure.5.1. From the nature of the graph, it is evident that film thickness increases almost linearly with the increase of deposition time.

The variation of deposition rate with deposition time at constant source to substrate distance and ambient pressure is shown in figure.5.2. From the nature of the graph, it is seen that deposition rate remains almost constant with the increase of deposition time.

The effect of source to substrate distance on film thickness was studied by depositing MnO_2 films of variable source to substrate distance. The result is illustrated in figure.5.3. The graph shows that the film thickness decreases with the increase of source to substrate distance.

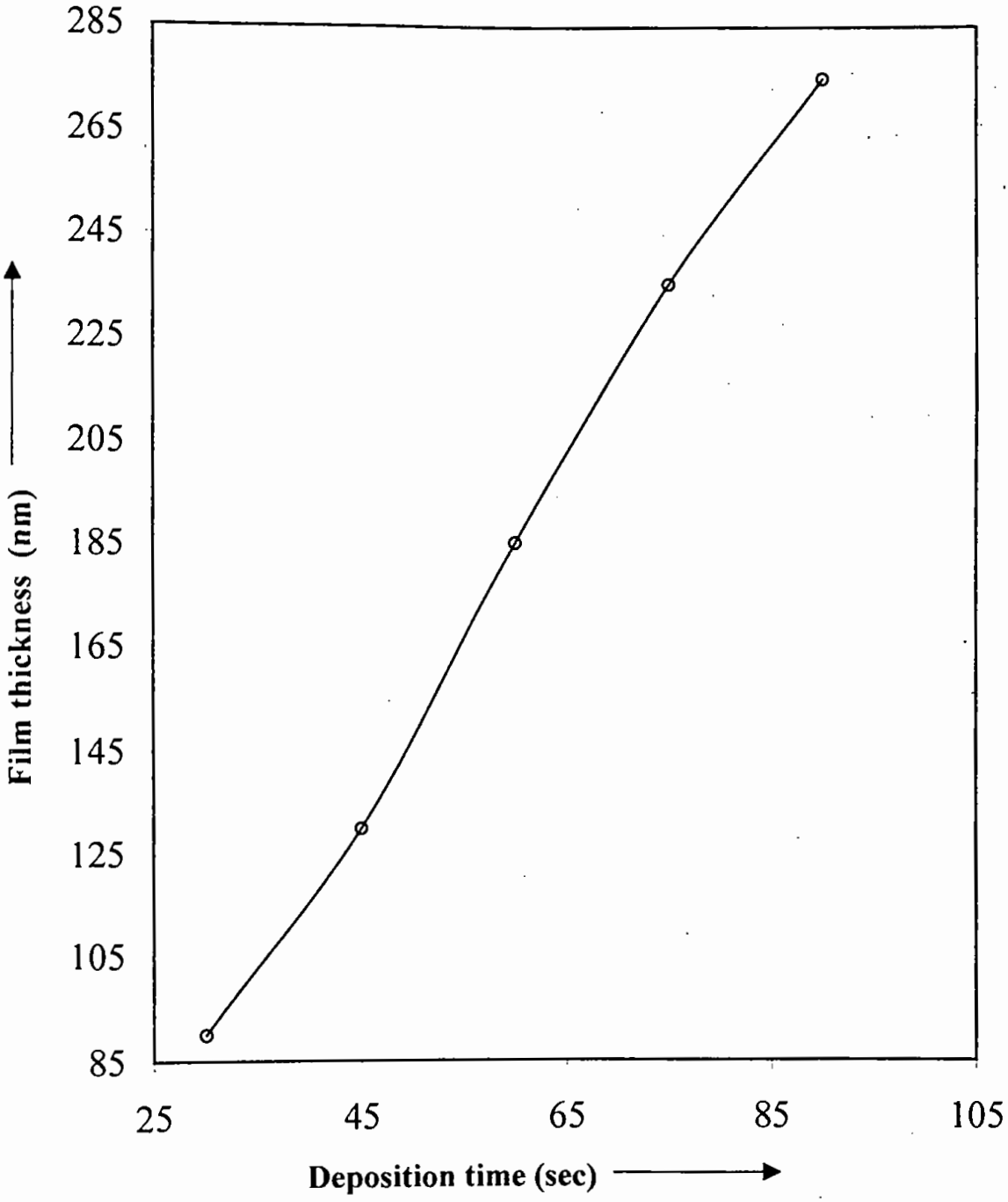

Fig: 5.1 Variation of film thickness with deposition time

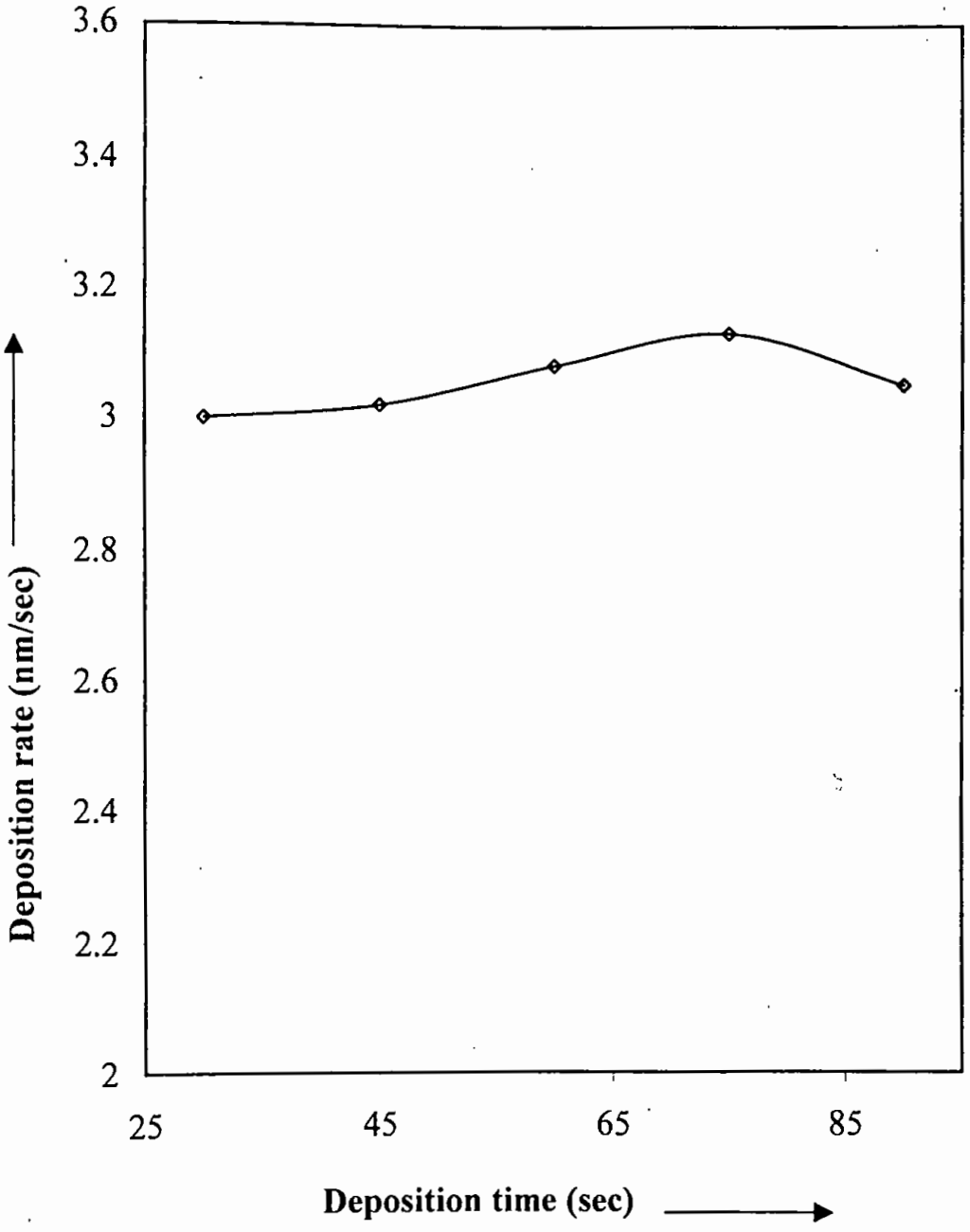

Fig: 5.2 Variation of diposition rate with deposition time

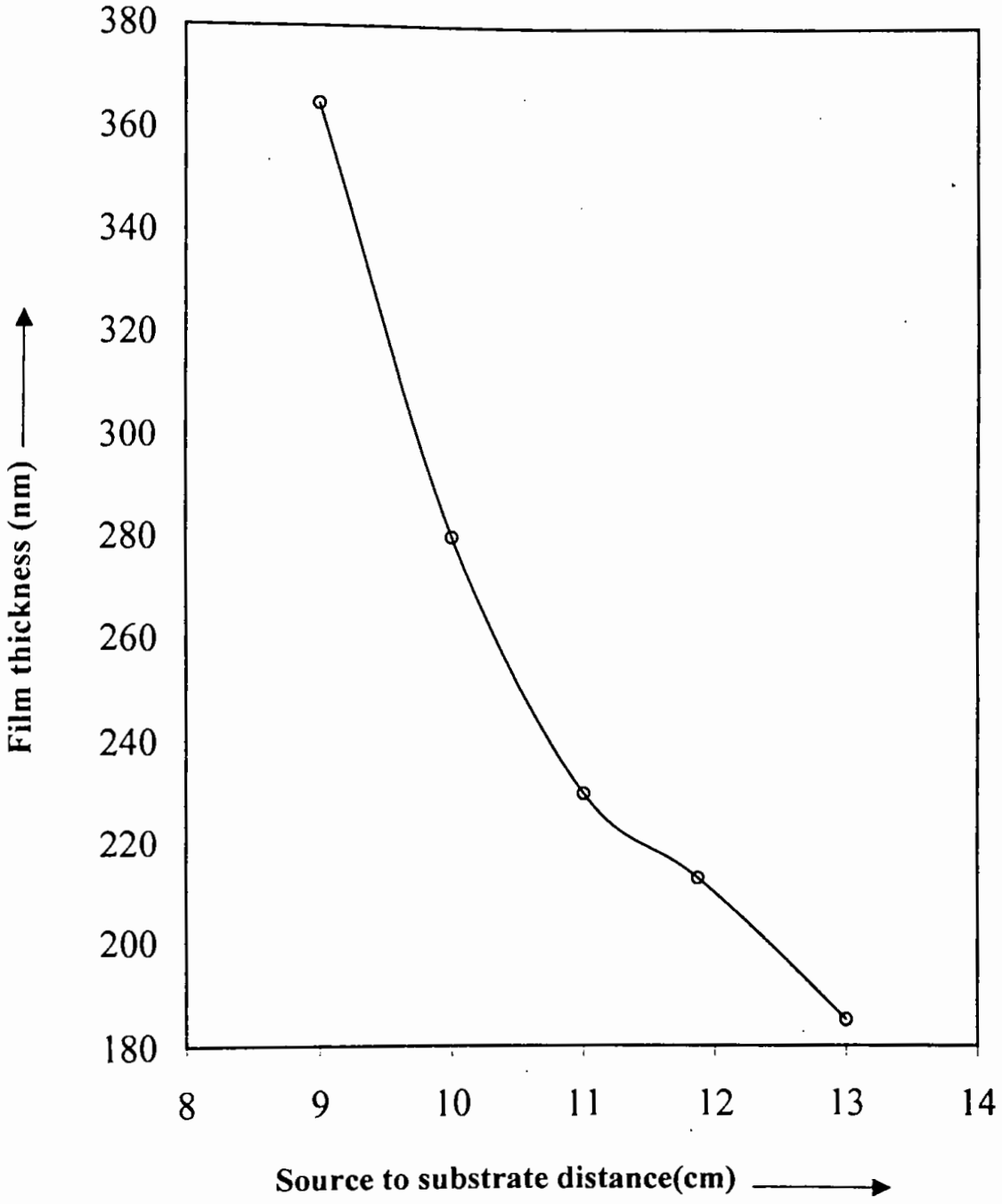

Fig: 5.3 Variation of film thickness with source to substrate distance at constant ambient pressure and deposition time

5.2 STRUCTURAL PROPERTIES

Figure 5.4 and 5.5 show the X-ray diffraction spectra of the MnO_2 films of thickness 120nm and 200nm, respectively. No distinct peaks are observed from these spectra which hints that the films are amorphous in nature.

5.3 TEMPERATURE DEPENDENCE OF ELECTRICAL CONDUCTIVITY OF SAMPLES PREPARED AT $2x10^{-5}$ TORR

Electrical conductivity is measured as a function of temperature from 303 to 403K. Figure 5.6 shows the plot of conductivity versus temperature curves for four samples of MnO_2 of thickness 80 nm, 120 nm, 180 nm, 220 nm, respectively. It is observed that the conductivity decreases with increasing temperature, which indicates metallic behavior. It is however, interesting to point out that this behavior is not linear over the entire range of temperature. From figure 5.6, it shows that there is an anomaly in conductivity in the conductivity versus temperature curve at a particular temperature near 323K. At this particular temperature of 323K the material shows an anomaly in conductivity which is well agreed with reports of previous workers. **(Bhide, 1960)**.

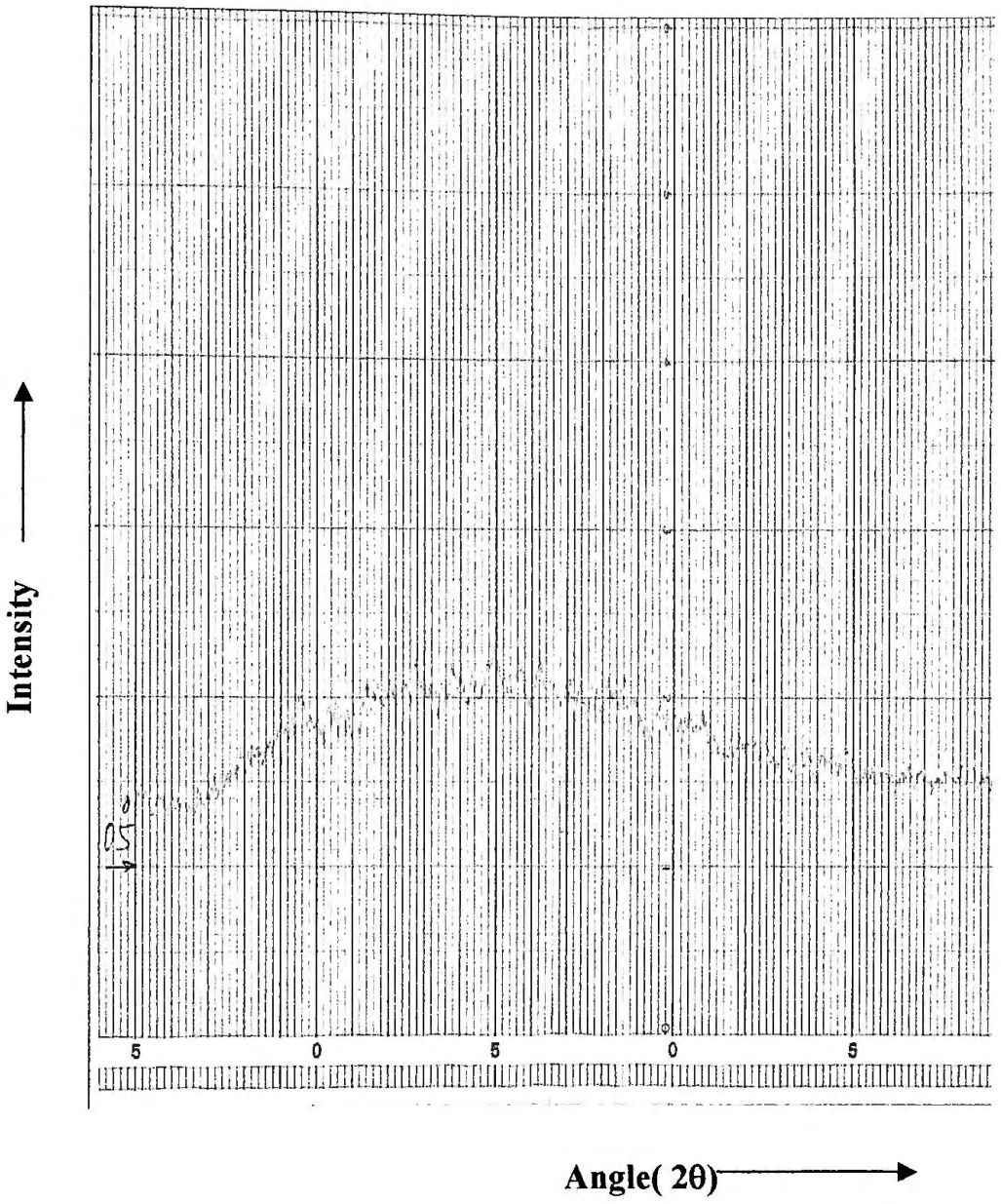

Fig: 5.4 XRD pattern for e-beam deposited MnO_2 thin film of thickness 120 nm.

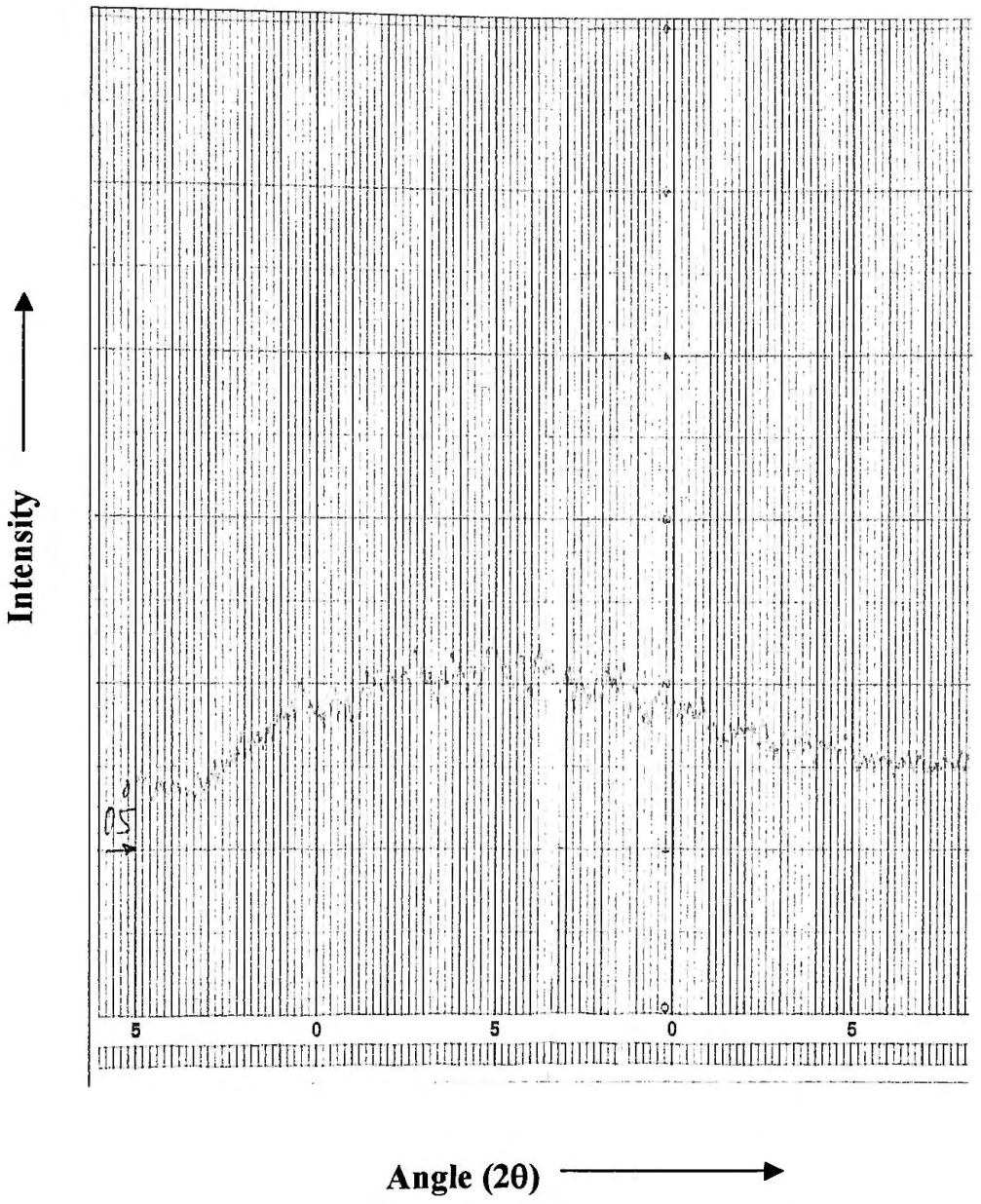

Fig : 5.5 XRD pattern for e-beam deposited MnO_2 thin film of thickness 200 nm.

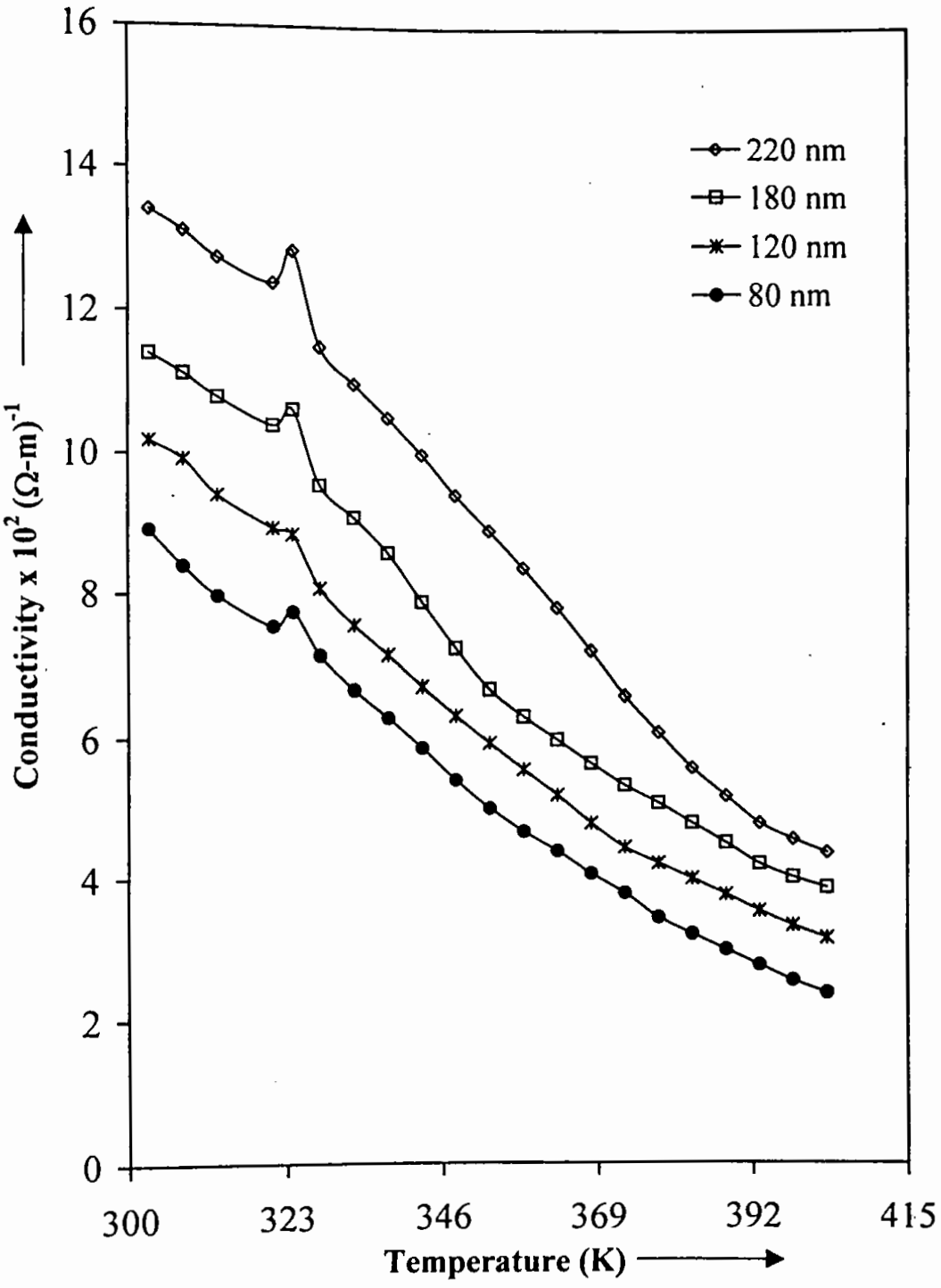

Fig:5.6 Variation of conductivity with temperature prepared at $2x10^{-5}$ torr.

5.4 ELECTRICAL PROPERTIES OF MnO_2 THIN FILMS PREPARED AT $6.0x10^{-6}$ torr

5.4.a ELECTRICAL CONDUCTIVITY

Electrical conductivity is measured as a function of temperature from 303 to 403K. Figure 5.7 shows the plots of conductivity versus temperature for four samples of MnO_2 of thickness 55 nm, 110 nm, 187 nm, 250 nm, respectively. It is seen that the conductivity increases with increasing temperature which indicates semiconducting behavior. It is however, interesting to point out that this behavior is not linear over the entire range of temperature. From figure 5.7, it shows that there is an anomaly in conductivity in the conductivity versus temperature curve at a particular temperature near 323K. It is note that the similar anomaly in conductivity also observed in the samples investigated in figure 5.6

The $Ln\sigma$ versus 1/T plots of figure 5.7 is shown in figure 5.8. The straight lines for the films of different thickness are drawn by using least mean square fitting method. From the slope of the straight lines, the activation energy has been calculated for the films of different thickness at the temperature below and above the anomaly temperature. Activation energy below and above the anomaly temperature is shown in figure 5.9. From the figure 5.9, it is seen that the activation energy for the four samples is fairly low and is of the order of 0.1 to 0.4 eV. Below the anomaly temperature the activation energy increases with increasing film

thickness. Above the anomaly temperature the activation energy decreases proportionally.

Film thickness t(nm)	Activation energy below the anomaly, ΔE (eV)	Activation energy above the anomaly, ΔE (eV)
55	0.181	0.162
110	0.332	0.151
187	0.381	0.141
250	0.400	0.119

5.4. b VARIATION OF SHEET RESISTANCE

Figure 5.10 shows the plots of sheet resistance with temperature for four samples of MnO_2 of thickness 55nm, 110nm, 187nm, 250nm, respectively. It is seen that the sheet resistance of all film decreases linearly with increasing temperature.

5.4.c VARIATION OF TEMPERATURE COEFFICIENT OF RESISTANCE (T.C.R.) WITH TEMPERATURE.

Figure 5.11 shows the temperature dependence of T.C.R. curves for eight samples of different thickness. Among the eight, four of the samples of thickness 80 nm, 120 nm, 180 nm, 220 nm, respectively are prepared at $2x10^{-5}$ torr, and the other four of thickness 55 nm, 110 nm, 187 nm, 250 nm, respectively are prepared at $6x10^{-6}$ torr. It is important to note from the graph that the films deposited at $2x10^{-5}$ torr show a positive T.C.R. which indicating metallic characteristics, whereas a negative T.C.R. indicating semiconducting behavior on all films prepared at $6x10^{-6}$ torr.

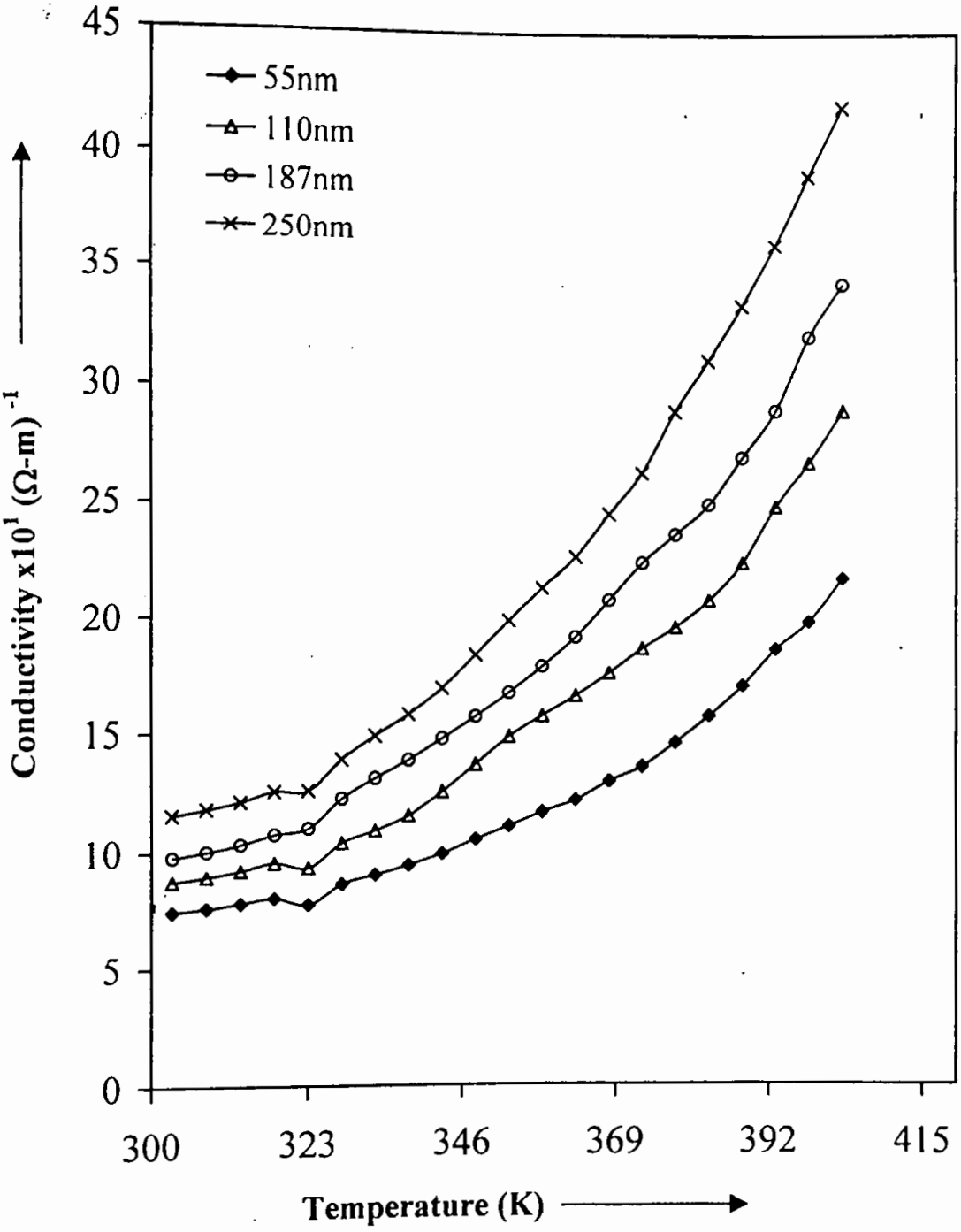

Fig : 5.7 Variation of conductivity with temperature prepared at 6x10^{-6} torr

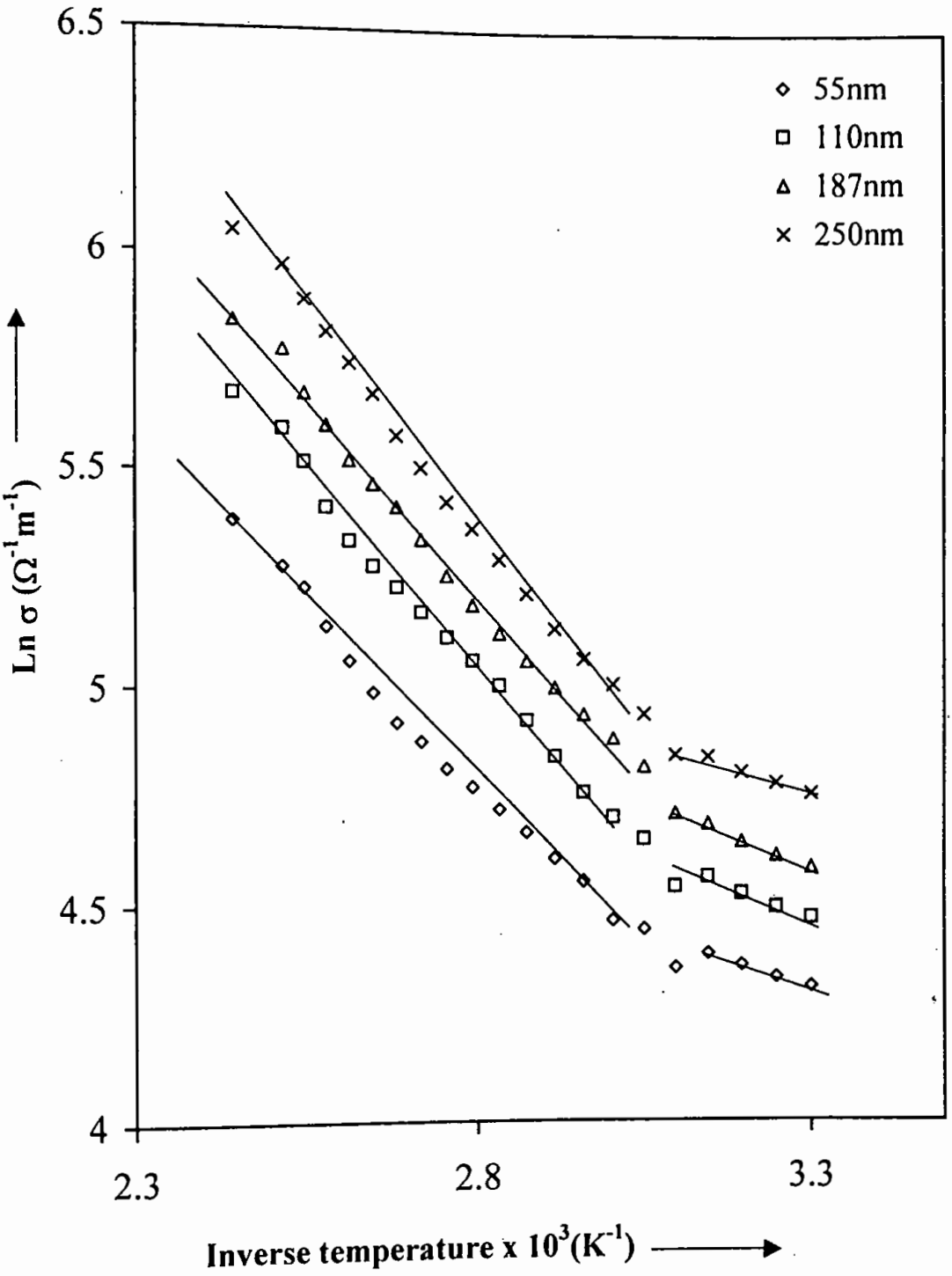

Fig : 5.8 Variation of Ln σ with inverse temperature

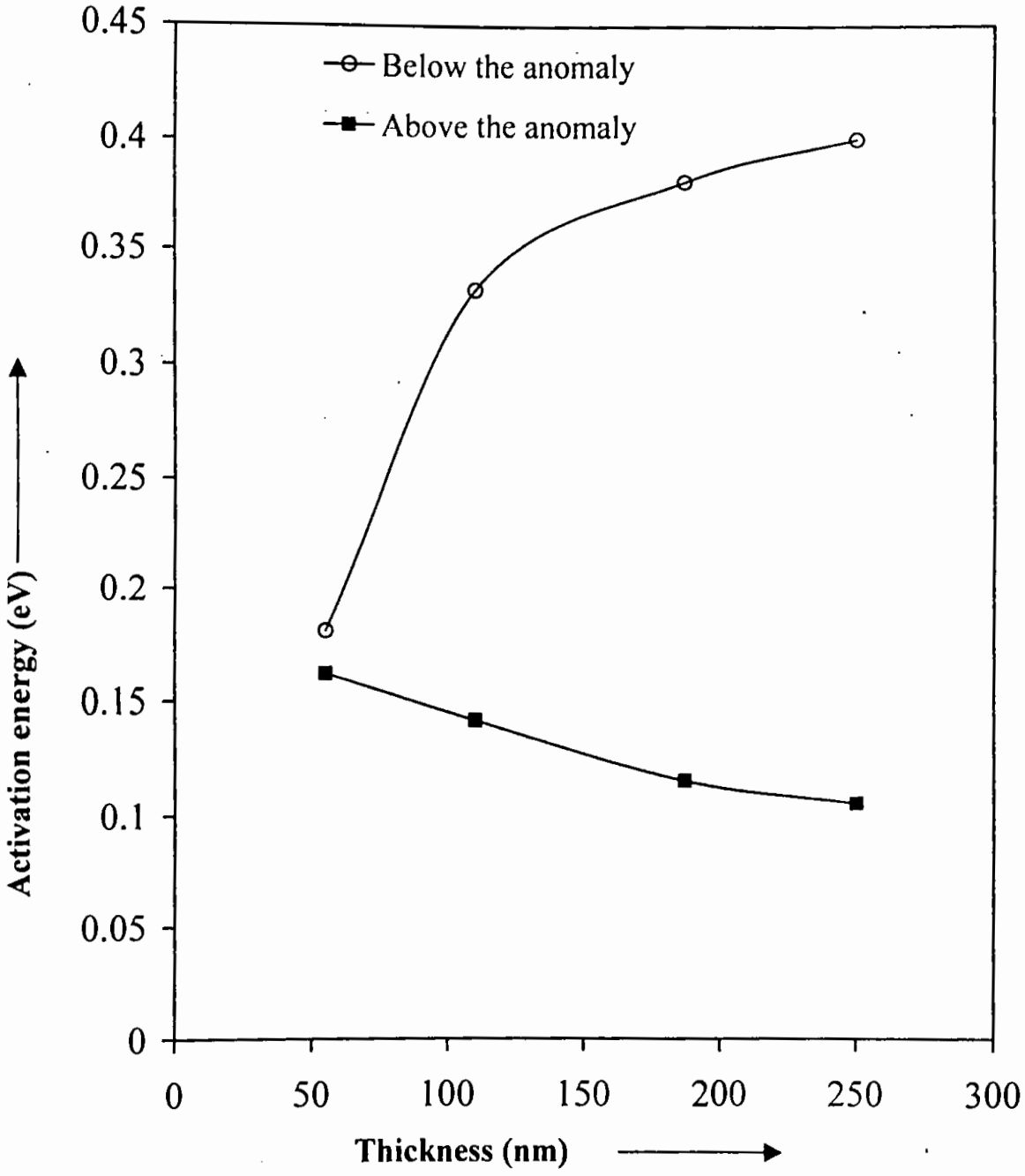

Fig: 5.9 Variation of activation energy with film thickness

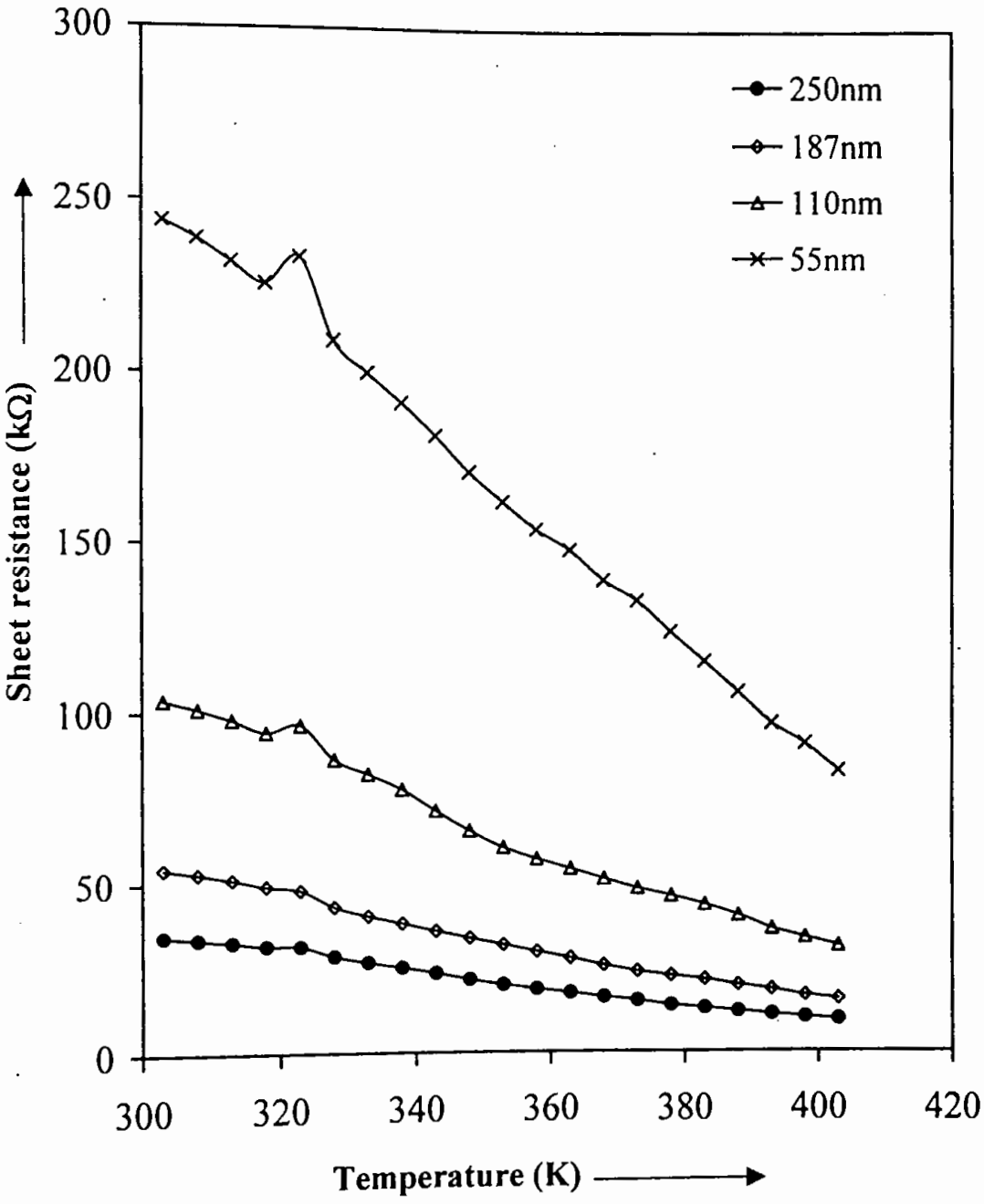

Fig : 5.10 Variation of Sheet resistance with temperature .

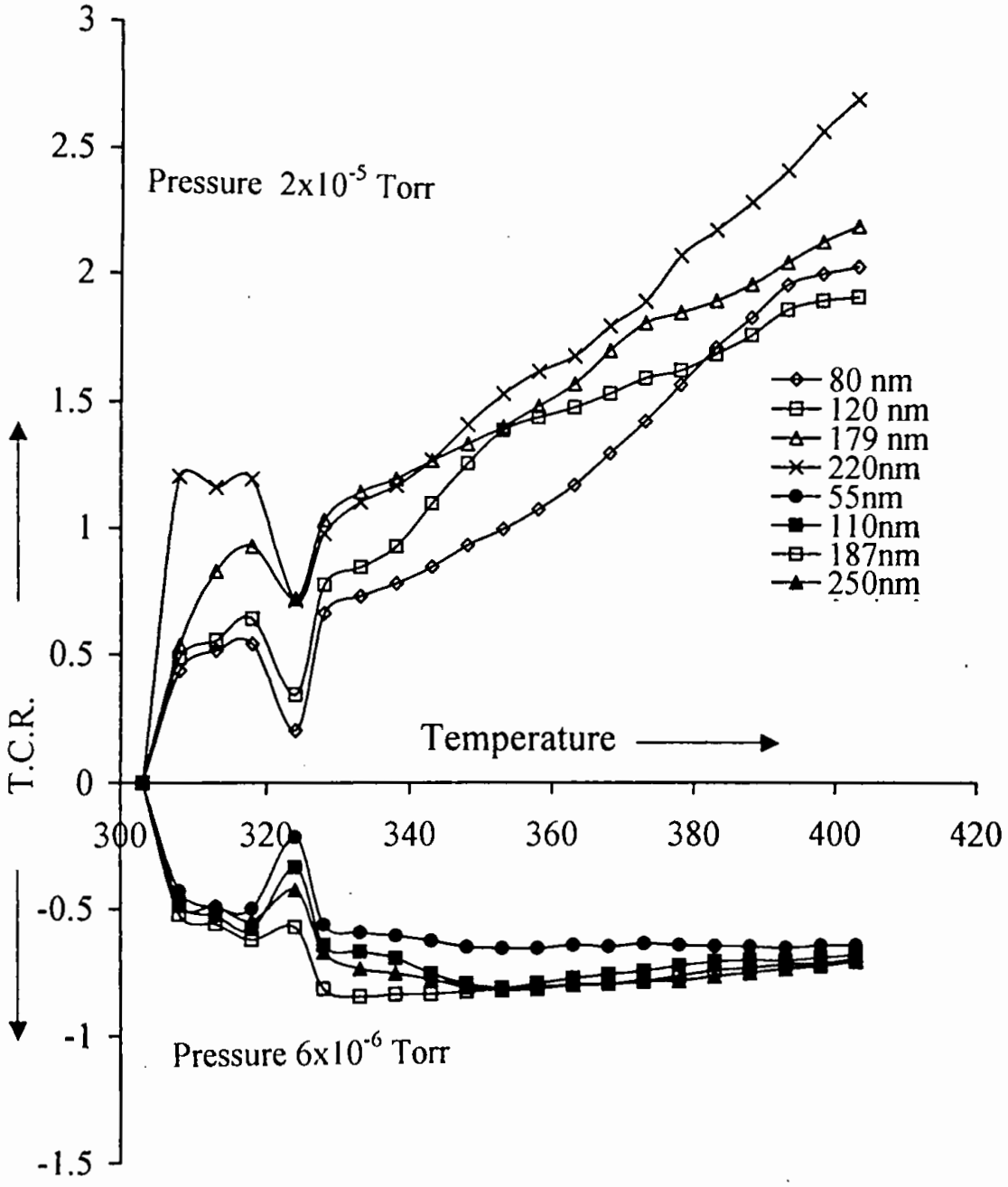

Fig:5.11 Variation of Temperature coefficient of resistance with temperature.

5.4.d VARIATION OF ELECTRICAL CONDUCTIVITY WITH FILM THICKNESS (SIZE EFFECT)

Electrical conductivity of the films for the thickness ranging from 55 nm to 300 nm has been investigated. Variation of electrical conductivity with thickness is shown in figure 5.12.

It is observed that the conductivity increases with thickness up to 200 nm range but above this range the films show the thickness independent behaviors.

5.4.e ANNEALING EFFECT ON MnO_2 THIN FILMS

To investigate the annealing effect, the films were annealed in open air for two hours at a constant temperature 523 K. Then the films were rapidly cooled in open air. Figure 5.13 shows the variation of conductivity versus temperature for both the as-deposited and annealed films. It is observed from the graph that the electrical conductivity of the annealed film is high than that of the as-deposited film and no anomaly is found in the annealed film.

5.4.f VARIATION OF ELECTRICAL CONDUCTIVITY WITH TIME (AGING EFFECT)

For aging effect study, the variation of conductivity with time for three samples of MnO_2 of thickness 250nm, 187nm, 110nm, respectively are shown in figure 5.14. It is observed that in all films, the electrical conductivity decreases with time and the conductivity decreases in thin film more rapidly than the thicker one.

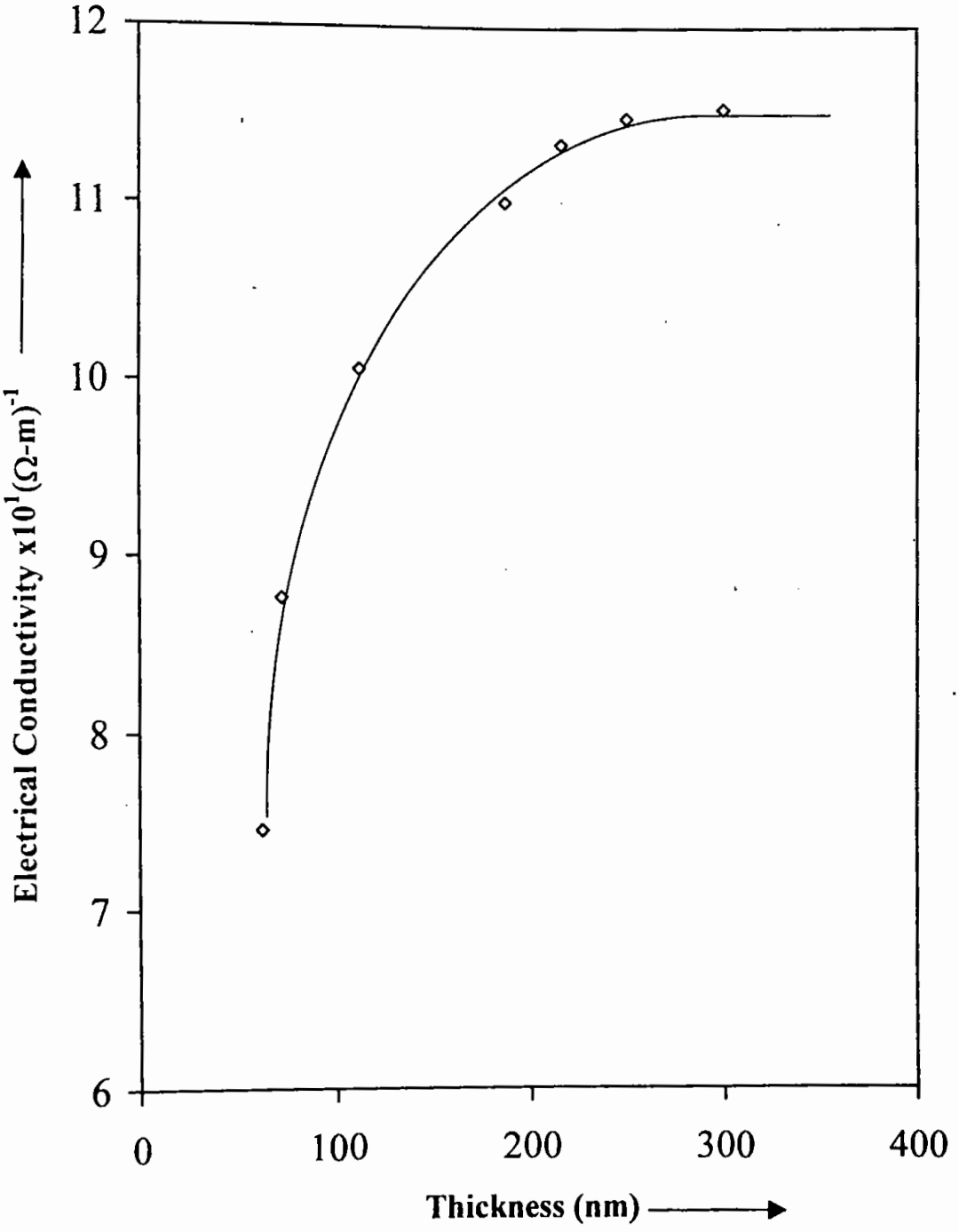

Fig: 5.12 Variation of electrical conductivity with thickness .

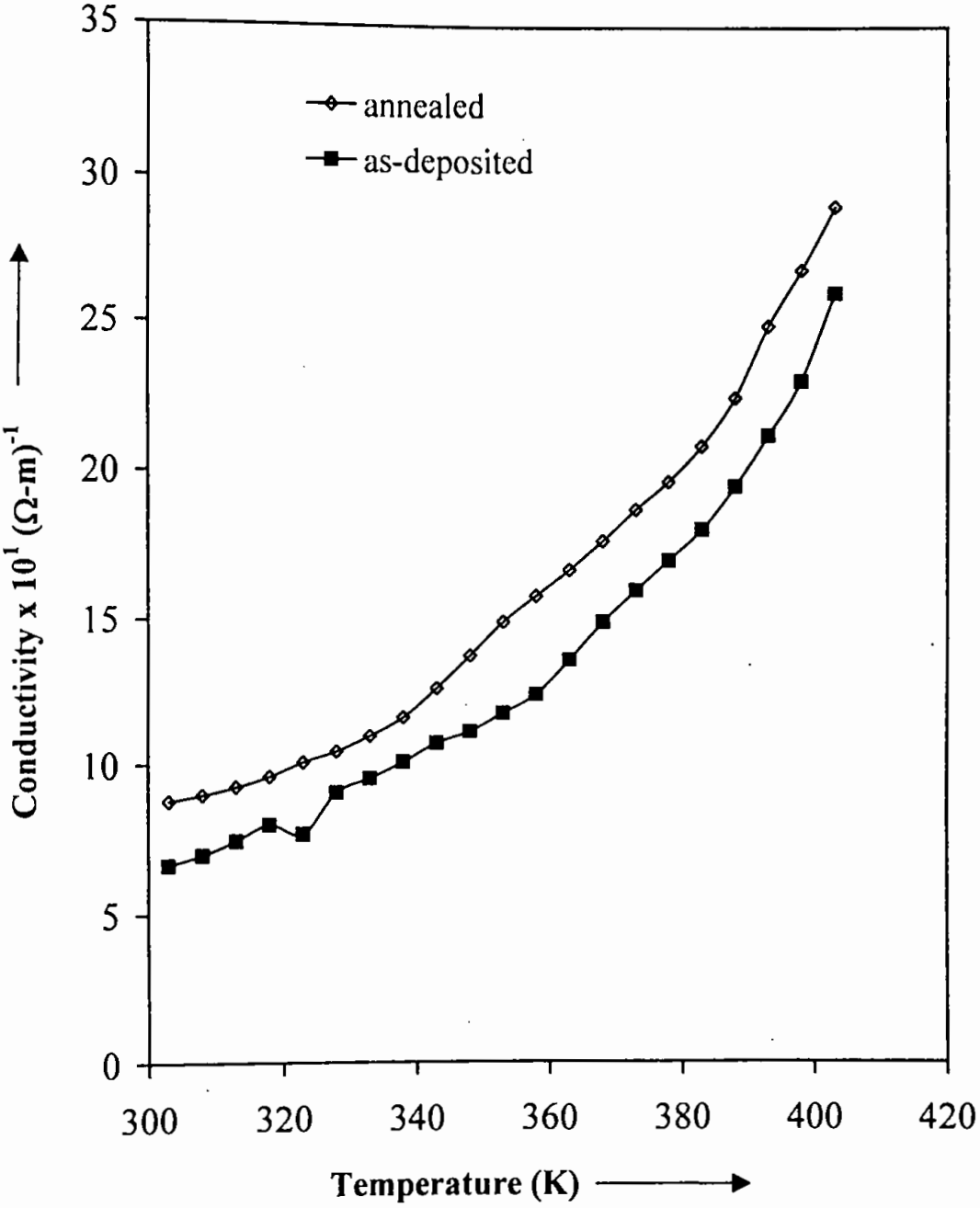

Fig : 5.13 Variation of conductivity with temperature for as- deposited and annealed films.

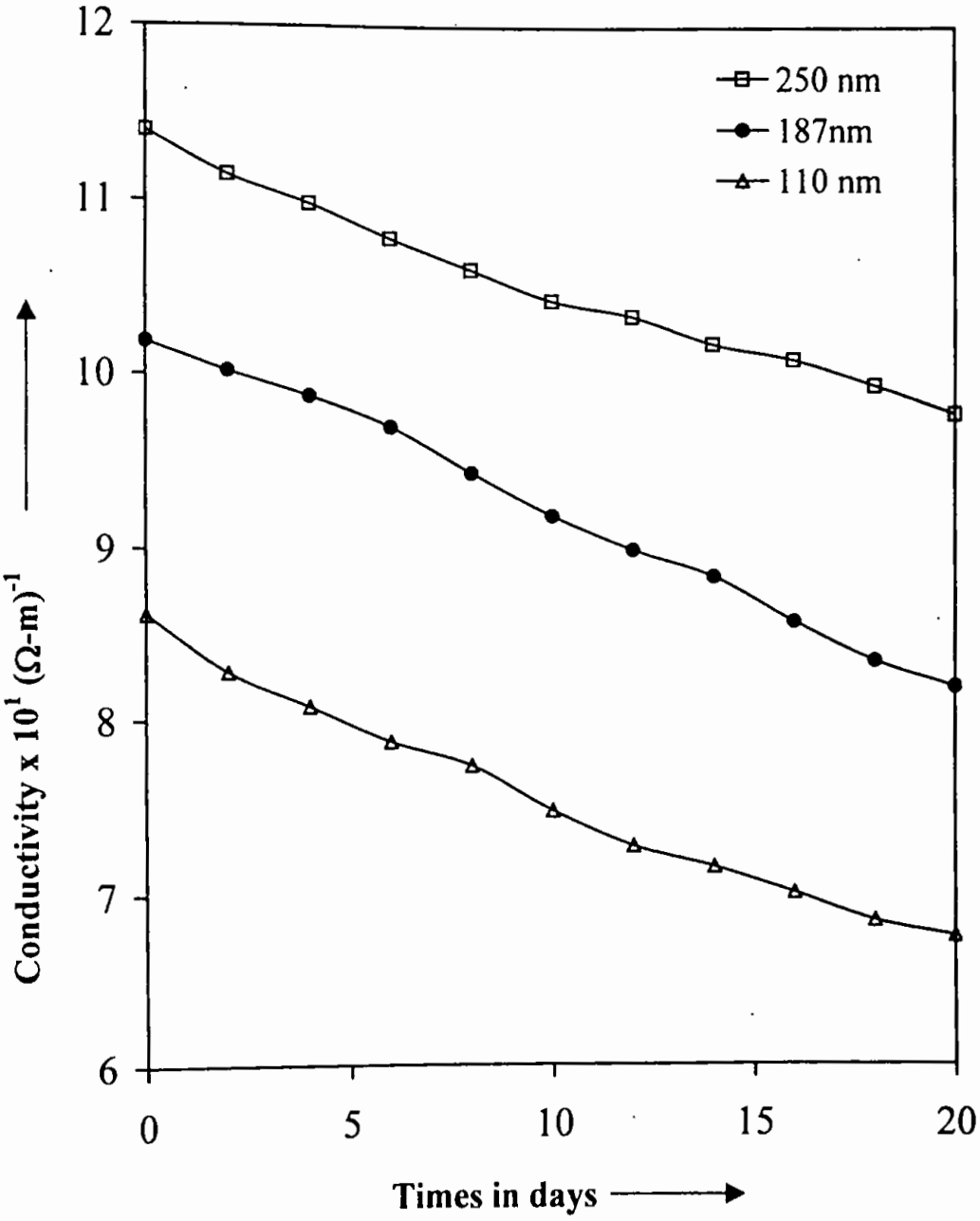

Fig : 5.14 Variation of film conductivity with time

5.5 HALL EFFECT

5.5.a THICKNESS EFFECT

The variation of Hall coefficient, carrier mobility and carrier concentration versus film thickness are presented in figures 5.15, 5.16, and 5.17, respectively. These figures interpret that Hall coefficient decreases while carrier mobility and carrier concentration increase with increasing thickness at constant magnetic field.

5.5.b MAGNETIC FIELD EFFECT

The effect of variation of magnetic field on Hall coefficient, carrier mobility and carrier concentration are represented in figures 5.18 to 5.20 for the films thickness 70nm, 110nm and 187nm,respectively.
It is observed that with increasing magnetic field both the Hall coefficient and carrier mobility increase whereas the carrier concentration decreases.

5.5.c TEMPERATURE EFFECT

The variation of carrier mobility, carrier concentration with temperature at constant magnetic field are shown in figures 5.21 and 5.22, respectively. From the figures it is seen that the carrier mobility and carrier concentration increase with increasing temperature.

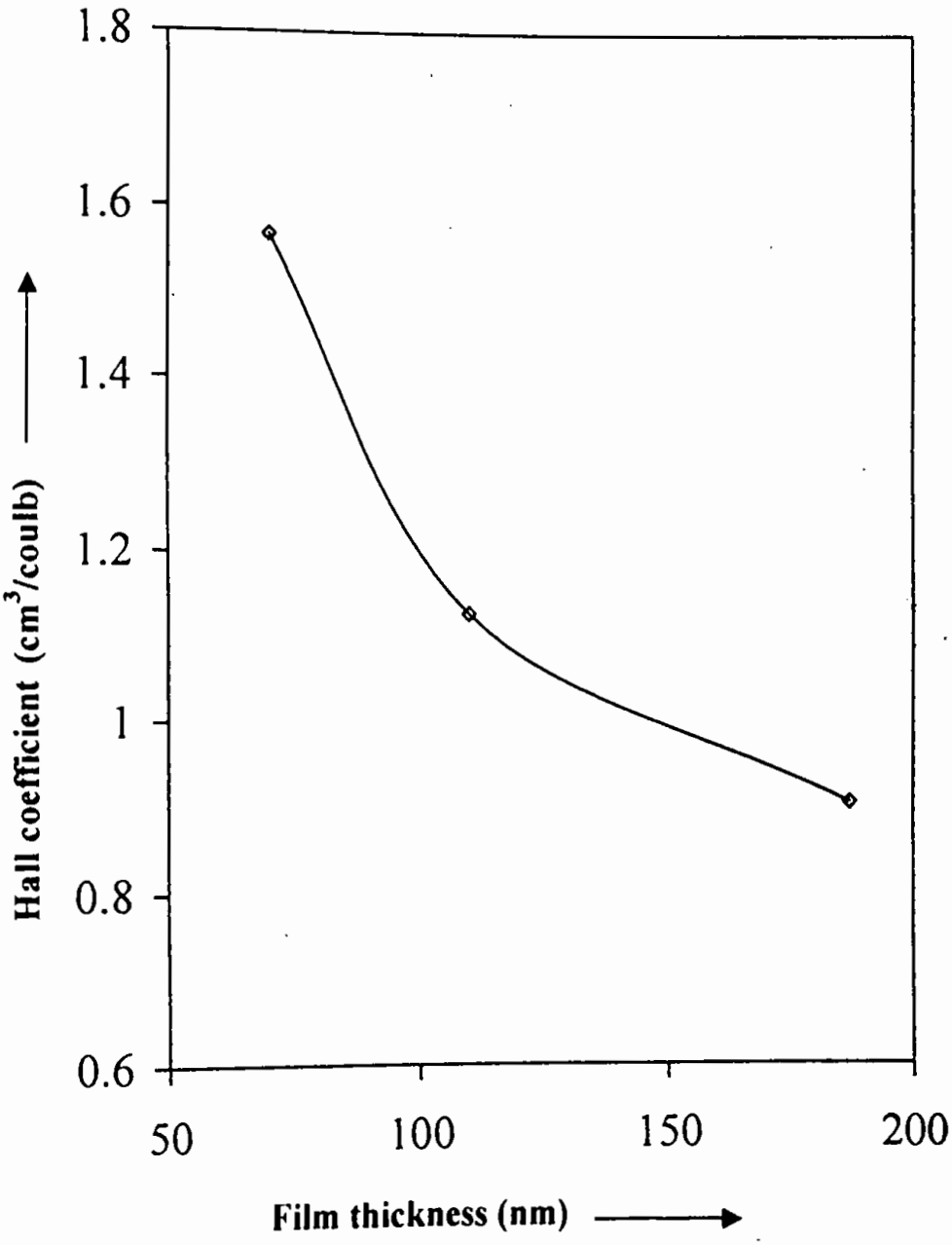

Fig:5.15 Variation of Hall coefficient with film thickness .

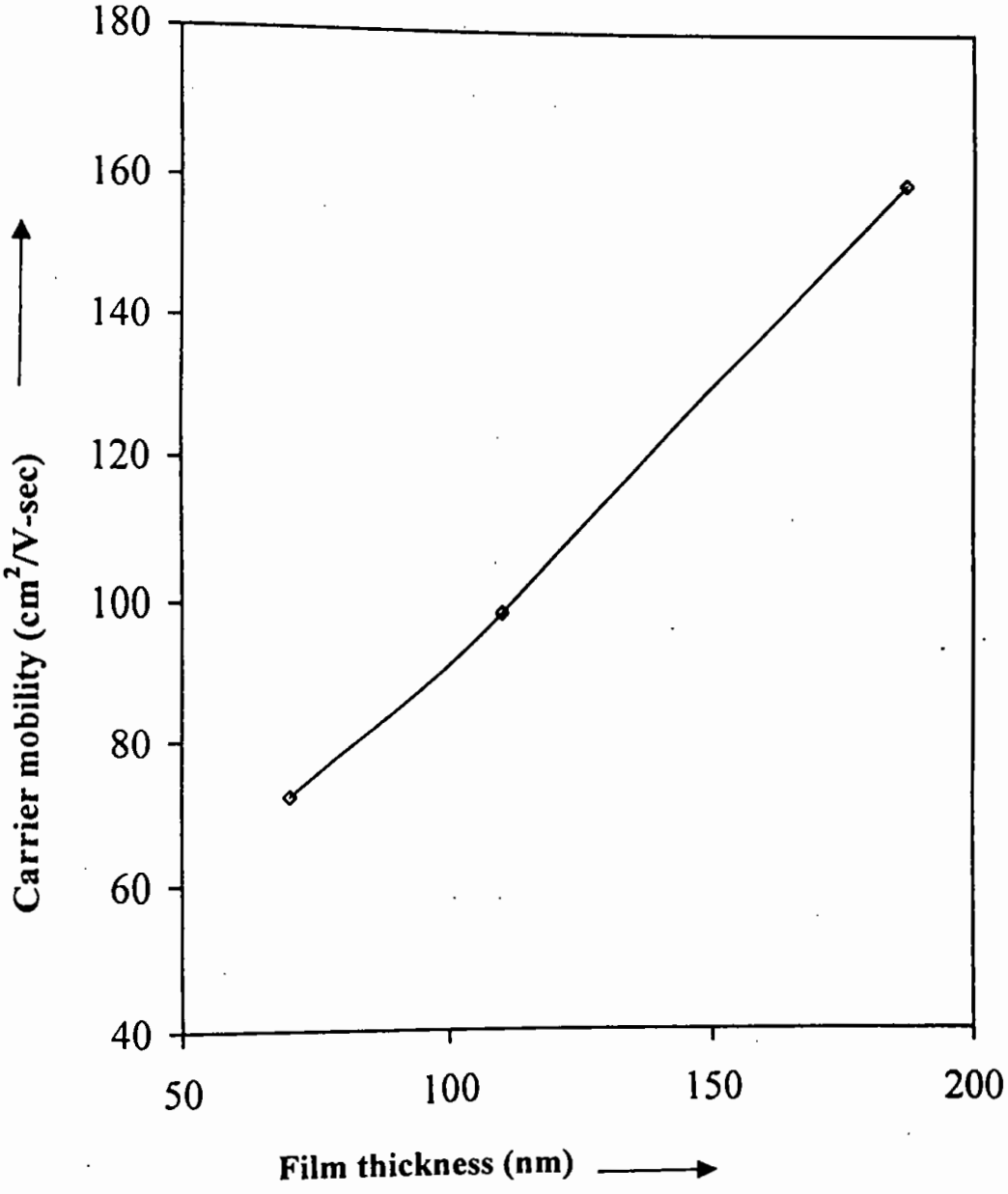

Fig: 5.16 Variation of carrier mobility with thickness .

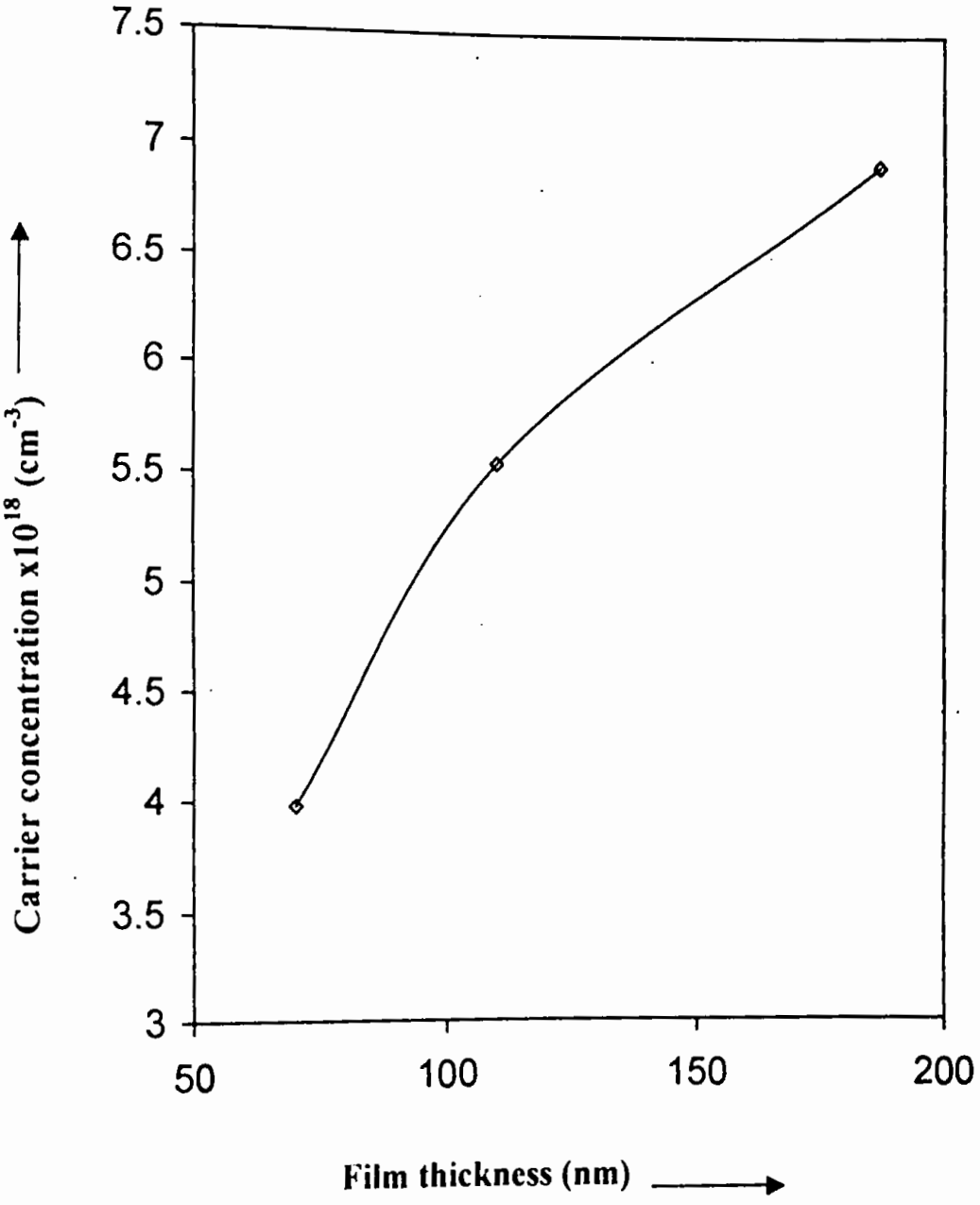

Fig: 5.17 Variation of carrier concentration with film thickness.

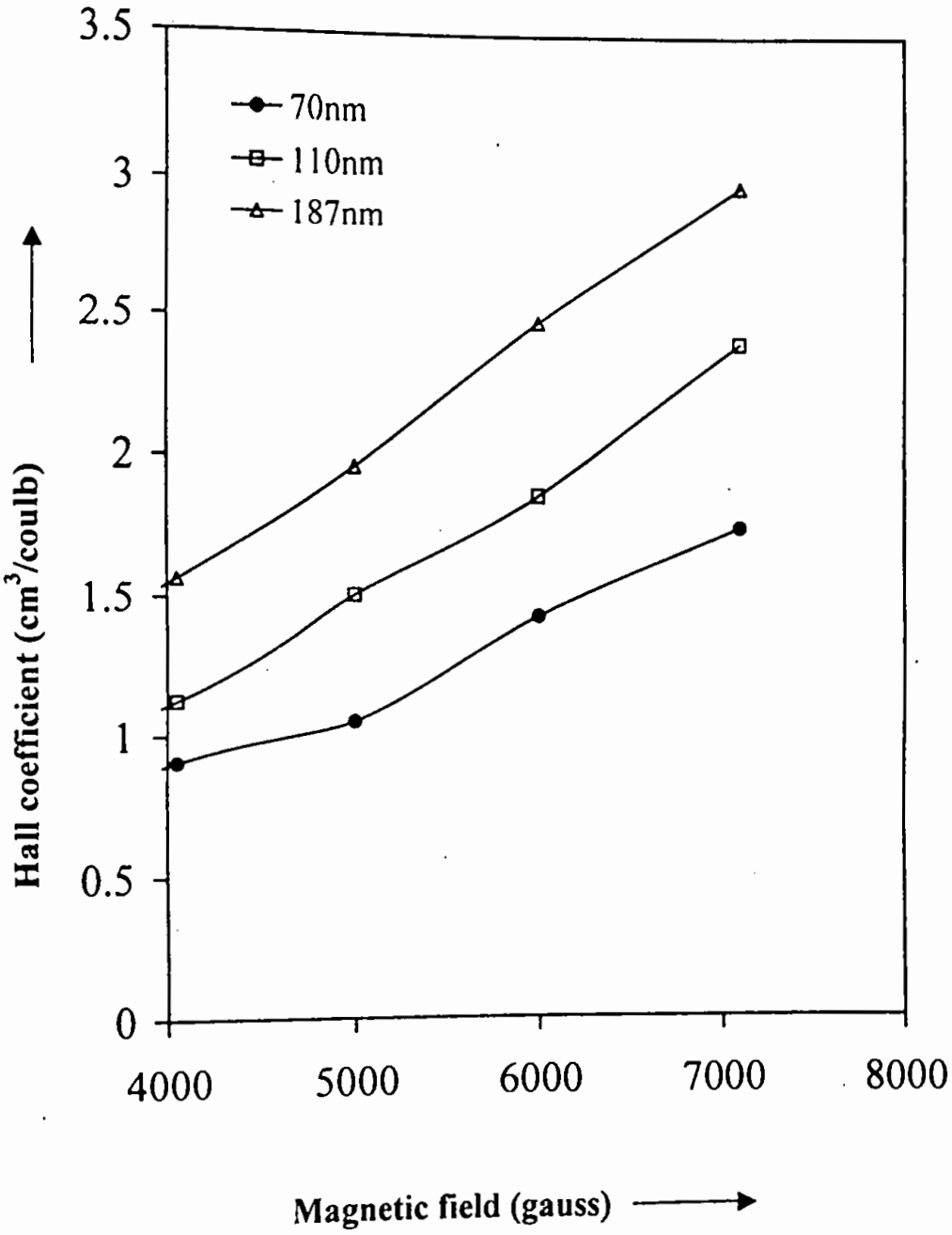

Fig :5.18 Variation of Hall coefficient with magnetic field

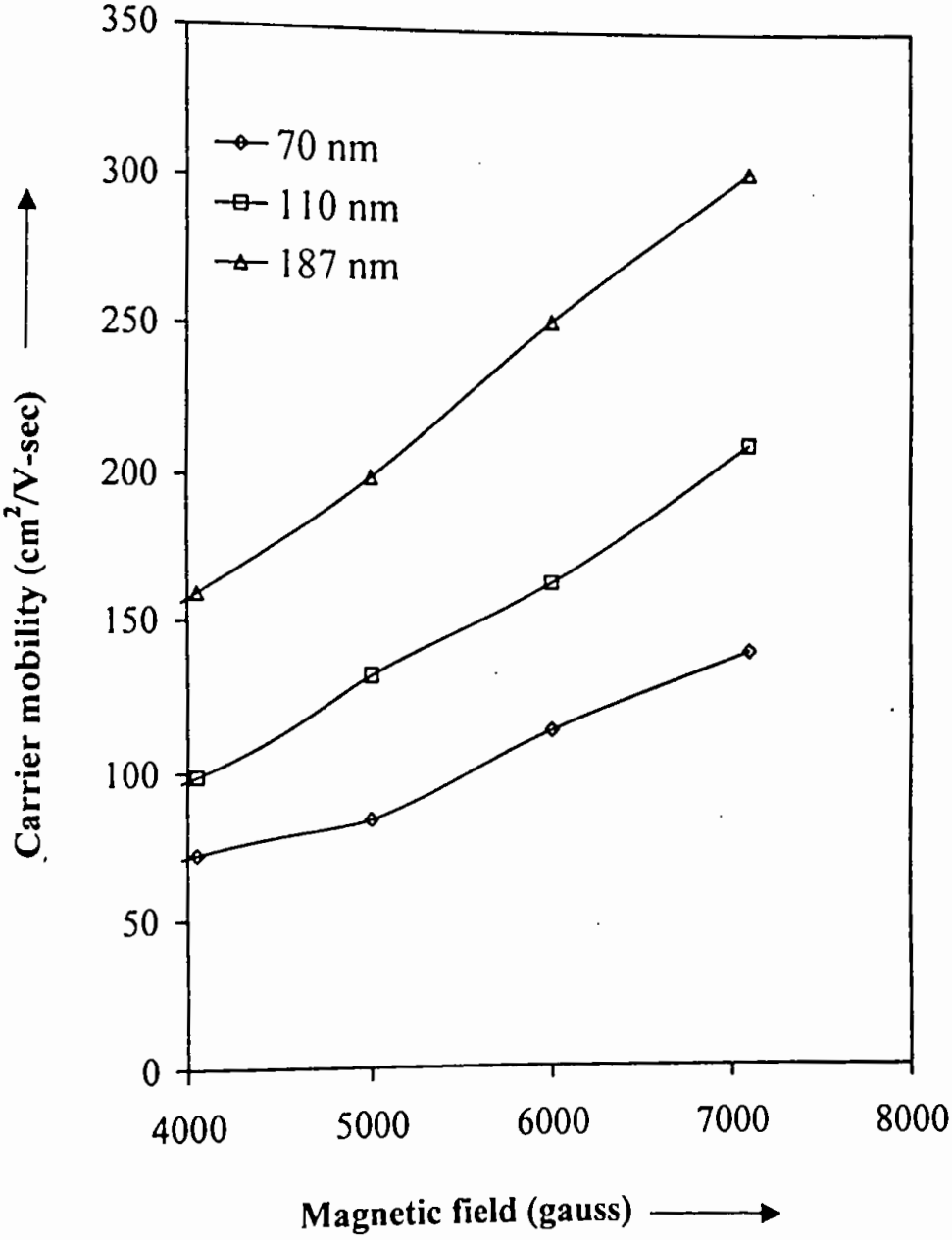

Fig : 5.19 Variation of carrier mobility with magnetic field

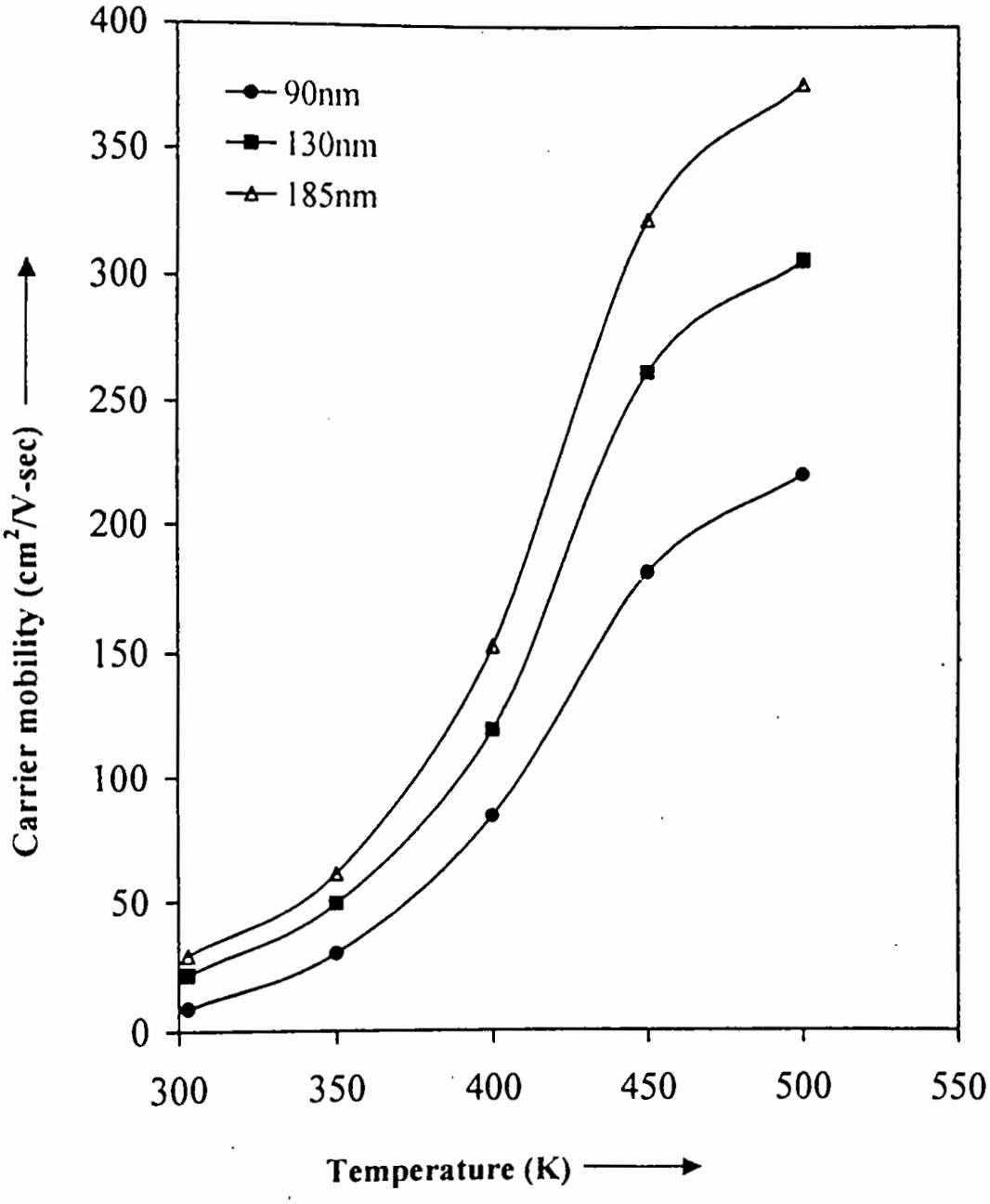

Fig: 5.21 Variation of carrier mobility with temperature.

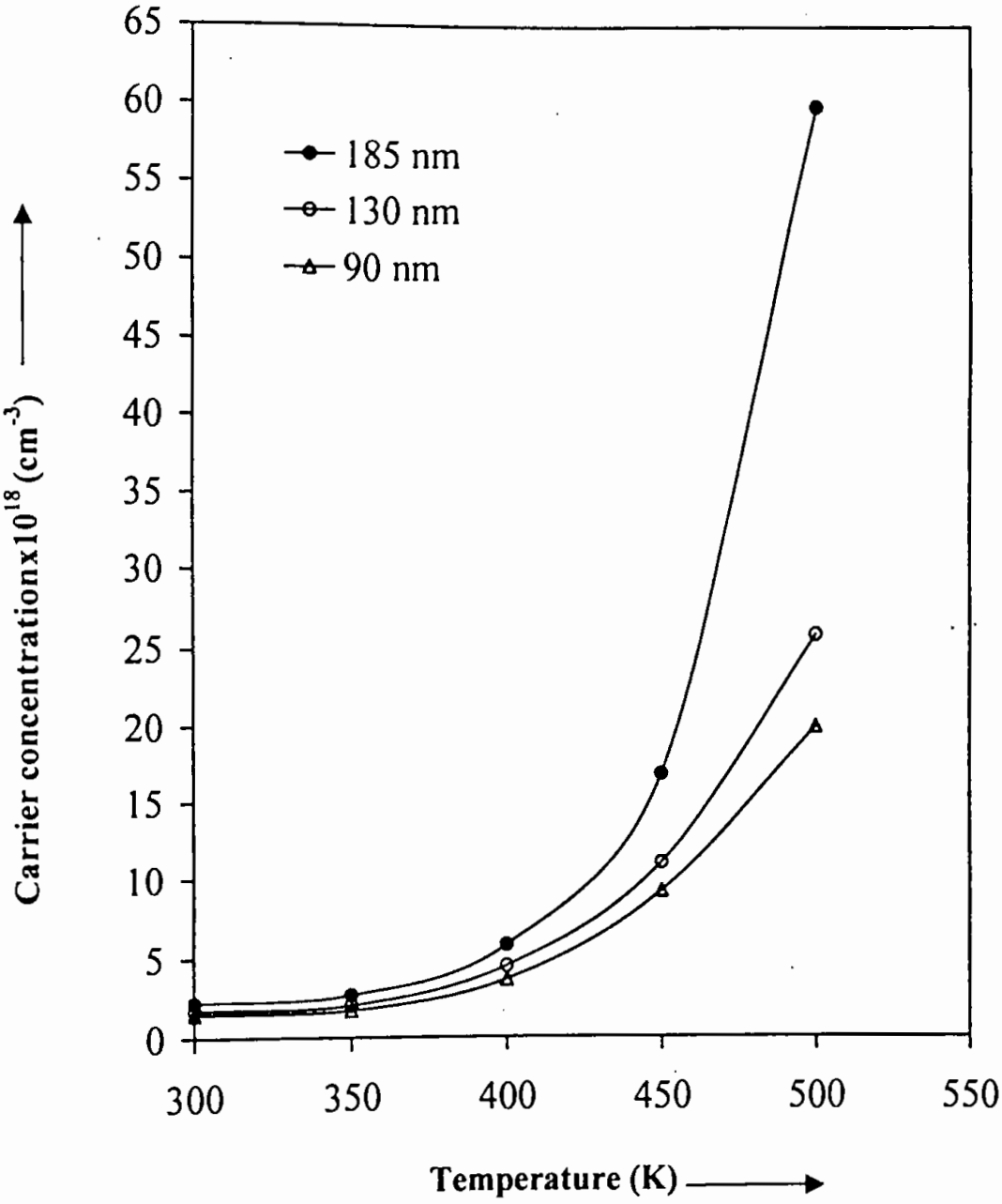

Fig:5.22 Variation of carrier concentration with temperature

Figure 5.23 shows the variation of $\ln R_H$ versus $\frac{1}{T}$ graph .The straight lines were drawn by using least mean square fitting method. From the slope, the band gap was calculated for the films having thickness 90nm, 130nm, 185nm,respectively. The results are tabulated below:

Film thickness (nm)	Band gap (eV)
90	0.277
130	0.276
185	0.278

From the table, it is observed that the band gap of the films of different thickness are almost identical. So the band gap of MnO_2 film is about 0.277 eV.

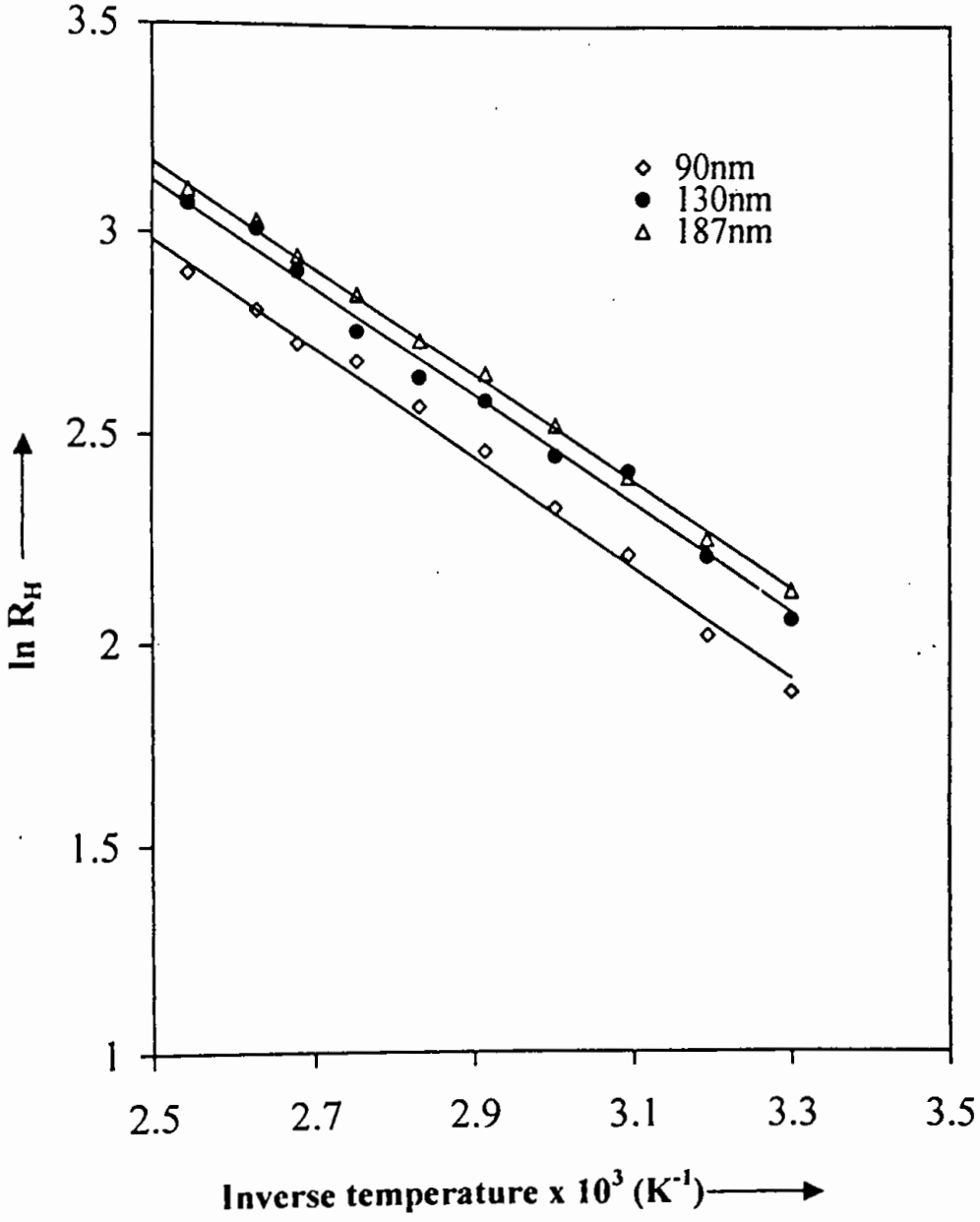

Fig :5.23 Variation of ln R_H with inverse temperature.

5.6 THERMO ELECTRICAL EFFECT

The thermal e.m.f. is measured as a function of temperature from 303 to 403K. Figure 5.24 shows the variation of thermoelectric e.m.f. with temperature for four samples of MnO_2 films of thickness 70nm, 110nm, 160nm, 210nm, respectively. It is seen that the thermal e.m.f. is found to be negative with respect to lead (Pb).

The thermoelectric power is calculated from the thermal e.m.f. and it is plotted in figure 5.25. It is clear from the figure that the thermoelectric power also found in negative.

5.7 OPTICAL PROPERTIES OF MnO_2 FILMS

The optical spectra of MnO_2 films shown in this section are made on glass substrates. All of the spectral transmittance and reflectance data are measured at room temperature. The spectral transmittance T (λ) in the wavelength range from 300 to 2500 nm for the films having thickness 70 nm, 110nm, 165 nm, 200 nm are shown in figure 5.26.Tranmittance and reflectance curve for a particular thickness 200 nm is shown in figure: 5.27.

It is seen from figure 5.26 that T (λ) increases very sharply in the ultraviolet region and then increases very slowly. The T (λ) curves remains almost constant in the entire near infrared wavelength range. The reflectance R (λ) in the figure 5.27 shows that R (λ) goes down in the visible region and then the value of the reflectance increases slowly and remains almost constant in the entire infrared wavelength range.

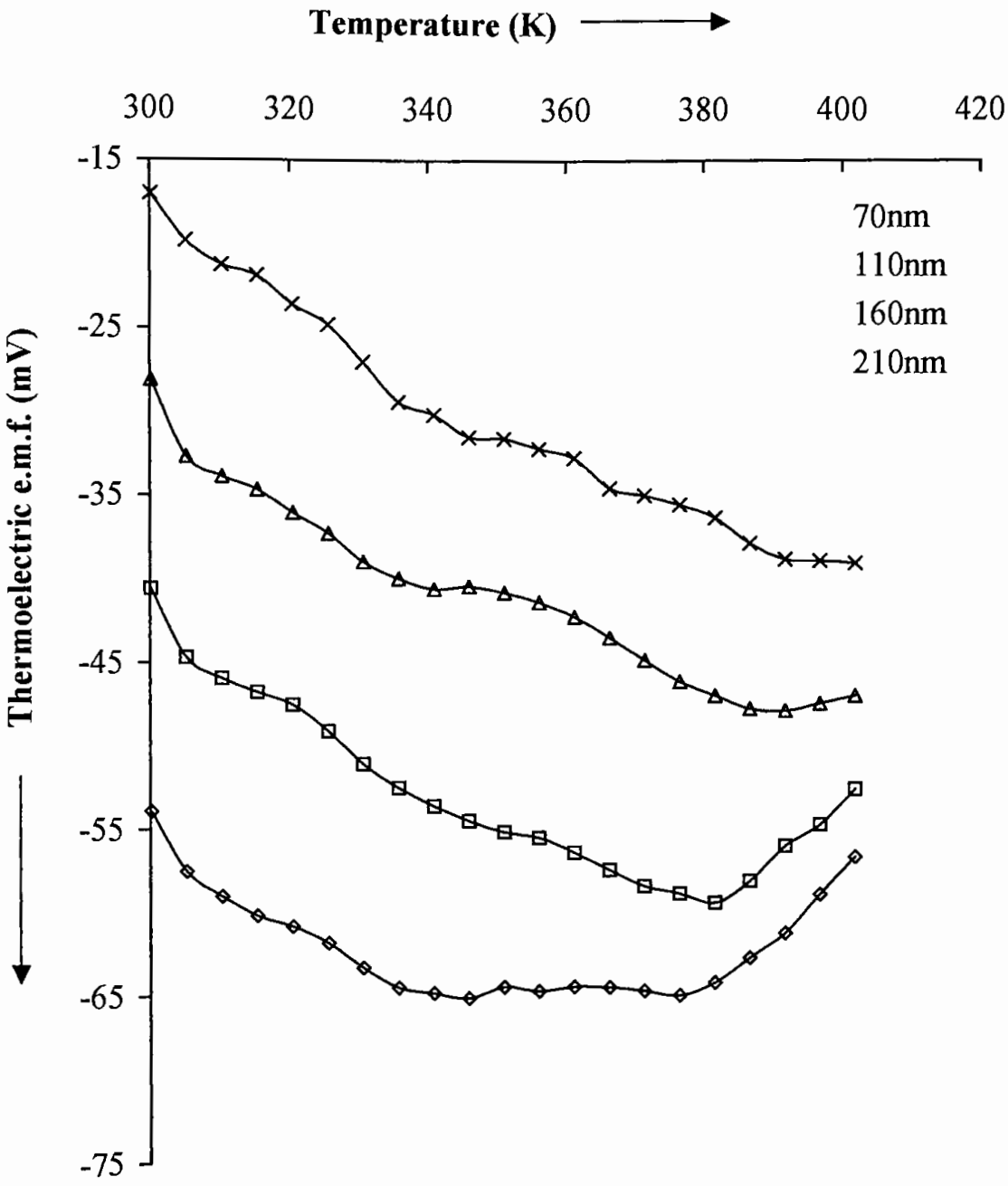

Fig : 5.24 Variation of thermoelectric e.m.f. with temperature

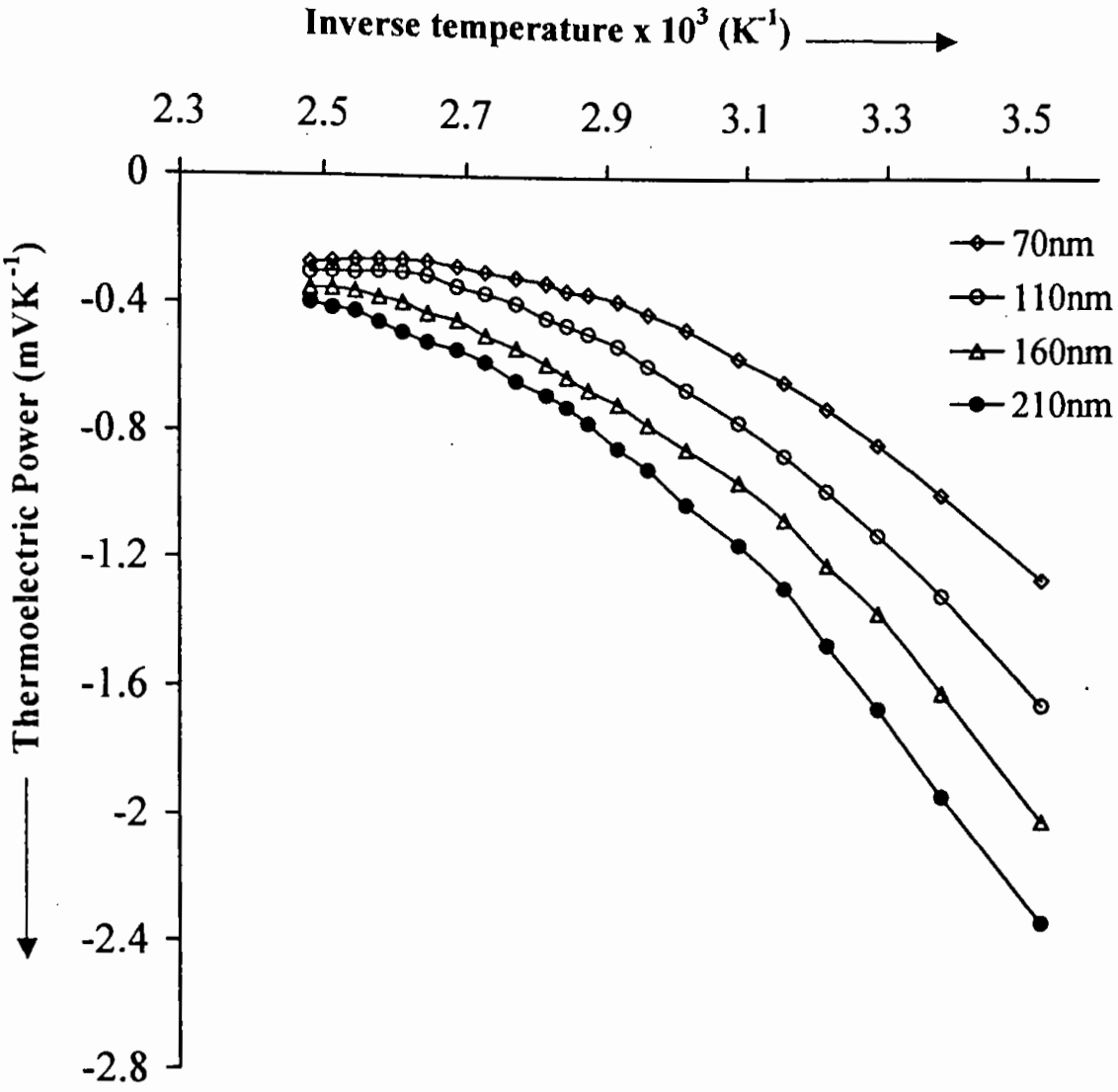

Fig: 5.25 Variation of thermoelectric power with inverse temprature

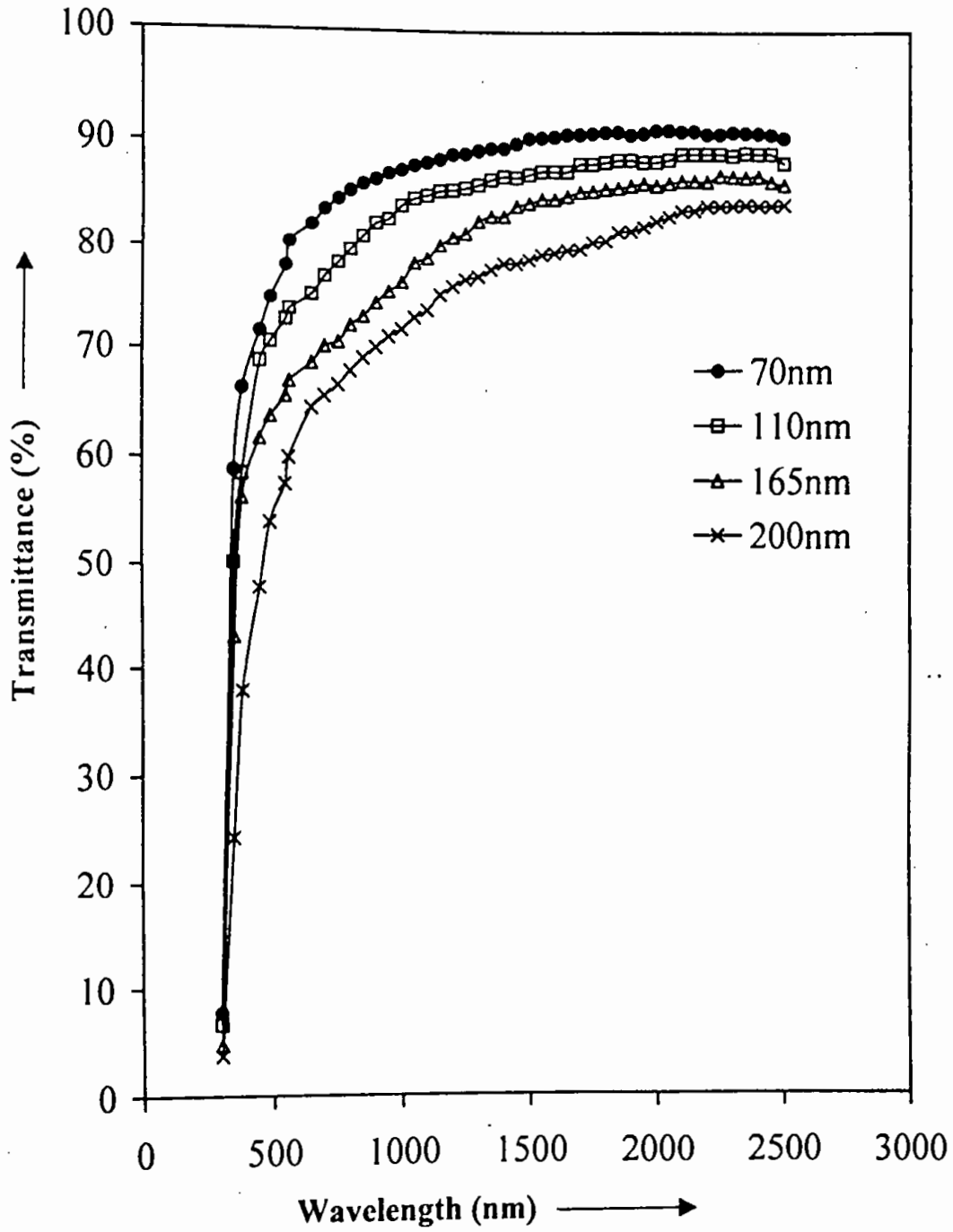

Fig: 5.26 Variation of transmittance with wavelength.

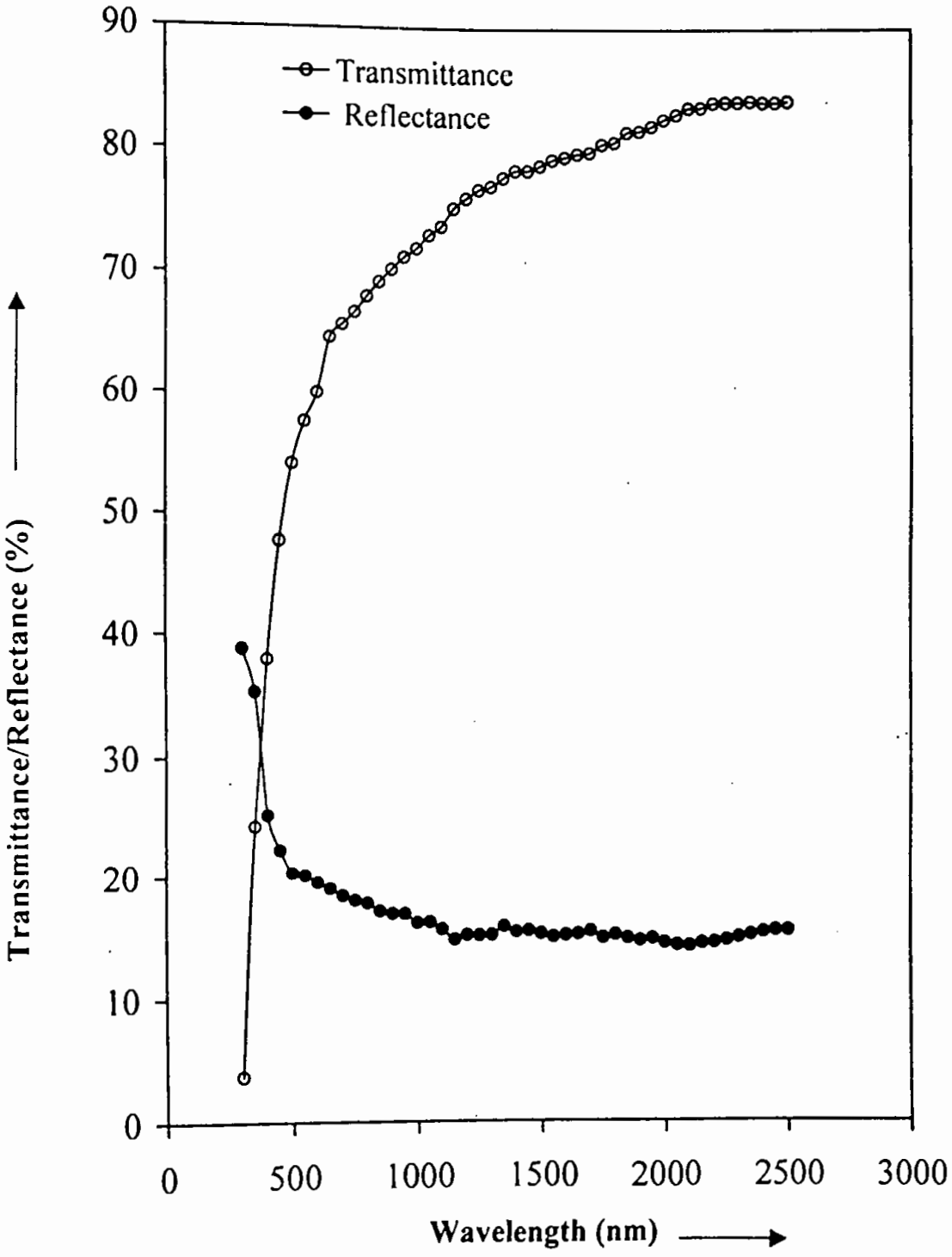

Fig :5.27 Variation of transmittance/reflectance with wavelength for a film of thickness 200nm

The plot of the absorption co-efficient versus wavelength is shown in figure 5.28. The absorption coefficient decreases with increasing wavelength.

Figure 5.29 and 5.30 show the plot of $(khv)^2$ versus hv and $(khv)^{1/2}$ versus hv for the direct allowed transition as well as indirect allowed transition.

The value of the tangent intercepting energy axis give the values of optical band gap. Comparing the nature of the plots of figure 5.29 and 5.30,it is seen that the best linearity of maximum experimental points is observed in figure 5.30, which signifies the transition is an indirect allowed type. The value of band gap is $\approx$ 0.250 eV, which is very close to the band gap of 0.277 eV measured by electrical measurement.

The luminous and solar transmittance as well as reflectance for various films are calculated from figures 5.26 and 5.27, respectively. Variation of luminous and solar transmittance value were found in the range 54.312 to 76.003 and 64.848 to 82.009 whereas the luminous and solar reflectance value lies in the range from 18.026 to 28.868 and 14.063 to 21.926, respectively.

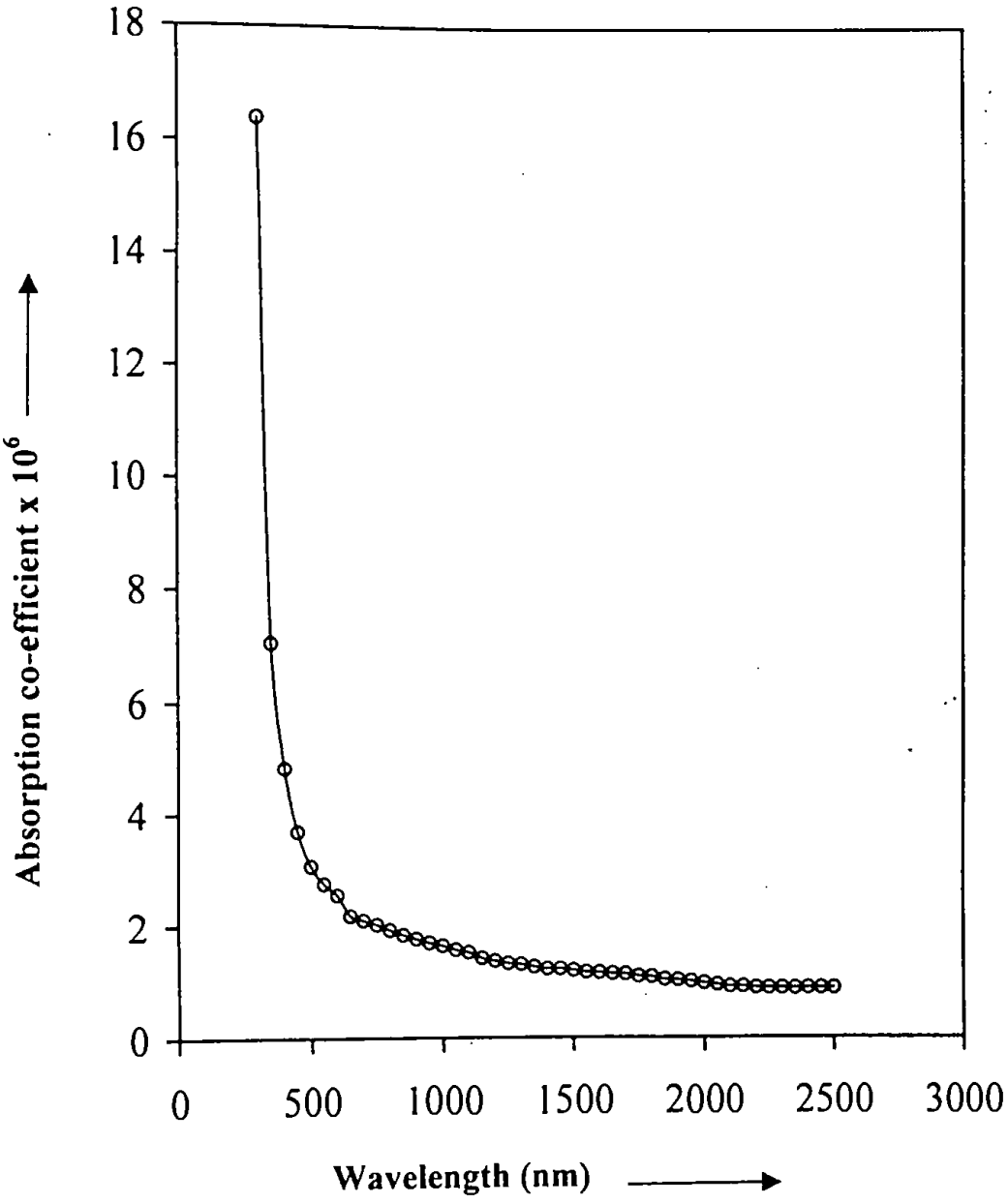

Fig: 5.28 Variation of absorption coeficient with wavelength

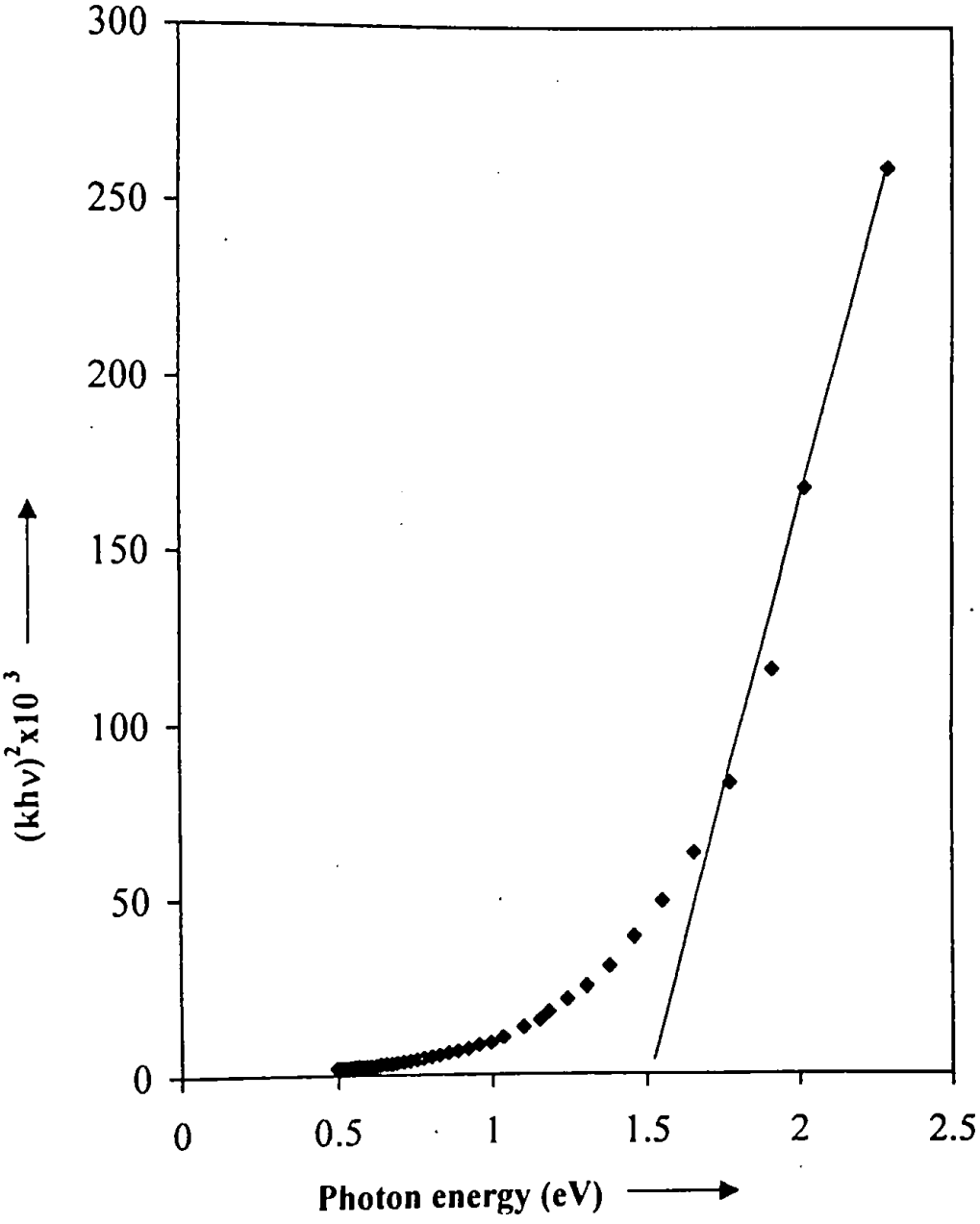

Fig : 5.29 Variation of (kh ν)² versus h ν for direct allowed transition.

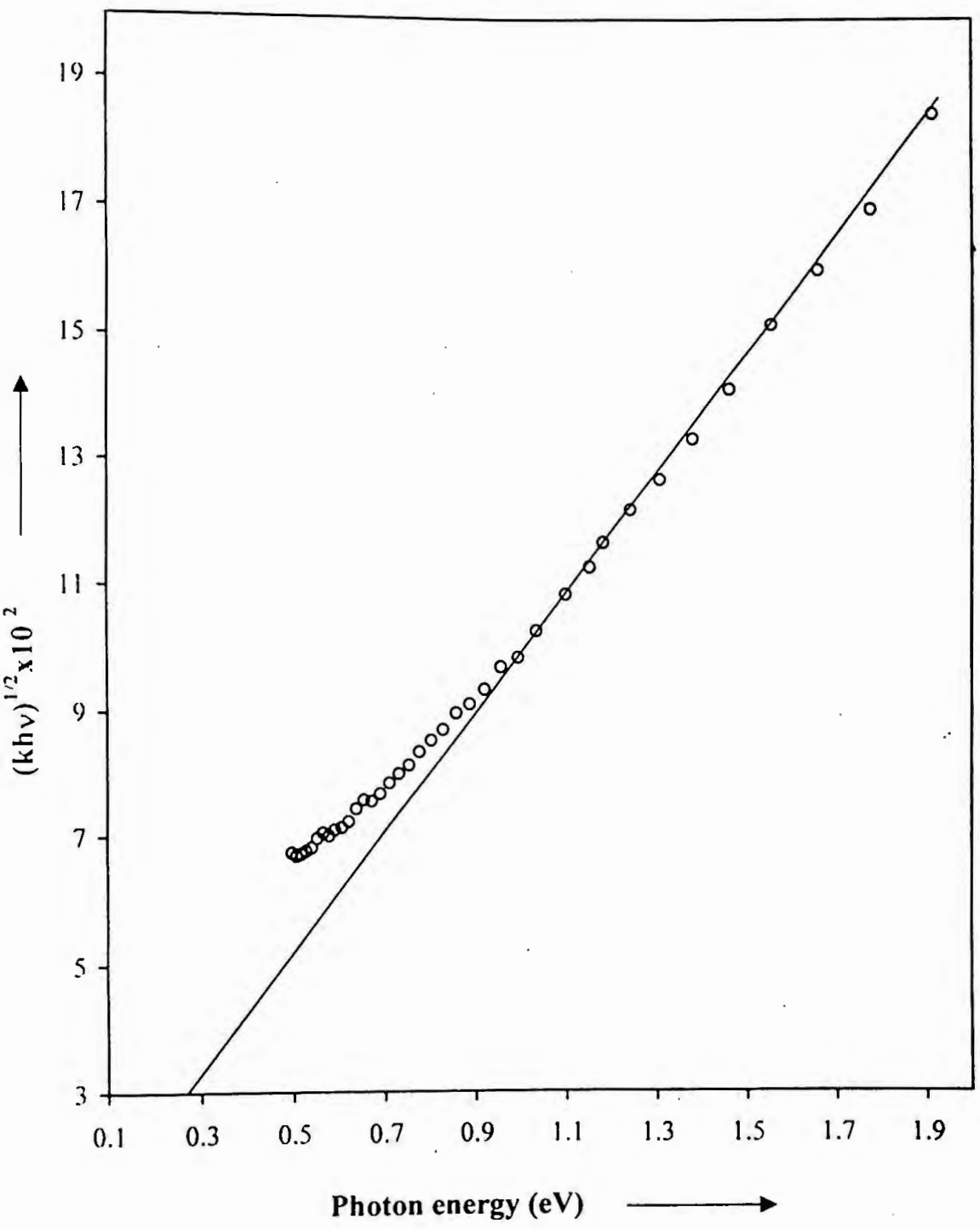

Fig : 5.30 V ariation of $(kh\nu)^{1/2}$ versus $h\nu$ for indirect allowed transition.

CHAPTER SIX

DISCUSSION AND CONCLUSION

DISCUSSION

6.1 EFFECT OF DEPOSITION PARAMETERS ON FILM THICKNESS

It has been seen in figure 5.1 that the film thickness increases linearly with the increase of deposition time. This is probably, after deposition to a certain thickness of the film, it is energetically favorable for the film to grow on the initially grown layer on the substrate **(Dale, 1932).**

It is observed from figure 5.3 that the film thickness decreases with increasing source to substrate distance. At small source to substrate distance, the maximum amount of vapor molecules, which come out from the source, can strike the substrate directly before getting the scope of distributing in the vacuum chamber. As the distance increase the vapor molecules get sufficient space to distribute laterally in the vacuum chamber. As a result a smaller quantity of vapor atom can reach the substrate and cause a decrease in deposition rate.

6.2 STRUCTURAL PROPERTIES

The X-ray diffraction pattern has been reported in figures 5.4 and 5.5, respectively. From the figures, it is found that there is no significant absorption peak in the X-ray diffraction pattern. The absence of any

absorption peak indicates that material is a non-crystalline or amorphous in nature.

6.3 TEMPERATURE EFFECT ON ELECTRICAL CONDUCTIVITY OF SAMPLES PREPARED AT $2x10^{-5}$ torr

The result presented in figure 5.6 helps us to conclude that the films deposited at about $2x10^{-5}$ torr show that the conductivity decreases with increasing temperature. The variation indicates a metallic behavior. This metallic characteristic may be explained due to scattering of oxygen or due to random impurities in higher pressure **(Adler, 1968)**. Figure 5.6 also shows that there is an anomaly in conductivity at a particular temperature near 323K, which is well agreed with reports of previous workers. **(Bhide, 1960).**

6.4 ELECTRICAL PROPERTIES OF MnO_2 THIN FILMS PREPARED AT $6.0x10^{-6}$ torr

6.4.a EFFECT OF TEMPERATURE

The result presented in figure 5.7 helps us to conclude that the films deposited at about $6x10^{-6}$ torr show that the conductivity increases with increasing temperature. The variation indicates a semiconducting behavior. In semiconducting material the number of carriers available for electrical conduction are increased with increasing temperature. These

carriers are thermally generated from the valance band to the conduction band and conduction does occur. So the conductivity is increased with temperature. The sheet resistance is inversely proportional to conductivity. So it decreases with increasing temperature.

Figure 5.8 shows the plots of lnσ versus 1/T.It would be straight line for an intrinsic semiconductor where thermal scattering is prominent **(Mckelvey, 1966)** and also in semiconductor where gain-boundary scattering is considerable **(Seto, 1975)**. In this work, all of the films show different straight lines having different ranges of slope.

Figure 5.9 indicates that the activation energy increases with decreasing film thickness above the anomaly temperature. This can be understood from the island structure theory based on tunneling of charged carriers between islands separated by a short distance. **(Neugebauer and Weeb, 1962)**. The activation energy required to move a charge from one island to the next is proportional to $e^2/\epsilon r$, where 'e' is the charge and 'r' is the linear dimension of the islands **(Gorter, 1951)**.

At the initial stage of the film growth discrete islands form on the substrate and with the increase of average film thickness these islands grow in size and subsequently merge to give a continuous film. With the decrease of average thickness of the film, crystallte size decreases and hence the increase of activation energy. This increase of activation energy with decreasing thickness is due to the complete isolation of the grains.

6.4.b VARIATION OF TEMPERATURE COEFFICIENT OF RESISTANCE (T.C.R.)

Figure 5.11 suggests that the films of thickness 55nm, 110nm, 187nm, 250nm, respectively deposited at pressure $6x10^{-6}$ torr show a negative T.C.R. indicating semi-conducting behavior whereas the films of thickness 80nm, 120nm, 180nm, 220nm, respectively deposited at pressure $2x10^{-5}$ torr show positive T.C.R. indicating metallic characteristics **(Bhide, 1960).** These metallic characteristics may be explained due to nonstoichiometry scattering of oxygen or due to random impurities in higher pressure **(Adler, 1968)**. This result, therefore, suggests that preparation and properties of MnO_2 is very much dependent on ambient pressure.

6.4.c EFFECT OF THICKNESS

Variation of electrical conductivity with film thickness is shown in figure 5.12. It is observed that conductivity increases sharply with thickness up to 200 nm and above that its value remains almost constant. In this range, the current density should be uniform and therefore, the calculated values are considered to give the volume conductivity, but not the surface conductivity in this thickness range.

Films thickness greater than 200 nm shows a bulk behavior. However, the lower of conductivity in comparison to even thick films can be attributed to inherent defects, such as point defects, vacancies, grain boundaries, dislocations, etc. which are always present even in comparatively thick 'as grown' film.

The electrical conductivity decreases sharply below 200nm, which is probably due to the discontinuous structure of the film. This thickness dependence of conductivity is well in conformity with the Fuch's-Sondheimer size effect theory **(Fuchs, 1938 & Sondheimer, 1952)**.

6.4.d ANNEALING EFFECT

It is observed from the figure 5.13 that the electrical conductivity of the annealed film is high than that of the as-deposited film, in same order of thickness of 200nm. It is also observed from the figure that there is no anomaly in conductivity in the annealing film. It indicates that the fundamental nonstoichiometry of oxygen vacancies in the film due to annealing is responsible for higher resistivity **(Moon, 1940).**

6.4.e AGING EFFECT

It has been observed from the figure 5.14 that the conductivity decreases with time and its conductivity decreases in thin film more rapidly than the thicker one. The observed irreversible changes in conductivity may be attributed due to the degradation of the sample through oxidation or contamination and in thin case the degradation occurs rapidly.

6.5 HALL EFFECT

From the measurement of Hall voltage, it is observed that all films studied are n-type semiconductors. Figure 5.15 shows that the Hall coefficient decreases with increasing thickness and figure 5.18 shows that

it is increasing with increasing magnetic field. It is also observed by previous works **(Chakrabarti & Pal, 1980), (Maissel &Glang, 1983).**

Figure 5.16 shows an increasing behavior of carrier mobility with increasing thickness. A similar behavior was also reported by previous works **(Yoshizumi Yasuoka &Toyoo Miya, 1979).**

It is observed from figure 5.17 that the carrier concentration increases with increasing thickness. The thickness dependence of carrier concentration may be due to the fact that this trapping of electron is dominant in thinner films than that of thicker one. Duga reported that trapping of electrons occur near the edge dislocation **(Duga, 1982).**

Figure 5.20 shows that the carrier concentration for different thickness decreasing with increasing magnetic field. It may be happened that due to the effect of magnetic field some trapped carrier become free to decreasing the carrier concentration.

Figure 5.22 show that the carrier concentration increases with increasing temperature. In semiconducting material carriers are thermally generated from the valence band to the conduction band and conduction does occur. Therefore carrier concentration is increases with temperature.

It is obtained from section 5.5 that the band gap of the author's sample of thickness 90nm, 130nm, 185nm are 0.277 eV, 0.276 eV, 0.278eV. These value of band gap agree well with the reported value of band gap 0.26 eV

and 0.28 eV by the previous workers **(Chevillot. et. al., 1959 & Druilhe et. al., 1967).**

6.6 THERMO ELECTRICAL EFFECT

Figure 5.24 shows the values of thermoelectric e.m.f. with temperatures for films of different thickness. It is observed that the thermo e.m.f. is negative with respect to lead. The negative sign in the thermoelectric e.m.f. measurement indicates that the carriers in the MnO_2 films are electrons and the films are n-type semiconductor. Similar observation was obtained from Hall effect measurements. Figure 5.25 shows the variation of the thermoelectric power with inverse temperature. It is observed from this figure that the thermoelectric power decreases continuously with increasing temperature and saturates in the higher temperature region. The rate of change of thermoelectric power with temperature is greater for films of higher thickness than that of lower one. The saturation of thermoelectric power with temperature also occurs at relatively higher temperature in the thicker films than that of thinner one.

To study the See-back effect the author also determined the thickness dependence of the thermoelectric power for different temperature and the thickness dependence thermoelectric power characteristics is shown in figure 6.1. It shows from the figure that at higher temperature thermoelectric power is almost thickness independent, while in the room temperature limit, it shows strong thickness dependence.

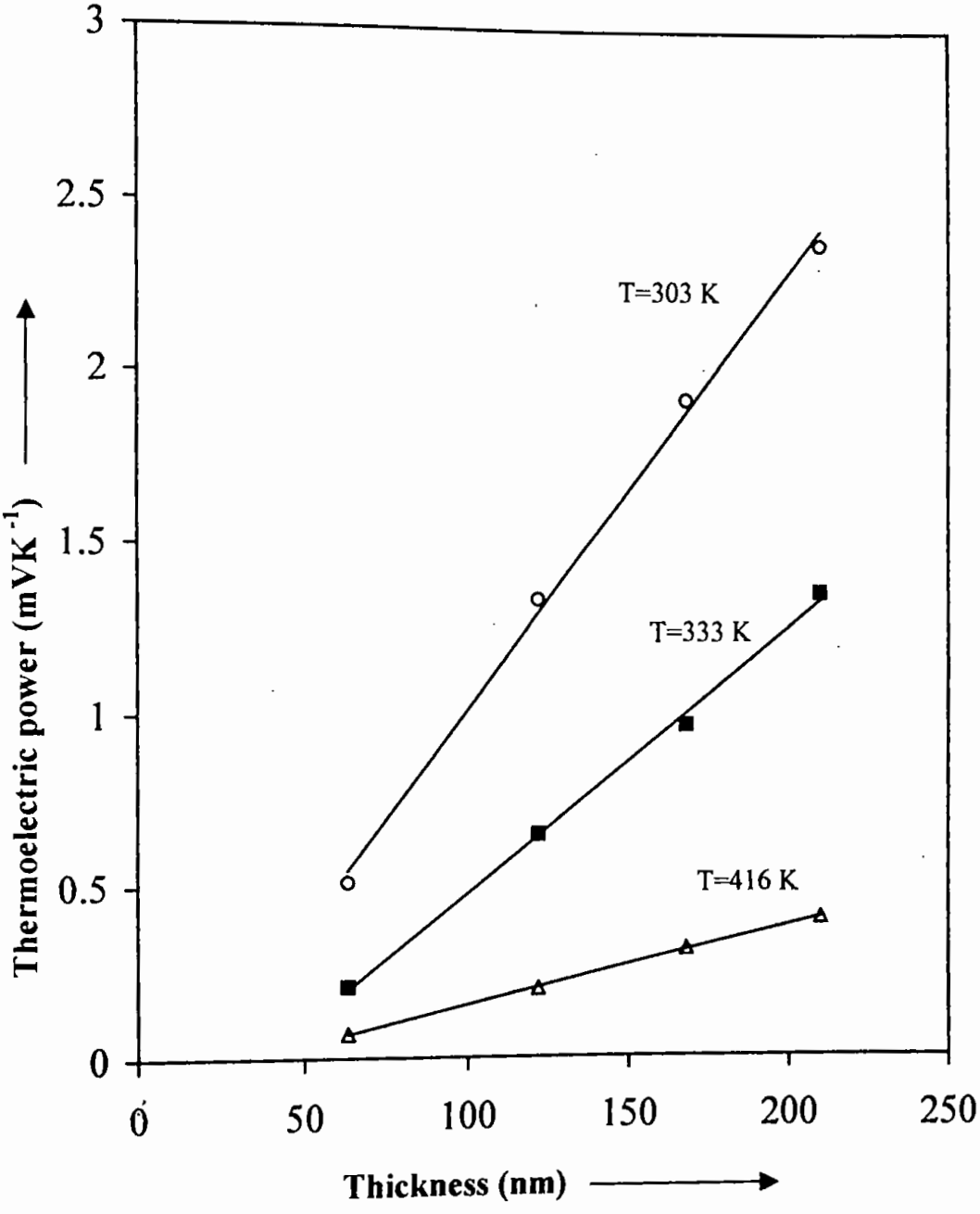

Fig: 6.1 Variation of thermoelectric power with thickness at three different temprature.

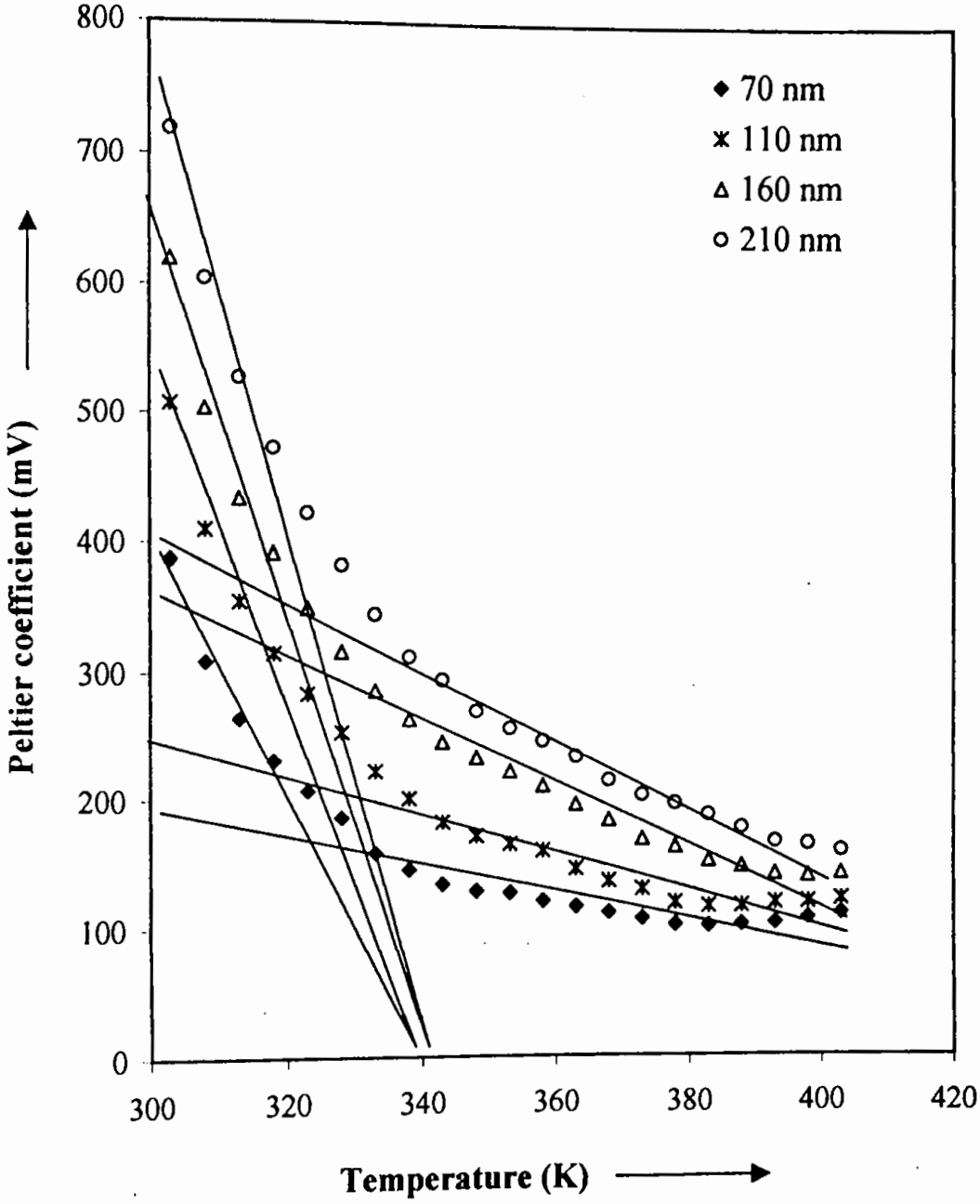

Fig : 6.2 Variation of Peltier coefficient with temperature

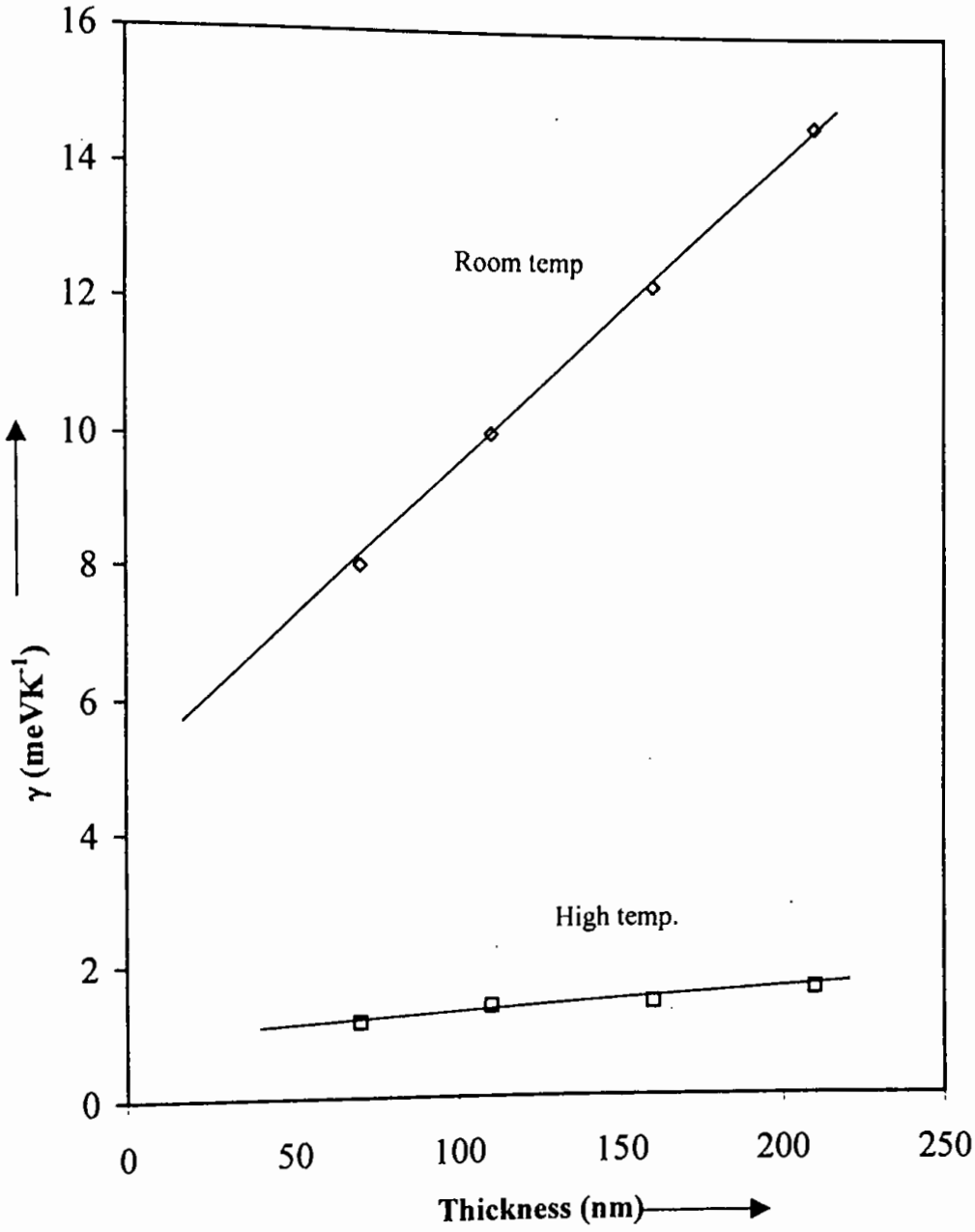

Fig : 6.3 Variation of temperature coefficient of activation energy with thickness at room temperature and high temprature.

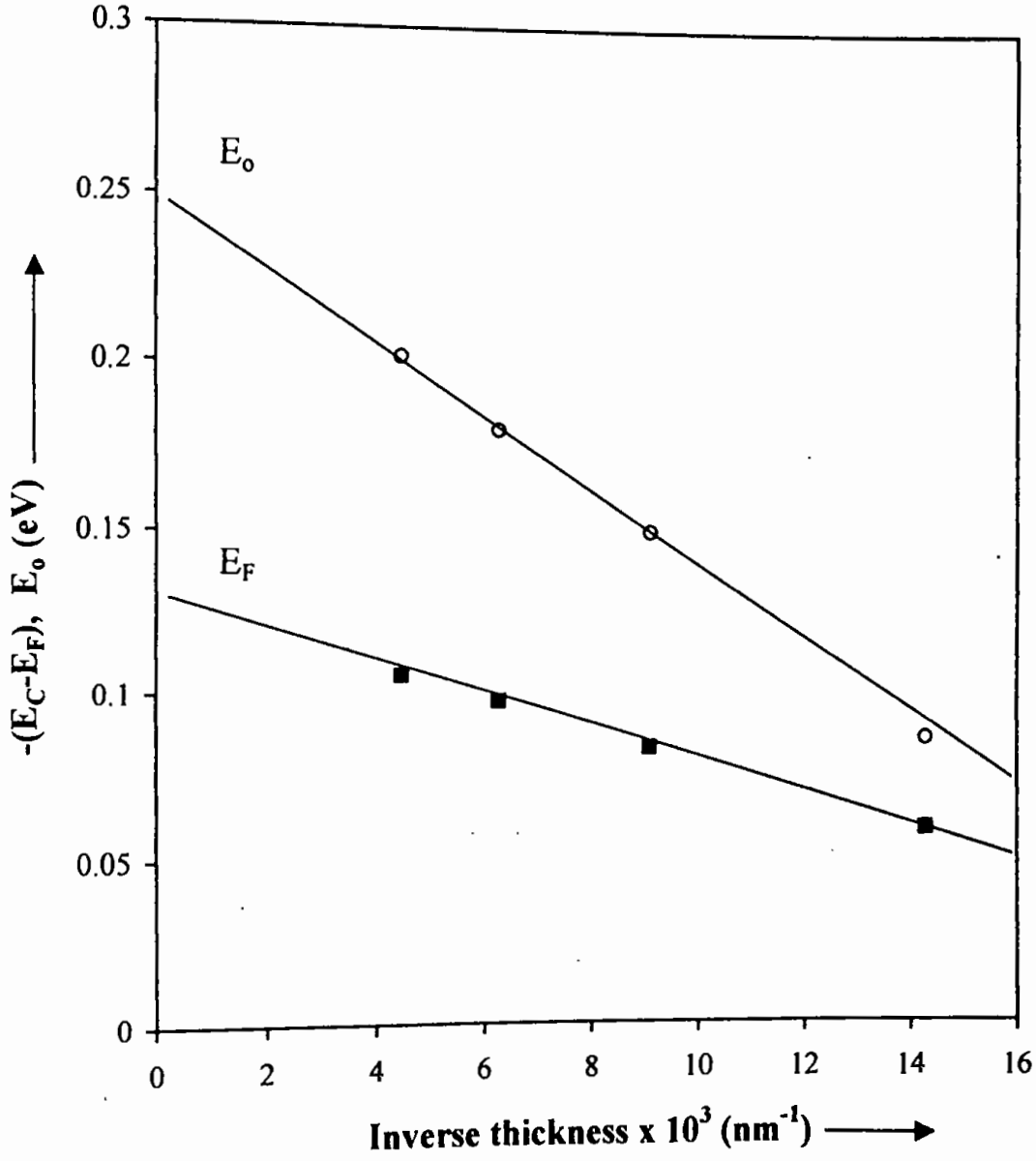

Fig: 6.4 Variation of E_o and Fermi energy E_F with inverse of thickness.

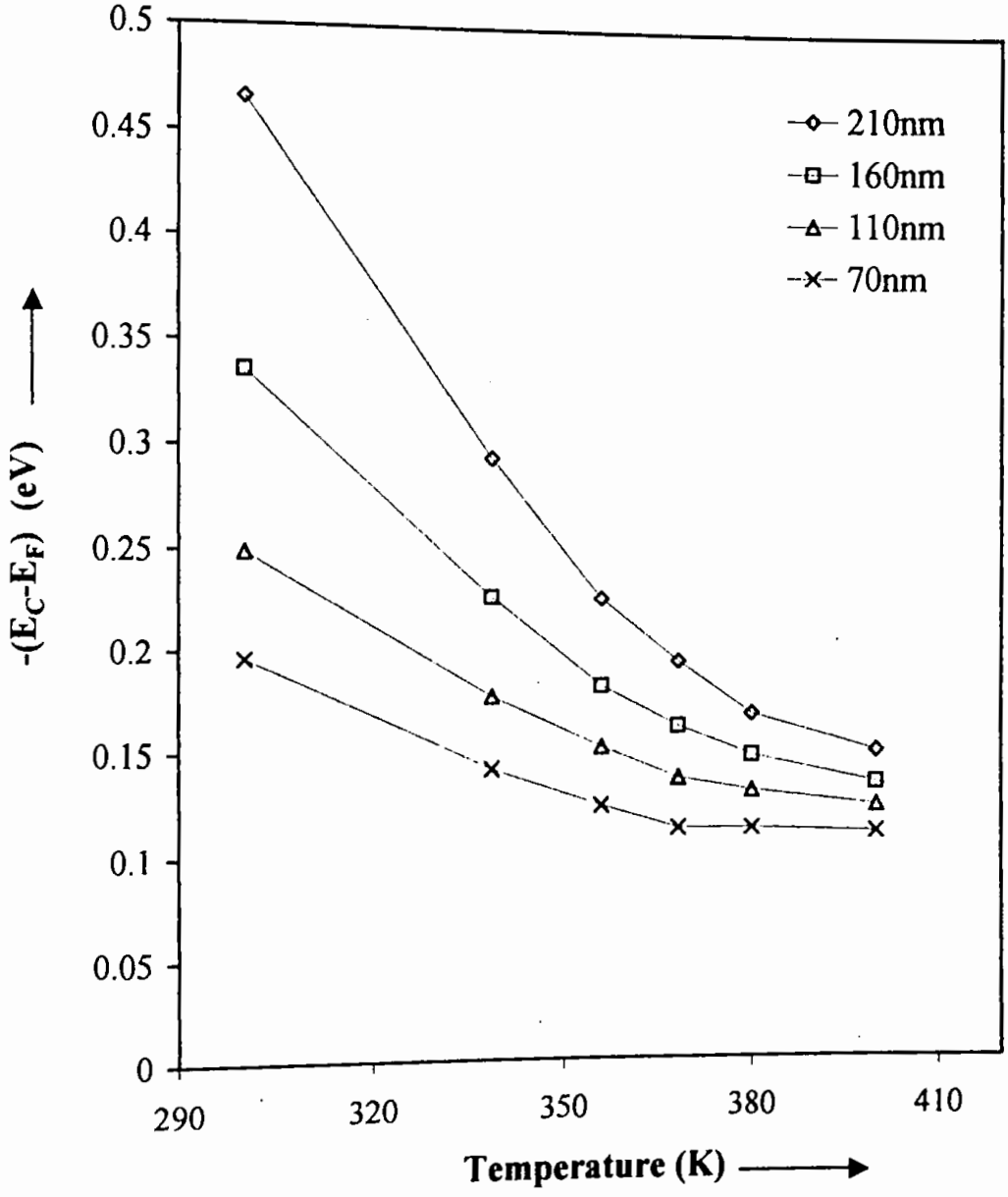

Fig: 6.5 Variation of Fermi level with temperature

The carrier concentration of the samples as obtained from the Hall effect is of the order of ~ 10^{18} cm^{-3} which helps to consider the samples as non-degenerate one. For a nondegenerate n-type crystalline semiconductor with spherical constant energy surface under thermal equilibrium the thermo electric power is given by **(Mott & Davis, 1979)**

$$Q = -\frac{K_B}{e}\left(\frac{E_c - E_F}{K_B T} + A\right) \text{----------(6.1)}$$

Where K_B is the Boltzmann constant and E_c is the energy of conduction band edge; A is a constant that depends on the nature of the scattering process. Normally, for a material like a Fermi glass, A runs between 2 and 4. If energy is measured with respect to the bottom of the conduction band then equation (6.1) reduces to

$$Q = -\frac{K_B}{e}\left(A + \frac{E_F}{K_B T}\right) \text{----------(6.2)}$$

Where E_F is the position of Fermi level in the band gap.

Harry et al **(Harry et al, 1973)** have pointed out that A = (5/2) - r, where r corresponds to the scattering index and is equal to - 0.5 for piezoelectric scattering and - 1.5 for ionized impurity scattering. Thus A= 4 for ionized impurity scattering and 3 for piezoelectric scattering. From equation (6.1) it is clear that A correspond to value of the thermo power at infinite temperature limit.

From figure 5.25 the extrapolated tangent at the higher temperature region of the curves approximately gives a common intercept at the ordinate from which the value of A has been obtained as 4.13. This value

corresponds to the scattering index = - 1.5 and is an indications that ionized impurity scattering is dominant in these MnO_2 films.

In all the author's samples it has been found that E_c - E_F varies with temperature and it can be assume that for a limited temperature range **(Mott & Davis, 1979).**

$$E_c - E_F = E_0 - \gamma T \text{----------(6.3)}$$

Where E_0 is the low -temperature limit of E_c - E_F and corresponds to the activation energy equivalent to the band gap, γ is the temperature coefficient of activation energy.

Putting equation (6.3) into equation (6.1); it is obtained the following equation

$$Q = -\frac{E_0}{eT} + \left(\frac{\gamma}{e} - \frac{AK_B}{e}\right) \text{----------(6.4)}$$

Now, the Peltier coefficient $\pi = QT$, is given by

$$\pi = -\frac{E_0}{e} + \left(\frac{\gamma}{e} - \frac{AK_B}{e}\right)T \text{----------(6.5)}$$

This equation shows that a π versus T plot should yield a straightest line and that value of γ can be obtained from its slope. Figure 6.2 shows such plots and it is observed that the slopes at room and higher temperature regions are different. Both slopes have been determined and using A=4.13, various values of γ were calculated for films of different thickness. These values of γ are plotted as a function of thickness in figure 6.3. It shows that at higher temperatures, γ is almost thickness independent, while in the room- temperature limit, it shows strong thickness dependence.

Using these values of γ at room temperature, the values of E_0 for the different film thickness may be calculated from equation (6.5), and the values of $E_c - E_F$ from equation (6.3). The variation of E_0 and of $E_c - E_F$ at room temperature as a function of inverse film thickness is shown in figure 6.4.

From figure 6.4 it is observed that E_0 has fair thickness dependence and its bulk value corresponding to inverse film thickness is 0.255 eV. This value agrees well with the band gap of MnO_2 crystal as reported previously **(Chevillot. et. al., 1959 & Druilhe et. al., 1967).** In extrinsic samples, the variation of E_0 with film thickness is obvious which is calculated from equation (6.3), is some type of thermal activation energy and depends on the detailed variations of the pattern of conduction and valance band edges with the structure of the film, including various defected. This is not necessarily a vertical transition. But the optical band gap corresponds to the optical absorption at same frequency and involves mostly vertical transitions between the bands. Thus the variation of optical band gap with thickness is not so straightforward as for E_0. Of course, carrier concentration plays an important role in the case.

Because, in the high-temperature region, the thermoelectric power saturates for all the samples (Figure 5.24 and 5.25) it suggests that the Fermi levels in these films are pinned near the band edge at higher temperature. This is now shown in figure 6.5 where this pinning can be clearly observed. The gradual decrease of thermoelectric power with inverse temperature as shown in figure 5.25, has also been reported by Huston **(Huston, 1959).** In thin film samples when the material behaves

like a Fermi glass, this type of variation is usual **(Mott & Davis, 1979)**. Author obtain some idea about this variation by differentiating equation (6.1) with respect to temperature, which yields

$$\frac{dQ}{dT} = -\frac{K_B}{e}\left[\frac{d(E_c - E_F)}{K_B T dT} - \left(\frac{E_c - E_F}{K_B T^2}\right) + \frac{dA}{dT}\right] \text{----------(6.6)}$$

From figure 6.5 it is observed that $-(E_c - E_F)$ decrease with temperature so that in the brackets the 1st term of equation (6.6) is positive. The second term is also positive because $(Ec - E_F)$ is negative and we have already ignored any possible temperature variation of A as it corresponds to the higher temperature limit of thermoelectric power. Thus the whole term in brackets is positive and hence dQ\dT is negative, which suggests a decrease of thermoelectric power with temperature. The minimum value of $-(E_c - E_F)$ as obtained from figure 6.5 is 0.11eV and is almost five times that of K_BT at in room temperature. Thus our previous consideration of a nondegenerate model is justified.

6.7 OPTICAL PROPERTIES OF MnO_2 FILMS

6.7.a BAND GAP

From the optical results, it is found that the best fit of the band gap is obtained for the indirect allowed transition. It may be conclude that MnO_2 thin film is an indirect band gap. The value of band gap is $\approx$ 0.250 eV ,which is very close to the band gap of 0.277 eV measured by electrical measurement and also agrees well with the band gap of MnO_2 crystal as reported previously **(Chevillot, et. al., 1959 & Druilhe, et. al., 1967).**

6.7.b INTEGRATED OPTICAL PROPERTIES

In order to utilize this material for selective surface coating for energy efficiency application, it is useful to assess its luminous and solar performance. In this section the author discusses the luminous and solar performance of this material for coatings of selective surface.

The integration could be done over the eye's sensitivity (0.4-0.7 μm) curve to get the luminous performance, over a typical solar spectrum (0.3-2.5 μm), over a blackbody spectrum (3-100 μm) to get the thermal performance, or over the atmospheric irradiant spectrum to find the radiative cooling performance

For assessing the performance pertinent to energy-efficient devices, it is convenient to introduce certain integrated optical quantities. These are the luminous (lum) and solar (sol) properties. Integrated luminous (lum) and solar (sol) quantities are computed from the relation

$$X\rho = \frac{\int d\lambda \phi_\rho(\lambda) X(\lambda)}{\int d\lambda \phi_\rho(\lambda)} \quad \text{--- --- -----(6.7)}$$

Where X denotes transmittance (T) or reflectance (R). The luminous quantities are obtained with $\phi_\rho = \phi_{lum}$ equal to the standard luminous efficiency for photopic vision **(Wyszecki, 1982)**. Solar properties are obtained with $\phi_\rho = \phi_{sol}$ given by the AM2 solar spectrum **(Moon, 1940)**.

Table 6.1 shows the solar and luminous values of transmittance as well as reflectance evaluated from figures 5.26 and 5.27, respectively.

Table 6.1 Data for thickness dependence of luminous and solar transmittance as well as reflectance of MnO_2 films.

Film thickness (nm)	T_{lum}(%)	T_{sol}(%)	R_{lum}(%)	R_{sol}(%)
70	76.003	82.009	18.026	14.063
110	70.558	76.998	24.315	19.184
165	64.157	70.846	26.592	20.574
200	54.312	64.848	28.868	21.926

CONCLUSION

The purpose of this section is to summarize the results obtained in this work. In practice, the work is to study the electrical, optical and structural properties of MnO_2 films for application in surface coating for energy-efficient devices.

The main results of this thesis can be summarized as follows:

i. Electron beam deposition is a suitable technique for production of MnO_2 thin film.

ii. X-ray diffraction pattern hints that MnO_2 is an amorphous material.

iii. Electrical conductivity measurement with temperature shows an anomaly in conductivity at a particular temperature near 323K, which is well agreed with reports of previous workers **(Bhide, 1960)**.

iv. The films deposited at about $2x10^{-5}$ torr show the electrical conductivity metallic in character by indicating positive Temperature Coefficient of Resistance (TCR), whereas a negative Temperature Coefficient of Resistance (TCR) indicating semiconducting behaviour exhibits on the films deposited at a pressure of about $6x10^{-6}$ torr. This result, therefore, suggests that preparation and properties of MnO_2 films are very much dependent on ambient pressure.

v. Activation energy for the samples are fairly low. It is inversely proportional with the film thickness above the anomaly and directly proportional below the anomaly temperature.

vi. Thickness-dependent electrical conductivity study was done in semiconducting MnO_2 films and it was seen that below 200nm thickness, the film shows thickness-dependent property and above this range the film has thickness-independent behaviour which is in good agreement with Fuchs-Sondheimer theory.

vii. The conductivity of the annealed film is higher than that of the as-deposited film.

viii. Studies on aging effect indicate that the sample degrades in conductivity with time, which may be due to oxidation or contamination.

ix. The value and sign of the Hall voltage of the measured samples signify that the samples are n-type in character. The value of band gap is found at approximately 0.277eV. This value agrees well with the band gap of MnO_2 crystal as reported previously **(Chevillot. et. al., 1959 & Druilhe et. al., 1967).**

x. The negative sign in the thermoelectric e.m.f. measurements indicates that the carriers in the MnO_2 films are electrons and the

films are n-type semiconductor. Similar observation was also obtained from Hall effect measurement.

xi. Thermoelectric power decreases continuously with increasing temperature and saturates in the higher temperature region. The rate of change of thermoelectric power with temperature is greater for films of higher thickness than that of lower one. In general the transport properties in these samples are controlled mainly by the ionized impurity scattering process corresponding to a scattering index of –1.5 obtained from thermoelectric power data. In the room temperature region coefficient of activation energy has strong thickness dependency while in the high-temperature region it is almost thickness independent.

xii. Optical studies in the wavelength range $300<\lambda<2500$ nm show that the material is highly transparent in the visible and infra-red range.

xiii. From the best linearity of $(kh\nu)^{1/2}$ versus $h\nu$ plot, it may be conclude that MnO_2 is an indirect allowed transition band gap semiconductor. The value of band gap is found to be ≈ 0.25 eV. The value of band gap is very close to the value obtained from electrically measured value of 0.27 eV.

xiv. For assessing the films in selective surface applications the integrated luminous and solar transmittance as well reflectance are

calculated. The integrated values of luminous transmittance (T_{lum}) and solar transmittance (T_{sol}) are of high order indicating that the material is a potential candidate for the applications in selective surface devices.

BIBLIOGRAPHY

BIBLIOGRAPHY

Advan. Phys., 1 (1952) 1

Adler,Rev, D. , Mod. Phys., 40 (1968) 714

Ames, I., Rev. Sci. Instr., 37 (1966) 213

Andrade, E.N. Trans. Faraday Soc., 31 (1935) 1137

Barden J., Blat F. J. and Hall, L. H. Photoconductivity

Beam, T., Rev. Sci. Instr., 35 (1964) 16

Bhide, V.G. Rev., physica, 26 (1960) 33-42

Bruck, L. Ann. Physik, 26 (1936) 233

Bunsen, R. J. Prakt. Chem., 56 (1852) 53 conference Eds. (1965).

Chakrabarti, B. & Pal. A.K. Jpn. J.Appl. Phys., 19 (1980) 591

Chevillot, J.P.; Brenet, J. ; C.R. Acad. Sci., 248, 776 (1959)

Chopra, K. L. " Thin Film Phenomena", Mc-Grow Hill Book Company, New York, (1969)

Conn, W. M. Phys. Rev., 79 (1950) 213 D.M. Mattox,

Dale, A.B. The Form and properties of Crystals, London: Cambridge University Press (1932)

Duga, J. J. Appl. Phys., 33 (1962) 169

Druilhe, R. ; Suchet, J. P., Czech. J. phys. B, 17, 337 (1967)

Ellis, S. G. J. Appl. Phys., 38 (1967) 2906

Faraday, M. phil. Trans. 147 (1857) 145

Fuchs, K. Proc. Cambridge Phil. Soc., 34(1938) 100

Gorter, C. J. ,Physica, 17 (1951) 77

Granqvist C. G. and Niklasson G.A., "Thin Film Technology", S-412 96 Gothenburg, Sweden

Ghosh, S. N. and Dev, S. A Synopsis of Physics. The World press Ltd., Calcutta, P.671 (1937)

Hall, E. H. phys. Rev., 2 (1879) 287

Harries, L. and Siegel, B. M. J. Appl. Phys., 19 (1984) 739W.R.

Harry, H. , Kwok, B. and Bube, R.H. , J. Appl. phys. 44(1973) 138

Holland, L. "Vacuum Deposition of Thin Films", John Wiley & Sons,Inc., New York (1956)

Hutson, A.R., ibid. 8 (1959) 467

Kundt, A. Ann. Physik, 31 (1888) 467

Langmur, I. Phys. Rev., 8 (1916) 149 and Frenkel, J. Zphysic, 26 (1924) 117

Levinstein, H. J. Appl. Phys., 20 (1949) 306

Lynn davis, International Journal on the science and Technology of Thin and Thick Films, 236 (1993) 1-5

Lucas, M. S. P. J. Appl. Phys., 36 (1965) 632

Mayadas, A. F. and Shatzkes, M. Phys. Rev., B1 (1970)

Matthews, J. W. Phil. Mag., 12 (1965) 1143

Maissel, L.I. & . Glang, R. "Handbook of Thin Film Technology",39(1983)

Mckelvey, J.P. , Solid state & Semiconductor Physics Harpar International Edition., N.Y.,1966

Megraw, H., Ferroelectricity in crystals, London: Methuen and Co., p. 14 (1957)

Moon, P. J., Franklin Inst., 230 (1940) 583

Mott, N.F. and Davis, E.A. "Electronic processes in non-crystalline materials", 2nd Edn (Clarendon press, Oxford, 1979)

Mullendore, A. W. and Rebarchik, F. N. J. Vacuum Sci. Tech., 4 (1967) 123

Neugebauer, G.A. Physics of Thin films, New York: Academic Press, 2 (1964).

Nahrwold, R. Ann. Physik, 31 (1887) 467

Neugebauer C. A. and Webb, M. B. J. Appl. Phys., 33 (1962) 74

Pashely, D. W. and Stowell, M. I., Jocobes M. H. and Law, T. J. , Phil. Mag., 10 (1964) 127

Pashley, D. W. and Stowell, M. J., in S. S. Breese (ed), Proc. 5th Intern. Congr. Electron microscope, (1962)

Pashely, D.W., Stowell, M. J., Jecobs, M.H. and Law, T. J. , phil. Mag., 10 (1964) 127

Pound, G. M., simnad ,M. T. and Yang, L. J. Chem. Phys., 22 (1954) 1215

Sayigh, A.A.M. and Thekaera, M.P., Solar Energy Engineering, New York: Academic Press(1977)

Semenoff, N. Z. Phys. Chem., B7 (1930) 741

Seto, J. Appl. phys., 46 (1975) 524

Sloope, B. W. and Tiller, C. O. J. Appl. Phys., 36 (1965) 317

Sondheimer, F. H. Phys. Rev. 80 (1950) 401

Sondheimer, F. H. Advan. phys., 1 (1952) 1

Smith, H. M. Appl. Opt., 4(1965) 147

Tolansky, S. " Multiple Beam Interferometry of Surfaces & Films" Oxford University Press, N. J. Fair Lawn (1948)

Thomson, J. J Proc. Cambridge Phil. Soc., 11 (1901)120

Touloukian, Y.S. and Dewitt, D.P, Thermophysical properties coatings, IFI/Plenum, New-York(1972)

Turner, J. A., Sci. Instr., 40 (1963)

Uyeda, R. Proc. Phys. Math. Soc. Japan, 24 (1942) 802

Volmer, M. and Weber, A. Z. Phys. Chem., 119 (1925) 277;

Volmer, M. "Kinetic der Phasenbildung", Theodor Steinkopf Verlagsbuchhandlung, Dresden-Leipzig, 1939 and W. Doring, Ann. Physik, 24 (1935) 719

Vander Pauw ,L. J. Philips. Res., 13 (1958)

Van, J. Rev. Sci. Instr., 36 (1965) 383

Vasudeva, D. N. "Fundamentals of Magnetism and Electricity", Chamad and Company Ltd., (1984)

Wiener, O. Wild. Ann., 31 (1887) 629

Wyszecki,G. and Stiles, W.S., Color Science, 2nd . Ed., New York: Wiley (1982)

Yoshizumi Yasuoka & Toyoo Miyata, Jpn. J.Appl.Phys., 18 (1979) 397